GLUTAMATERGIC SYNAPTIC PLASTICITY IN DOPAMINE D1 AND D2 RECEPTOR-EXPRESSING STRIATAL NEURONS AND ALCOHOL USE DISORDER

A Dissertation

by

JIAYI LU

Submitted to the Office of Graduate and Professional Studies of
Texas A&M University
in partial fulfillment of the requirements for the degree of

DOCTOR OF PHILOSOPHY

Chair of Committee,	Jun Wang
Committee Members,	William H. Griffith
	Jianrong Li
	Laura N. Smith
Head of Program,	Carol Vargas

December 2020

Major Subject: Medical Sciences

ABSTRACT

The dorsomedial striatum (DMS) of the basal ganglia is critically involved in drug and alcohol abuse and contains medium spiny neurons (MSNs) expressing dopamine D1 receptors (D1Rs) or D2Rs. D1-MSNs positively and D2-MSNs negatively control reward-driven behaviors. However, how different glutamatergic inputs onto distinct MSNs are altered by alcohol and how such alcohol-evoked aberrant plasticity drives reinforcement behaviors remain unclear. Thus, I first examined how excessive alcohol intake alters glutamatergic transmission at striatal synapses expressing distinct presynaptic dopamine receptors. Then I investigated the causality between alcohol-evoked plasticity and reinforcement behaviors and whether reversal of this plasticity persistently reduced alcohol-seeking. Lastly, I examined the selectivity of extra-striatal afferents in their innervations of D1-MSNs and D2-MSNs.

First of all, I found larger excitatory postsynaptic currents at the synapses between the extra-striatal D2R-expressing afferents and D1-MSNs (D2→D1), as compared with those observed at the other tested synapses (D1→D1, D1→D2, and D2→D2). I further discovered that excessive alcohol consumption induced a long-lasting potentiation of glutamatergic transmission at the corticostriatal D2→D1 synapse. Secondly, I found that mimicking alcohol-evoked potentiation at glutamatergic synapse between medial prefrontal cortex (mPFC) and D1-MSNs using *in vivo* dual-channel optogenetic self-stimulation of this synapse to induce LTP was sufficient to drive reinforcement of lever pressing in rat operant behaviors. Conversely, *in vivo* LTD

induction at this synapse with time locked to lever presses persistently decreased alcohol-seeking behavior. Lastly, I discovered that pDMS D1-MSNs preferentially received inputs from orbital frontal cortex, secondary motor and visual cortex, as well as cingulate cortex, whereas D2-MSNs received primary motor, primary sensory, and thalamic inputs. Taken together, my graduate study suggests that 1) chronic alcohol exposure selectively strengthened glutamatergic transmission from cortical inputs, e.g. D2R-expressing inputs or mPFC inputs, onto DMS D1-MSNs. 2) Glutamatergic synaptic plasticity at mPFC→D1-MSNs was sufficient to drive the reinforcement behavior and contributed to alcohol-seeking behavior. 3) pDMS D1-MSNs and D2-MSNs received differential innervation from extra-striatal regions. These data will enrich and help specify the understanding of how glutamatergic plasticity at striatal circuits controls alcohol-induced addictive behaviors.

ACKNOWLEDGEMENTS

I would like to thank my committee chair, Dr. Jun Wang, and my committee members, Dr. William H. Griffith, Dr. Jianrong Li, and Dr. Laura N. Smith for their guidance and support throughout the course of this research.

Thanks also go to my relatives and friends (Ms. Lily Bloodworth, Mr. Robert Bloodworth, Ms. Jennifer Bloodworth, Ms. Stacy Bloodworth, Ms. Xueyang Zhang, and Mr. Yuanning Zhen) and colleagues (especially Dr. Yifeng Cheng, Dr. Tengfei Ma, Dr. Xiaowen Zhuang, Ms. Xuehua Wang, Mr. Xueyi Xie, Mr. Himanshu Gangal, Dr. Amanda Mahnke, Ms. Nihal Salem, Mr. Dae Chung, Mr. Nathaniel Teplitskiy, Ms. Kayla Woodson, Ms. Emily Disney, Ms. Jordan Bonifacio, Mr. Craig Kemper, and Mr. Kassidy Bego) and the departmental faculty (Dr. Warren Zimmer, Dr. Jun-Yuan Ji, Dr. Xin Wu, Dr. Rajesh Miranda, and Dr. Rahul Srinivasan) and staff for making my time at Texas A&M University a great experience.

Finally, thanks to my parents (Ms. Yongmei Ye and Mr. Jianqi Lu) for their encouragement and to my husband (Mr. Yen-Nan Lin) for his patience and love.

CONTRIBUTORS AND FUNDING SOURCES

This work was supervised by a dissertation committee consisting of Associate Professor Jun Wang [adviser], Professor William H. Griffith, and Assistant Professor Laura N. Smith in the Department of Neuroscience and Experimental Therapeutics and Associate Professor Jianrong Li in the Department of Veterinary Integrative Biosciences.

The stereotaxic infusion for Chapter II was assisted by Dr. Yifeng Cheng. The confocal images analysis and neuron counting for Chapter II, III, and IV were conducted by Mr. Craig Kemper, Ms. Emily Disney, Ms. Kayla Woodson, Ms. Jordan Bonifacio, Mr. Xueyi Xie, and Mr. Yifeng Cheng. The electrophysiology experiments for Chapter III (Figure 3.2 G-J) were provided by Dr. Tengfei Ma. The behavior experiments for Chapter III was assisted by Mr. Yifeng Cheng, Mr. Xueyi Xie, Ms. Kayla Woodson, and Mr. Kassidy Bego. All experimental animals were bred and genotyped by Ms. Xuehua Wang. All other work conducted for the dissertation was completed by the graduate student, Ms. Jiayi Lu, independently.

Graduate study was supported by [NIH/NIAAA] under Grant Number [R01AA021505] (JW), [R01AA027768] (JW), [U01AA025932] (JW), and by Texas Research Society on Alcoholism (TxRSA) (JL).

ABBREVIATIONS

AUD	Alcohol Use Disorder
AMPAR	α-amino-3-hydroxy-5-methyl-4-isoxazolepropionic Acid Receptor
AD	Anterior Dorsal Thalamus
AV	Anterior Ventral Thalamus
BLA	Basolateral Amygdala
BNST	The Bed Nucleus of the Stria Terminalis
CIN	Cholinergic Interneurons
CB1R	Cannabinoid Type I Receptor
CeA	Central Nucleus of the Amygdala
Cg	Cingulate Cortex
CM	Central Thalamic Nucleus
DLS	Dorsolateral Striatum
DMS	Dorsomedial Striatum
D1Rs	Dopamine D1 receptors
D2Rs	Dopamine D2 receptors
eCB	Endocannabinoid
EPSC	Excitatory Postsynaptic Current
EP	Entopeduncular Nucleus
GP	Globus Pallidus
GPe	External Part of Globus Pallidus

LTP	Long-term Potentiation
LTD	Long-term Depression
LHb	Lateral Habenula
MSN	Medium Spiny Neuron
M2	Secondary Motor Cortex
M1	Primary Motor Cortex
MD	Mediodorsal Thalamic Nucleus
mPFC	Medial Prefrontal Cortex
NMDAR	N-methyl-D-aspartate Receptor
oPSD	Optogenetic Postsynaptic Depolarization
PPR	Paired-Pulse Ratio
PrL	Prelimbic Cortex
Pf	Parafasicular Thalamic Nucleus
PVT	Paraventricular Thalamic Nucleus
Po	Posterior Thalamic Nucleus
SNc	Substantia Nigra Pars Compacta
SNr	Substantia Nigra Pars Reticulata
STDP	Spike Timing-Dependent Plasticity
S1	Primary Sensory Cortex
VTA	Ventral Tegmental Area
VM	Ventromedial Thalamic Nucleus

TABLE OF CONTENTS

Page

LIST OF FIGURES

Page

LIST OF TABLES

Page

CHAPTER I

INTRODUCTION AND LITERATURE REVIEW

1.1. Overview

Alcohol is one of the most commonly used addictive substance today (Rehm et al., 2009; Whiteford et al., 2013). When people suffer from the inability to control alcohol use due to both a physical and emotional dependence on alcohol, they will be diagnosed as alcohol use disorder (AUD) (Rehm et al., 2009; Whiteford et al., 2013; Kranzler and Soyka, 2018). Chronic and heavy alcohol use leads to many health problems, including liver diseases, cardiovascular problems, diabetes complications, and other mental health issues (Rehm et al., 2009; Kranzler and Soyka, 2018). The World Health Organization revealed that more than 76 million people worldwide have AUD, and AUD are responsible for 5 million death per year (Whiteford et al., 2013; Jeanblanc, 2015). The individual, social and economic burden of AUD are extraordinarily high (Rehm et al., 2009; Batman and Miles, 2015; Volkow et al., 2016; Kranzler and Soyka, 2018). The economic costs to treat alcohol-related problems is nearly $250 billion annually in the United States alone (Sacks et al., 2015). Unfortunately, there are only a few available medications for AUD with limited efficacy and often fail to prevent relapse (Kranzler and Soyka, 2018; Ehrie et al., 2020). Approaches to solving this crisis include basic and preclinical research on underlying neurobiological mechanisms, which seeks to deepen understanding of circuits, neurotransmitters and molecules that underline alcohol use and abuse to increase our ability to devise new treatments.

The striatum, the main component of the basal ganglia has emerged as a critical hub for alcohol and drug addiction. Increasing studies showed that the dorsomedial striatum (DMS) is particularly relevant for alcohol addiction (Wang et al., 2007; Wang et al., 2010; Wang et al., 2012a; Wang et al., 2015; Cheng et al., 2017; Ma et al., 2018; Roltsch Hellard et al., 2019). In animal models, acute and chronic alcohol exposure alters DMS glutamatergic and GABAergic signaling (Wang et al., 2007; Wang et al., 2010; Wang et al., 2011; Wang et al., 2012a; Cheng et al., 2017; Ma et al., 2017) and manipulation of DMS function impacts excessive alcohol consumption and alcohol self-administration (Cheng et al., 2017; Ma et al., 2018; Roltsch Hellard et al., 2019). Thus, understanding the role of DMS circuits in excessive alcohol consumption and alcohol self-administration is of great significance.

1.2. Medium spiny neurons (MSNs) in the DMS play critical roles in AUD

Medium spiny neurons are GABAergic projection neurons representing 95% of striatal cells (Kreitzer and Malenka, 2008; Cheng et al., 2017). They are characterized by their high spiny density and very negative resting potentials (Kreitzer and Malenka, 2008; Cheng et al., 2017). Due to the expression of inwardly rectifying potassium channels (Kir) and activation of other potassium channels at depolarizing voltages, MSNs showed a slow depolarization and delay of the first spike (Surmeier et al., 1989; Surmeier et al., 1991; Shen et al., 2004; Shen et al., 2005). Previous studies have revealed that *in vivo* MSNs exhibit two different membrane potential: up-state of MSNs with more depolarized membrane potential and down-state of MSNs with hyperpolarized membrane potentials (Wilson and Kawaguchi, 1996; Kreitzer, 2009).

The shifting of down- and up-state depends on the intrinsic membrane properties of MSNs and the magnitude and timing of glutamatergic inputs from the cortex and thalamus (Blackwell et al., 2003). High levels of Kir stabilize the MSNs membrane potentials at down-state, whereas sufficient glutamatergic inputs shift MSNs from down-state to up-state.

DMS MSNs are not homogeneous. Based on the dopamine expression pattern and axonal projection, MSNs can be categorized into two different subtypes. D1-MSNs exhibit high expression of dopamine D1 receptors (D1Rs), and directly project to internal globus pallidus and substantia nigra pars reticulata, forming the direct-pathway (Kreitzer and Malenka, 2008; Cheng et al., 2017). In contrast, D2-MSNs express high levels of D2Rs and send axons to the external globus pallidus, forming the indirect-pathway (Kreitzer and Malenka, 2008; Cheng et al., 2017). The direct-pathway circuits disinhibiting the excitatory thalamocortical projections result in activation of cortical circuits and facilitation of action selection and movement (Kreitzer and Malenka, 2008; Cheng et al., 2017). The indirect-pathway circuits contribute to the inhibition of thalamocortical neurons and lead to the suppression of cortical circuits and movement (Kreitzer and Malenka, 2008; Cheng et al., 2017). Thus, D1-MSNs positively and D2-MSNs negatively control rewarding behaviors (Kreitzer and Malenka, 2008; Cheng et al., 2017).

Both types of DMS MSN receive glutamatergic inputs from cortex, thalamus and amygdala (Wall et al., 2013; Hunnicutt et al., 2016; Smith et al., 2016; Ma et al., 2017). In addition to the excitatory glutamatergic inputs, MSNs receive dopaminergic inputs

from substantia nigra pars compacta (SNc) (Wall et al., 2013; Hunnicutt et al., 2016). Dopamine can regulate the activity of MSNs via D1Rs and D2Rs. Both D1Rs and D2Rs are G protein-coupled receptors, but they have distinct downstream signaling pathways and kinetic property. In the striatum, activation of D1Rs enhances cAMP and PKA signaling and facilitates the trafficking of α-amino-3-hydroxy-5-methyl-4-isoxazolepropionic acid receptors (AMPARs) and N-methyl-D-aspartate receptors (NMDARs) (Beaulieu and Gainetdinov, 2011). In contrast, activation of D2Rs triggers increases in potassium efflux via GIRK channel and the inhibition of trafficking of AMPARs. Given that D1Rs are low-affinity dopamine receptors whereas D2Rs are with high affinity, phasic dopamine release mainly activates D1Rs and enhances the activity of direct-pathway circuits, facilitating the goal-directed behaviors. Changes in tonic dopamine level or phasic pause of dopamine release mainly disinhibit D2Rs and enhances the activity of indirect-pathway circuits, suppressing the goal-directed behaviors (Bromberg-Martin et al., 2010; Durieux et al., 2012).

Growing evidence has indicated that both D1-MSNs and D2-MSNs play critical roles in the drug and alcohol addiction. Systematic administration of D1R antagonist impaired alcohol intake and alcohol condition place preference (Bahi and Dreyer, 2012; Pina and Cunningham, 2014). Inhibition of D1-MSNs via optogenetics or chemogenetics reduced sensitization of amphetamine and alcohol consumption (Hikida et al., 2010; Lobo et al., 2010; MacAskill et al., 2014; Cheng et al., 2017). Optogenetic or chemogenetic activation of D2-MSNs enhances the sensitization of amphetamine,

craving for cocaine and alcohol (Hikida et al., 2010; Lobo et al., 2010; MacAskill et al., 2014; Cheng et al., 2017).

1.3. Presynaptic dopamine receptors as a critical regulator of AUD

Dopamine signaling in the corticostriatal circuit is centrally involved in reward-driven behaviors (Bamford et al., 2018). Many learned behaviors depend on the coordinated activation and inhibition of pathways in the striatum (Bamford et al., 2018). By acting on different glutamatergic synapses, striatal dopamine regulates specific excitatory inputs from the cortex and thalamus onto two types of MSNs, contributing to the selection of appropriate "Go" or "NoGo" action (Bamford et al., 2018). Dopaminergic modulation is mainly mediated by D1Rs and D2Rs, which are highly expressed in DMS D1-MSNs and D2-MSNs (Beaulieu and Gainetdinov, 2011; Wei et al., 2018). Activation of D1Rs and D2Rs leads to an opposite regulation of glutamatergic receptor and play an opposite role in addiction (Shen et al., 2008). Anatomical evidence has indicated that, in addition to postsynaptic neurons, D1Rs and D2Rs are present at presynaptic cortical terminals in the striatum (Wang and Pickel, 2002; Dumartin et al., 2007). These presynaptic dopamine receptors facilitate dopamine-mediated regulation of excitatory signaling to specific striatal pathways (Bamford et al., 2018). Altered dopaminergic transmission is a common mechanism underlying drug and alcohol abuse (Koob and Volkow, 2010; Luscher and Malenka, 2011). It has long been known that all addictive drugs elevate levels of dopamine in the brain (Koob and Volkow, 2010; Luscher and Malenka, 2011). Since D1Rs and D2Rs are activated by elevated dopamine after *in vivo* alcohol exposure, it is plausible that glutamatergic transmission in D1-

MSNs and D2-MSNs is differentially regulated by alcohol consumption. However, how excessive alcohol consumption affects glutamatergic synapses expressing particular pre- and postsynaptic dopamine receptors is poorly understood. Therefore, in chapter II, I used whole-cell patch-clamp recording to explore the effect of excessive alcohol intake in glutamatergic transmission of corticostriatal synapses expressing distinct presynaptic dopamine receptors. I discovered that DMS synapses containing presynaptic D2Rs and postsynaptic D1Rs (D2→D1) exhibited strongest glutamatergic connectivity, as compared with those observed at the other tested synapses (D1→D1, D1→D2, and D2→D2). Excessive alcohol intake selectively potentiated glutamatergic transmission at the corticostriatal D2→D1 synapse. Lastly, I confirmed that D2R-mediated inhibition of glutamatergic transmission in the DMS is mediated by distinct pre- and postsynaptic mechanisms.

1.4. Glutamatergic plasticity in the DMS and AUD

Both D1-MSNs and D2-MSNs in the DMS receive a number of different inputs, including glutamatergic inputs from the cortex, which convey sensory, motor, and other information that may stimulate alcohol-seeking and alcohol-taking behaviors (Wall et al., 2013; Hunnicutt et al., 2016; Smith et al., 2016; Ma et al., 2017). The glutamatergic inputs from the amygdala, which mediates emotional stimuli such as stress are able to enhance alcohol intake, as well as those from the thalamus (Wall et al., 2013; Hunnicutt et al., 2016; Smith et al., 2016; Ma et al., 2017). Striatal glutamatergic activity is critically involved in regulating behaviors related to alcohol intake and other drugs of abuse (Wang et al., 2007; Belin and Everitt, 2008; Wang et al., 2010). For example,

inhibition of striatal glutamatergic activity in the dorsal striatum suppresses operant alcohol self-administration and cocaine relapse (Wang et al., 2007; Belin and Everitt, 2008; Wang et al., 2010). The dorsal striatum contains AMPAR and NMDAR glutamatergic receptors. AMPARs mediate fast synaptic transmission and NMDARs control the induction of long-term potentiation (LTP) of AMPAR-mediated synaptic transmission (Calabresi P, 1992; Partridge JG, 2000; Shen et al., 2008). Recent studies reported that excessive alcohol exposure induced the phosphorylation of NR2B subunits of the NMDAR, which results in long-lasting facilitation of GluN2B-containing NMDAR activity (Wang et al., 2007; Wang et al., 2010). These adaptations enhance striatal LTP induction and occur preferentially in the DMS (Wang et al., 2007; Wang et al., 2010). Although striatal glutamatergic activity plays a critical role in regulating alcohol intake, much remains unknown about where and how glutamatergic receptors are activated in striatal circuits to promote pathological addiction-related behaviors.

AUD is a psychiatric illness involving a transition from recreational use to compulsive alcohol-seeking and alcohol-taking (Luscher et al., 2020). This behavioral transition is proposed to be controlled by alcohol-evoked plasticity. LTP, particularly NMDAR-dependent LTP, and LTD are synaptic processes underlying learning and memory (Yin et al., 2007; Luscher and Malenka, 2011; McCool, 2011). Addiction, including AUD, is generally considered drug-evoked, abnormally enhanced learning and memory (Luscher and Malenka, 2011; Ma et al., 2018). Medications fail to persistently prevent alcohol-seeking and relapse, perhaps because they do not reverse the alcohol-evoked long-term synaptic plasticity, which is thought to be a cellular substrate of

alcohol addiction (Luscher and Malenka, 2011; Ma et al., 2018). Emerging evidence suggests that such drug-evoked aberrant plasticity shares similar mechanisms with LTP and LTD, which can reverse one another (Malenka and Bear, 2004; Luscher and Malenka, 2011; Pascoli et al., 2012; Ma et al., 2018). Thus, mimicking alcohol-evoked plasticity by inducing LTP, or reversing this plasticity by inducing LTD, will provide a new understanding of how this plasticity controls alcohol-seeking behavior.

In chapter III, using whole-cell patch-clamp recording, I found that excessive alcohol consumption selectively potentiated glutamatergic transmission from medial prefrontal cortex (mPFC) to D1-MSNs (mPFC→D1-MSNs). To further understand the role of this corticostriatal plasticity at mPFC→D1-MSNs in reinforcement behaviors, I mimicked this alcohol-evoked aberrant plasticity via *in vivo* optogenetic LTP induction. I found that the corticostriatal plasticity is sufficient to drive reinforcement in rat operant behaviors. Importantly, I also use *in vivo* dual-channel optogenetics to selectively suppressing neural activity within DMS circuits during alcohol self-administration to better understand how DMS processing underlies alcohol self-administration in real time. I discovered that reversing alcohol-evoked synaptic plasticity at D1-MSNs using a behavior-locked LTD-inducing protocol persistently reduced alcohol-seeking behavior.

To test the hypothesis that *in vivo* LTD induction at the mPFC inputs onto DMS D1-MSNs leads to a sustained reduction in alcohol-seeking behavior, I combined dual-channel optogenetics and spike timing-dependent plasticity (STDP) to induce circuit-specific LTD at the mPFC inputs onto DMS D1-MSNs. The dual channel optogenetic approach, whereby two channelrhodopsins are expressed, allows me to selectively

control the activity of pre- and postsynaptic components simultaneously by delivering different wavelengths of light. In the STDP induction, the relative timing of presynaptic and postsynaptic action potentials determines the direction and strength of synaptic potentiation or depression. The “post-pre”-STDP protocol is used for LTD induction, in which repeated postsynaptic spike arrives a few milliseconds before presynaptic action potential. Since LTD induction requires both pre- and postsynaptic activity, precise time control of activation using dual channel optogenetics will provide circuit-specific induction.

1.5. Excitatory inputs of striatum and their functional organization

The striatum receives and sorts excitatory inputs from the cortex, thalamus, and amygdala to basal ganglia, and it is involved in diverse psychological functions, e.g. movement control, action selection and reward-related processes (Hunnicutt et al., 2016). The striatum can be anatomically and functionally divided into three parts: DMS, dorsolateral striatum (DLS) and ventral striatum. While all regions participate in movement control, DMS regulates action-outcome association, goal-directed strategy, and higher cognitive behaviors, whereas DLS mediated habit in the familiar environment (Kreitzer and Malenka, 2008; Cheng et al., 2017). The ventral striatum exhibits a prominent role in reward-related behaviors (Kreitzer and Malenka, 2008; Cheng et al., 2017). Based on the specific input to striatum, the striatum is thought to contain three functional domains: sensorimotor, associative and limbic domains, which correspond to the DLS, DMS and ventral striatum, respectively (Hunnicutt et al., 2016). Although striatal inputs differentially innervate subregions of striatum, their innervation selectivity

on different striatal neurons is poorly understand. The DMS plays critical roles in goal-directed behaviors, but D1-MSNs and D2-MSNs provide opposite roles during this process (Cheng et al., 2017). To fully understand how information flows from striatum to basal ganglia, we need to know how upstream inputs distinctly innervate the direct- and indirect-pathway.

In chapter IV, I utilized the recently developed rabies virus-mediated monosynaptic tracing approach to label brain-wide neurons that project to pDMS D1-MSNs or D2-MSNs. I found that MSN subtypes received asymmetric inputs throughout the whole brain. These findings lay a foundation for future understanding of how pDMS sorts information from multiple upstream brain regions to determine the action.

CHAPTER II

ALCOHOL INTAKE ENHANCES GLUTAMATERGIC TRANSMISSION FROM D2 RECEPTOR-EXPRESSING AFFERENTS ONTO D1 RECEPTOR-EXPRESSING MEDIUM SPINY NEURONS IN THE DORSOMEDIAL STRIATUM*

2.1. Overview

Dopaminergic modulation of corticostriatal transmission is critically involved in reward-driven behaviors. This modulation is mainly mediated by dopamine D1 receptors (D1Rs) and D2Rs, which are highly expressed in medium spiny neurons (MSNs) of the dorsomedial striatum (DMS), a brain region essential for goal-directed behaviors and addiction. D1Rs and D2Rs are also present at presynaptic cortical terminals within the DMS. However, it is not known how addictive substances alter the glutamatergic strength of striatal synapses expressing presynaptic dopamine receptors. Using cell type-specific Cre mice in combination with optogenetic techniques, we measured glutamatergic transmission at D1R- or D2R-expressing afferents to DMS MSNs. We found larger excitatory postsynaptic currents at the synapses between the extra-striatal D2R-expressing afferents and D1R-expressing MSNs (D2→D1), as compared with those observed at the other tested synapses (D1→D1, D1→D2, and D2→D2).

---

* Parts of this chapter have been reprinted with permission from "Alcohol intake enhances glutamatergic transmission from D2 receptor-expressing afferents onto D1 receptor-expressing medium spiny neurons in the dorsomedial striatum" by Jiayi Lu, Yifeng Cheng, Xuehua Wang, Kayla Woodson, Craig Kemper, Emily Disney, Jun Wang, 2019. *Neuropsychopharmacology*, 44, 1123-1131, Copyright [2019] by Springer Nature.

Additionally, excessive alcohol consumption induced a long-lasting potentiation of glutamatergic transmission at the corticostriatal D2→D1 synapse. Furthermore, we demonstrated that activation of postsynaptic, but not presynaptic, D2Rs inhibited corticostriatal transmission in an endocannabinoid-dependent manner. Taken together, these data provide detailed information on the mechanisms underlying dopamine receptor-mediated modulation of brain reward circuitry.

2.2. Introduction

Dopamine signaling in the corticostriatal circuit is centrally involved in reward-driven behaviors (Bamford et al., 2018). By acting on different glutamatergic terminals, striatal dopamine regulates specific excitatory inputs from the cortex and thalamus onto MSNs, contributing to the selection of appropriate behaviors (Bamford et al., 2018). Dopaminergic modulation is mainly mediated by D1Rs and D2Rs (Beaulieu and Gainetdinov, 2011; Wei et al., 2018), which are highly expressed in the DMS, a brain region essential for goal-directed behaviors and addiction (Lovinger, 2010; Cheng et al., 2017). DMS MSNs express D1Rs or D2Rs (Kreitzer and Malenka, 2008) and anatomical evidence indicates that these receptors are present at presynaptic cortical terminals in the striatum (Wang and Pickel, 2002; Dumartin et al., 2007). These presynaptic receptors facilitate dopamine-mediated regulation of excitatory signaling to specific striatal pathways (Bamford et al., 2018). Altered dopaminergic transmission is a common mechanism underlying drug and alcohol abuse (Koob and Volkow, 2010; Luscher and Malenka, 2011). However, it is not known how excessive alcohol consumption affects glutamatergic synapses expressing particular pre- and postsynaptic dopamine receptors.

The medial prefrontal cortex (mPFC) afferent input to the DMS has been extensively implicated in drug and alcohol addiction (Balleine and O'Doherty, 2010; Corbit et al., 2013; Ma et al., 2014). Excessive alcohol exposure has been reported to enhance glutamatergic responses at mPFC inputs to the DMS (Ma et al., 2017), and this enhancement was recently shown to contribute to a long-lasting enhancement of alcohol-seeking and alcohol-taking behaviors (Ma et al., 2018). The neuronal subtypes within the mPFC can also be distinguished based on their expression of D1Rs and D2Rs (Wei et al., 2018). However, it is not known how excessive alcohol consumption distinctly alters D1R- or D2R-expressing mPFC afferents onto striatal MSNs.

In this study, we measured the effects of excessive alcohol intake on glutamatergic transmission at DMS synapses expressing different pre- and postsynaptic dopamine receptors. We discovered that synapses containing presynaptic D2Rs and postsynaptic D1Rs (D2→D1) exhibited stronger glutamatergic connectivity than the other tested synapses (D1→D1, D1→D2, and D2→D2). Excessive alcohol intake induced a long-lasting potentiation of glutamatergic transmission at the corticostriatal D2→D1 synapse. In addition, we demonstrated that D2R-mediated inhibition of glutamatergic transmission in the DMS is mediated by distinct pre- and postsynaptic mechanisms. These findings contribute to the elucidation of the detailed mechanisms underlying the dopaminergic modulation of different brain reward circuitry. Our results also identified alcohol-evoked circuit-specific plasticity in the DMS, which may contribute to excessive alcohol consumption.

2.3. Results

2.3.1. DMS glutamatergic synapses containing different pre- and postsynaptic dopamine receptors exhibit distinct connectivity

To achieve selective activation of D1R- or D2R-expressing neurons, we crossed D1-Cre or D2-Cre mice, in which Cre expression was driven by the D1R or D2R promotor, with a channelrhodopsin-2 (ChR2)-enhanced yellow fluorescent protein (EYFP) Cre reporter line, Ai32 (Gong et al., 2007; Madisen et al., 2012). We recently verified that Cre expression in these mouse lines reliably represented D1R- and D2R-expressing neurons outside the striatum (Wei et al., 2018). In D1-Cre; Ai32 and D2-Cre;Ai32 mice, we observed intense expression of EYFP in the dorsal striatum and at the projection targets of D1-MSNs and D2-MSNs (Figure 2.1 A, B), confirming ChR2 expression in these neurons. We utilized a biophysical approach to identify MSN subtypes. In D1-Cre;Ai32 mice, D1-MSNs expressed ChR2 and responded distinctly to 2-ms and 500-ms light stimulations (Cruikshank et al., 2010) (Figure 2.2 Ai, B). Conversely, D2-MSNs in these animals did not express ChR2, but received glutamatergic afferents expressing D1Rs and ChR2; in these cells, 500-ms light stimulation did not significantly alter the width of the response to 2-ms light stimulation (Figure 2.2 Aii, B). The same approach was used to identify D1-MSNs and D2-MSNs in D2-Cre;Ai32 mice (Figure 2.2 C).

Next, we measured the light-evoked response in the presence of an AMPAR antagonist, DNQX (10 μM), and found that the responses at D1→D2 and D2→D1 synapses were completely blocked (Figure 2.2 D, E). In contrast, the light-evoked

responses of D1→D1 or D2→D2 were partially suppressed due to a large postsynaptic ChR2-mediated depolarization (Figure 2.2 F). This ChR2-mediated direct depolarization may cause a space-clamp error, which affects the accuracy of measurements of D1→D1 and D2→D2 connectivity. To overcome this space-clamp issue, we measured the strontium (Sr^{2+})-induced asynchronous excitatory postsynaptic currents (aEPSCs) evoked by light stimulation (Ding et al., 2008; Mateo et al., 2017). We found that the aEPSC frequency was significantly higher at the D2→D1 synapse than at the other three synapse types (Figure 2.1 C, D; $F_{(3,49)} = 32.88$, $p < 0.001$), and that the aEPSC amplitude was identical in these four types of synapse (Figure 2.1 C, E; $F_{(3,49)} = 0.14$, $p > 0.05$).

The higher aEPSC frequency indicated that the D2→D1 synapse may show the strongest connectivity. To confirm this, we compared the light-evoked AMPAR-EPSCs at D1→D2 and D2→D1 synapses; these can be measured directly, without interference from postsynaptic ChR2-mediated depolarization (Figure 2.1 F). We found significantly larger EPSC amplitudes at D2→D1 synapses than at D1→D2 synapses (Figure 2.1 G; $t_{(16)} = -2.543$, $p < 0.05$). Lastly, we confirmed that D1-Cre and D2-Cre mice crossed with reporter lines expressed the same proportions of D1R- and D2R-expressing neurons (Figure 2.3).

Together, these results suggest that DMS glutamatergic synapses containing different pre- and postsynaptic dopamine receptors exhibit distinct connectivity, and that the D2→D1 connectivity is stronger than that of the other tested connections.

Figure 2.1 Striatal glutamatergic synapses with different pre- and postsynaptic dopamine receptor expression exhibit distinct strengths.
A, A sagittal section from a D1-Cre;Ai32 mouse counterstained with NeuroTrace red (NT-Red) showed intense ChR2-EYFP expression in D1-MSNs, and in their projections to the internal segment of the globus pallidus (GPi) and the substantia nigra pars reticulata (SNr). Scale bar: 1 mm. The boxed area is presented at higher magnification in the left-hand panels showing three striatal neurons stained with NT-Red (top); two neurons (arrowheads) expressing EYFP on the cell membrane (middle), and the merged image (yellow; bottom). Scale bar: 4 μm. **B,** A sagittal section from a D2-Cre;Ai32 mouse counterstained with NT-Red showed intense ChR2-EYFP expression in D2-MSNs and in their target, the external segment of the globus pallidus (GPe). Scale bar: 1 mm. The left-hand panels showed two NT-Red-stained striatal neurons (top), one of which expressed EYFP (middle, arrowhead). Scale bar: 4 μm. **C,** Sample traces of Sr^{2+}-induced asynchronous excitatory postsynaptic currents (aEPSCs) at synapses expressing pre- and postsynaptic D1Rs (D1→D1), presynaptic D1Rs and postsynaptic D2Rs (D1→D2), presynaptic D2Rs and postsynaptic D1Rs (D2→D1), and pre- and postsynaptic D2Rs (D2→D2). The EPSCs were evoked by 2-ms 470-nm light in the presence of 2.5 mM Sr^{2+}. **D-E,** Bar graphs summarizing asynchronous EPSC frequency (D) and amplitude (E) after light stimulation of D1→D1, D1→D2, D2→D1, and D2→D2 synapses; ***$p < 0.001$ versus the other three synapses (D), one-way ANOVA, post hoc SNK tests; n = 14 neurons, 4 mice (D1→D1); 12 neurons, 4 mice (D1→D2); 13 neurons, 4 mice (D2→D1); 14 neurons, 4 mice (D2→D2). **F,** Top, schematic of whole-cell recordings of DMS D2-MSNs in D1-Cre;Ai32 mice (left) and of DMS D1-MSNs from D2-Cre;Ai32 mice (right). Presynaptic neurons expressed ChR2 on the cell membrane (represented in green). Bottom, representative traces of light-evoked EPSCs in the absence and presence of DNQX (10 μM) at D1→D2 (left) and D2→D1 (right) synapses. Scale bars: 20 ms, 80 pA. **G,** Bar graphs comparing the amplitudes of AMPAR-EPSCs at D1→D2 and D2→D1 synapses; *$p < 0.05$, unpaired t test; n = 6 neurons, 5 mice (D1→D2); 12 neurons, 6 mice (D2→D1).

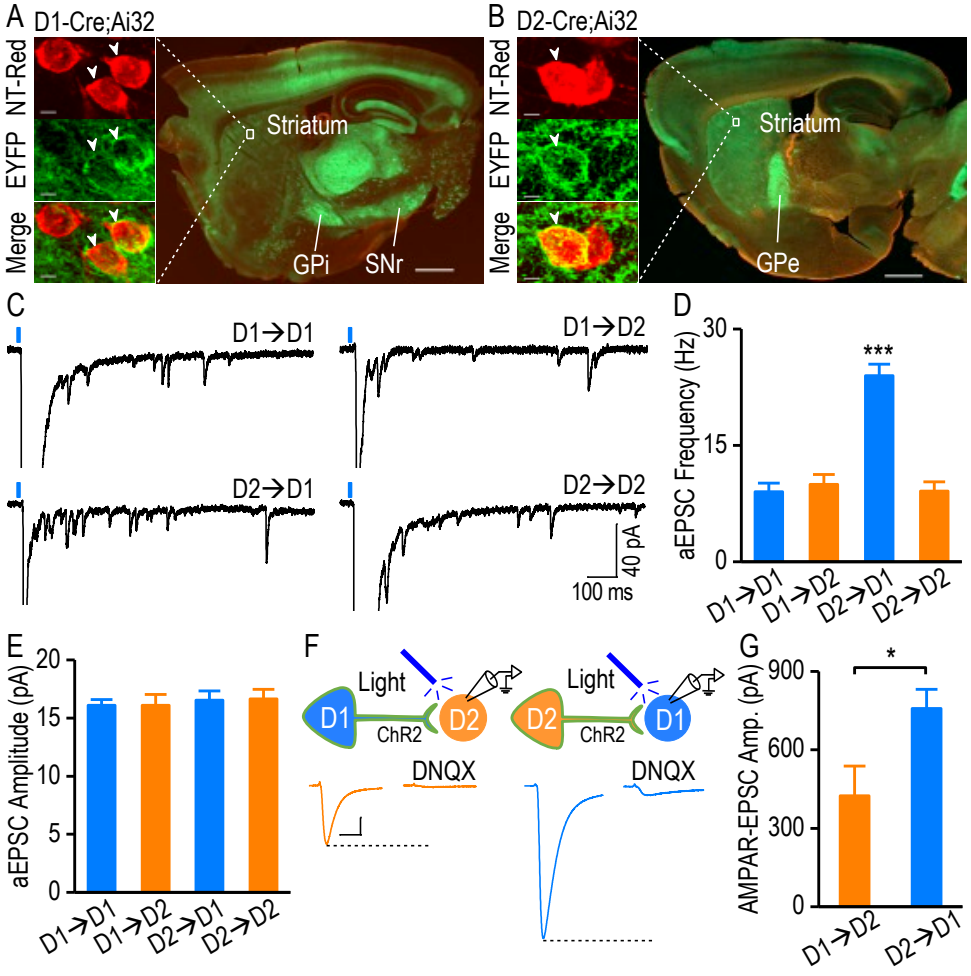
A
D1-Cre;Ai32
NT-Red
EYFP
Merge
Striatum
GPi
SNr
B
D2-Cre;Ai32
NT-Red
EYFP
Merge
Striatum
GPe
C
D1→D1
D1→D2
D2→D1
D2→D2
40 pA
100 ms
D
aEPSC Frequency (Hz)
30
15
0
***
D1→D1
D1→D2
D2→D1
D2→D2
E
aEPSC Amplitude (pA)
20
15
10
5
0
D1→D1
D1→D2
D2→D1
D2→D2
F
Light
D1
ChR2
D2
DNQX
Light
D2
ChR2
D1
DNQX
G
AMPAR-EPSC Amp. (pA)
900
600
300
0
*
D1→D2
D2→D1

Figure 2.2 Identification of MSNs and validation of DMS glutamatergic synapses. **A,** Left, an illustration showed the whole-cell recording at D1→D1 (i) and D1→D2 (ii) synapses in DMS slices from D1-Cre;Ai32 mice. Presynaptic D1R-expressing neurons and postsynaptic D1-MSNs, but not postsynaptic D2-MSNs, expressed ChR2. Right, representative traces indicated the membrane depolarization recorded in putative DMS D1-MSNs (i) and D2-MSNs (ii) in response to 2-ms (black) or 500-ms (red) light stimulation. Scale bars: 100 ms, 30 pA (A); 100 ms, 200 pA (B). Extended light stimulation caused significantly different responses in ChR2-expressing D1-MSNs and ChR2-negative D2-MSNs. **B-C,** Quantification of the half-width of 2-ms and 500-ms light-evoked responses in D1- and D2-MSNs from D1-Cre;Ai32 mice (B; n = 14 neurons, 6 mice [D1→D1]; 15 neurons, 6 mice [D1→D2]) and from D2-Cre;Ai32 mice (C; n = 14 neurons, 5 mice [D2→D1]; 13 neurons, 4 mice [D2→D2]). Note that a prolonged 500-ms light stimulation caused sustained ChR2-mediated direct depolarization at D1→D1 and D2→D2 connections, but not at D1→D2 or D2→D1 synapses. ###$p < 0.001$, two-way RM ANOVA; ***$p < 0.001$, n.s. (not significant), $p > 0.05$, post hoc SNK test. **D-E,** Time course of light-evoked responses before and during bath application of DNQX in putative D1- and D2-MSNs from D1-Cre;Ai32 mice and D2-Cre;Ai32 mice. DNQX (10 μM) completely abolished light-evoked responses in D2-MSNs of D1-Cre;Ai32 mice (D; DNQX: 6.18 ± 1.29% of baseline, $t_{(5)} = 72.82$, $p < 0.001$) or in D1-MSNs of D2-Cre;Ai32 mice (E; DNQX: 7.73 ± 0.73% of baseline, $t_{(11)} = 126.51$, $p < 0.001$), indicating exclusive glutamatergic transmission at the D1→D2 and D2→D1 synapse. In contrast, DNQX caused a partial, but significant reduction of the light-evoked response in D1-MSNs of D1Cre;Ai32 mice (D; DNQX: 82.08 ± 2.73% of baseline, $t_{(10)} = 6.57$, $p < 0.001$) or in D2-MSNs of D2Cre;Ai32 mice (E; DNQX: 87.61 ± 2.39% of baseline, $t_{(9)} = 5.18$, $p < 0.001$). These results suggested that light stimulation triggered synaptic transmission, which was blocked by DNQX, and direct ChR2-mediated depolarization at the D1→D1 and D2→D2 synapse. n = 11 slices, 6 mice (D; D1→D1); 6 slices, 5 mice (D; D1→D2), 12 slices, 6 mice (E; D2→D1), and 10 slices, 8 mice (E; D2→D2). **F,** Left, sample traces of light-evoked responses in the absence and presence of DNQX at D1→D1 (top) and D2→D2 (bottom) synapses. Scale bars: 20 ms, 150 pA (top); 20 ms, 200 pA (bottom). Right, bar graphs compared the amplitudes of the light-evoked D1→D1 and D2→D2 responses in the absence and presence of DNQX, as well as the change induced by DNQX. n.s., not significant, $p > 0.05$, two-way RM ANOVA followed by post hoc SNK test. n = 12 neurons, 6 mice (D1→D1); 10 neurons, 8 mice (D2→D2).

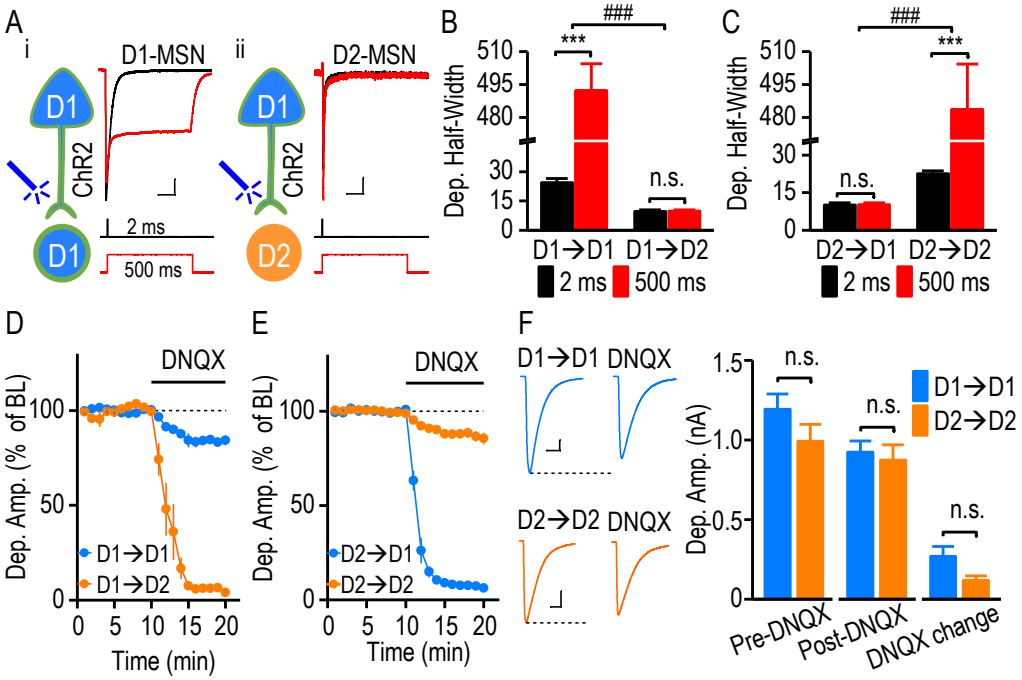
A
i
D1-MSN
D1
ChR2
D1
2 ms
500 ms
ii
D2-MSN
D1
ChR2
D2
B
Dep. Half-Width
510
495
480
30
15
0
###
***
n.s.
D1→D1 D1→D2
2 ms 500 ms
C
Dep. Half-Width
510
495
480
30
15
0
###
***
n.s.
D2→D1 D2→D2
2 ms 500 ms
D
DNQX
Dep. Amp. (% of BL)
100
50
0
D1→D1
D1→D2
0 5 10 15 20
Time (min)
E
DNQX
Dep. Amp. (% of BL)
100
50
0
D2→D1
D2→D2
0 5 10 15 20
Time (min)
F
D1→D1 DNQX
D2→D2 DNQX
Dep. Amp. (nA)
1.5
1.0
0.5
0
n.s.
n.s.
n.s.
D1→D1
D2→D2
Pre-DNQX
Post-DNQX
DNQX change

Figure 2.3 Identical representation of dopamine receptor expression in D1-Cre and D2-Cre mice.

To compare the reliability of Cre representation of D1R-expressing neurons in D1-Cre mice and of D2R-expressing neurons in D2-Cre mice, we crossed these mice with a tdTomato Cre reporter line, Ai14. **A-B,** Representative fluorescent image (A) and summarized data (B) for histological comparison. We infused AAV-CAG-Flex-GFP into the mPFC of D1-Cre;Ai14 (A; left) and D2-Cre;Ai14 mice (A; middle and right), and prepared coronal sections 10 days after the infusion. A high magnification image of the viral infusion site of a D2-Cre;Ai14 mouse showed co- expression of GFP and tdTomato (A; right). Note that the D1R (D1-Cre mice) or D2R (D2-Cre mice) promotor drove Cre expression to turn on the viral-mediated GFP expression and Ai14-drived tdTomato expression. Thus, GFP represented neurons that currently expressed D1Rs or D2Rs, whereas tdTomato indicated neurons that historically (e.g., during development) and currently expressed these receptors. Summarized data (B) showed that the percentage of mPFC neurons co-expressing GFP and tdTomato (yellow) in cells that express tdTomato (red) did not differ between D1-Cre and D2-Cre mice. Scale bar: 500 μm (left and middle); 15 μm (right). n.s., $p > 0.05$, unpaired t test; n = 9 sections, 3 mice per group. **C-H,** Pharmacological comparison of Cre line efficiency. Red tdTomato-expressing ($tdTomato^+$) neurons in the mPFC of D1-Cre;Ai14 or D2-Cre;Ai14 mice were recorded in the current-clamp mode in the presence of DNQX (10 μM), APV (50 μM), and picrotoxin (100 μM) to block both excitatory and inhibitory synaptic transmission. A 500-ms current step was injected every minute to evoke firing in the absence and presence of a D1R or D2R agonist. Baseline and post-agonist firing frequencies were averaged from 1 to 5 min and from 11 to 15 min, respectively. Those neurons with ≥ 20% change in their post-agonist firing were operationally considered as D1R/D2R-expressing ($D1R^+$/ $D2R^+$) neurons, and the remaining neurons were considered as D1R/D2R-negative ($D1R^-$/$D2R^-$) cells. Panel C showed representative DIC (grey) and fluorescent (red) images of $tdTomato^+$ pyramidal cells in the mPFC slice. Scale bar, 20 μm. Panel D showed sample traces of membrane potentials in the red $D1R^+$ (top) and $D1R^-$ (bottom) cells in response to a step current injection before (left, baseline) and during (right) bath application of a D1R agonist, SKF 38393 (20 μM) in the D1-Cre;Ai14 mice. Panel E showed the time course of averaged responses in evoked firing frequency before and during SKF38393 application in the red $D1R^+$ (blue) and $D1R^-$ (black) cells of D1-Cre;Ai14 mice. In 16 neurons from 4 D1-Cre;Ai14 mice, 12 of them were responsive to D1R agonist application. Sample traces (F) showed evoked firing of red $D2R^+$ (top) and $D2R^-$ (bottom) neurons before and during bath application of quinpirole (20 μM) in D2-Cre;Ai14 mice. Time course of averaged responses in evoked firing frequency before and during quinpirole application in the red $D2R^+$ (orange) and $D2R^-$ (black) cells of D2-Cre;Ai14 mice (G). In 16 neurons from 4 D2-Cre;Ai14 mice, 13 of them were responsive to D2R agonist application. Bar graph (H) summarized the percentage of $tdTomato^+$ neurons responded to the D1R/D2R agonist between D1-Cre;Ai14 and D2-Cre;Ai14 mice. D1-Cre and D2-Cre mice have identical reliability to represent the D1R-expressing neurons and D2R-expressing neurons; n.s., $p > 0.05$; n = 16 neurons, 4 mice per group.

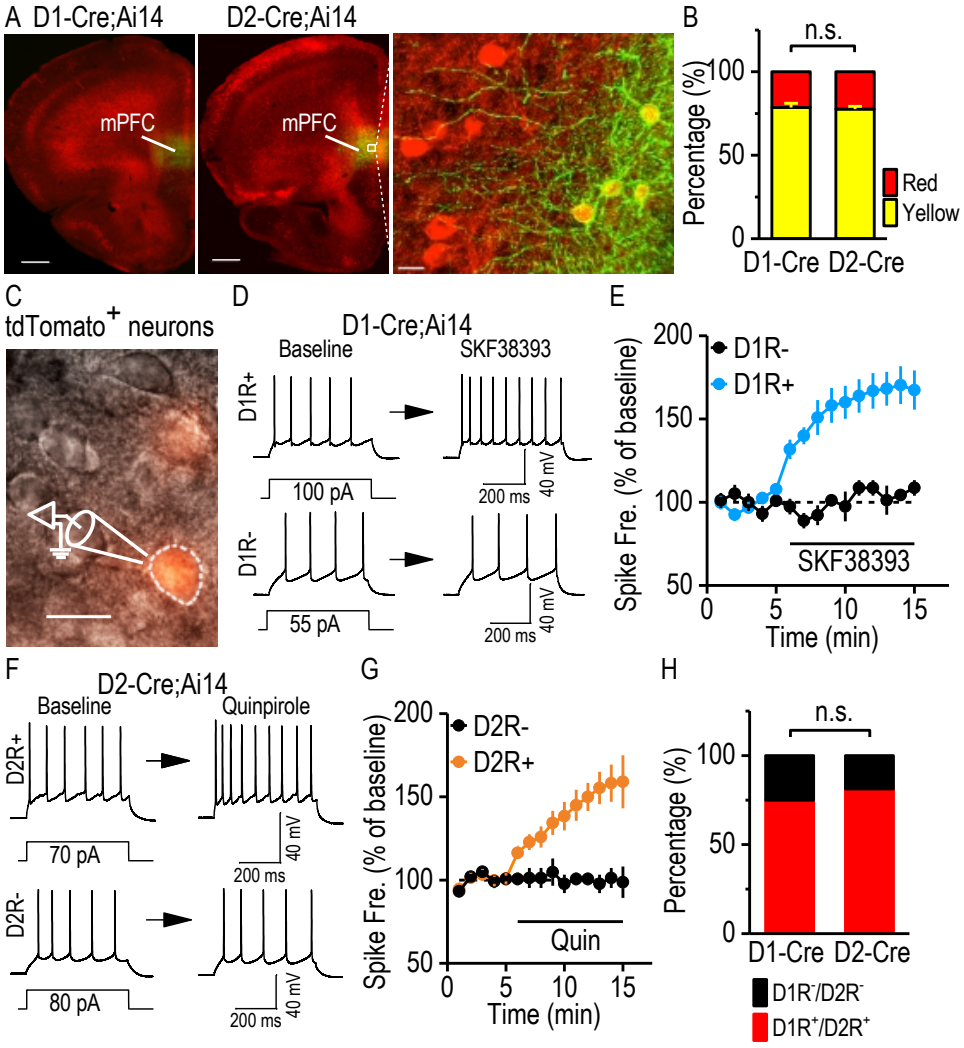
A D1-Cre;Ai14
D2-Cre;Ai14
mPFC
mPFC
B
n.s.
Percentage (%)
100
50
0
Red
Yellow
D1-Cre D2-Cre
C
tdTomato+ neurons
D
D1-Cre;Ai14
Baseline
SKF38393
D1R+
100 pA
200 ms
40 mV
D1R-
55 pA
200 ms
40 mV
E
Spike Fre. (% of baseline)
200
150
100
50
D1R-
D1R+
SKF38393
0
5
10
15
Time (min)
F
D2-Cre;Ai14
Baseline
Quinpirole
D2R+
70 pA
200 ms
40 mV
D2R-
80 pA
200 ms
40 mV
G
Spike Fre. (% of baseline)
200
150
100
50
D2R-
D2R+
Quin
0
5
10
15
Time (min)
H
n.s.
Percentage (%)
100
50
0
D1-Cre D2-Cre
D1R-/D2R-
D1R+/D2R+

2.3.2. DMS-projecting extra-striatal neurons preferentially express D2Rs

We next explored the potential mechanism underlying the relatively greater strength of the DMS D2→D1 synapse. Previous anatomical studies indicated that cortical fibers in the dorsal striatum contain abundant D2Rs, and fewer D1Rs (Wang and Pickel, 2002; Dumartin et al., 2007). It was therefore possible that there were more D2R-expressing fibers, as compared with those expressing the D1R. To test this, we employed D1-Cre;Snap25 and D2-Cre;Snap25 mice where D1R- and D2R-expressing neurons expressed green fluorescent protein (GFP), respectively (Figure 2.4 A). A retrograde virus encoding tdTomato (AAVretro-CAG-tdTomato) was infused into the DMS in order to label DMS-projecting neurons (Figure 2.4 A). Co-expression of tdTomato and GFP was visualized as a yellow signal (Figure 2.4 A-D).

We observed that more of the mPFC projections to the DMS expressed the D2R, as compared with the D1R (Figure 2.4 B). We counted yellow neurons in other extra-striatal areas of both hemispheres throughout the entire brain. To compensate for infusion and expression variations, we normalized the number of yellow neurons to the number of red neurons in the mPFC. This analysis of brain-wide inputs to the DMS found that significantly more DMS-projecting neurons expressed the D2R, as compared with the total number of neurons that expressed the D1R (Figure 2.4 E; $t_{(4)} = -3.03$, $p < 0.05$). Additionally, many individual brain sections contained significantly more D2R-expressing neurons than D1R-expressing cells (Figure 2.4 F; $F_{(1,130)} = 8.92$, $p < 0.05$). Interestingly, we discovered that the posterior brain regions tended to have more D2R- than D1R-expressing DMS-projecting neurons (Figure 2.4 G; $t_{(4)} = -4.03$, $p < 0.05$),

while the anterior regions showed no significant differences between the D1R-expressing and D2R-expressing cells (Figure 2.4 G; $t_{(4)} = -2.04$, $p > 0.05$). These data suggest that extra-striatal D2R-expressing inputs to the DMS are more prevalent than D1R-expressing inputs, and that presynaptic D2Rs may therefore play a stronger regulatory role than D1Rs.

Figure 2.4 DMS-projecting extra-striatal neurons preferentially express dopamine D2Rs versus D1Rs.

A, Illustration of the strategy used to target D1R-expressing ($D1R^+$) DMS-projecting extra-striatal neurons. We employed D1-Cre;Snap25 transgenic mice, where D1R-expressing neurons were labeled by GFP (green). The AAVretro-CAG-tdTomato was infused into the DMS of these mice, which labeled DMS-projecting neurons with a red fluorescent protein, tdTomato. Note that neurons co-expressing tdTomato and GFP were D1R-expressing DMS-projecting neurons (yellow). **B-D,** Representative fluorescent images of D1R-expressing inputs (top) and D2R-expressing inputs (bottom) to the DMS from the cortex (B and C) and amygdala (D) following viral infusions in the DMS of D1-Cre;Snap25 and D2-Cre;Snap25 mice as indicated. Boxes (B, right-hand panels) indicated the zone shown in the left-hand panels (B) at a higher magnification. Note that the number of yellow neurons was higher in D2-Cre;Snap25 mice than in D1Cre;Snap25 mice, although the numbers of red neurons were identical. Coronal sections were prepared 10 days after the viral infusion. Scale bar: 30 μm (B, left); 500 μm (B, right); 700 μm (C); 800 μm (D). **E,** Bar graphs indicated that the total number of extra-striatal D2R-expressing neurons (D2-neuron) that projected to the DMS was significantly higher than that of extra-striatal D1R-expressing DMS-projecting neurons (D1-neuron). The total number of D1-neurons or D2-neurons was normalized to the red neurons in the mPFC; $*p < 0.05$, unpaired t test, n = 3 mice per group. **F,** Analysis of the distribution of D1-neurons and D2-neurons from the anterior to posterior (starting at 3.2 mm relative to Bregma and continuing in 200-μm steps) identified a significant difference between these neuronal types; $\#p < 0.05$, two-way RM ANOVA, n = 102 sections, 3 mice per group. **G,** Bar graphs comparing the number of D1-neurons and D2-neurons in the anterior (starting at 3.2 mm and ending at -0.2 mm relative to Bregma, where the anterior commercial crossed) and posterior (starting at -0.2 mm and ending at -3.6 mm relative to Bregma) regions; $*p < 0.05$ (posterior), $p > 0.05$ (anterior), unpaired t test; n = 3 mice per group.

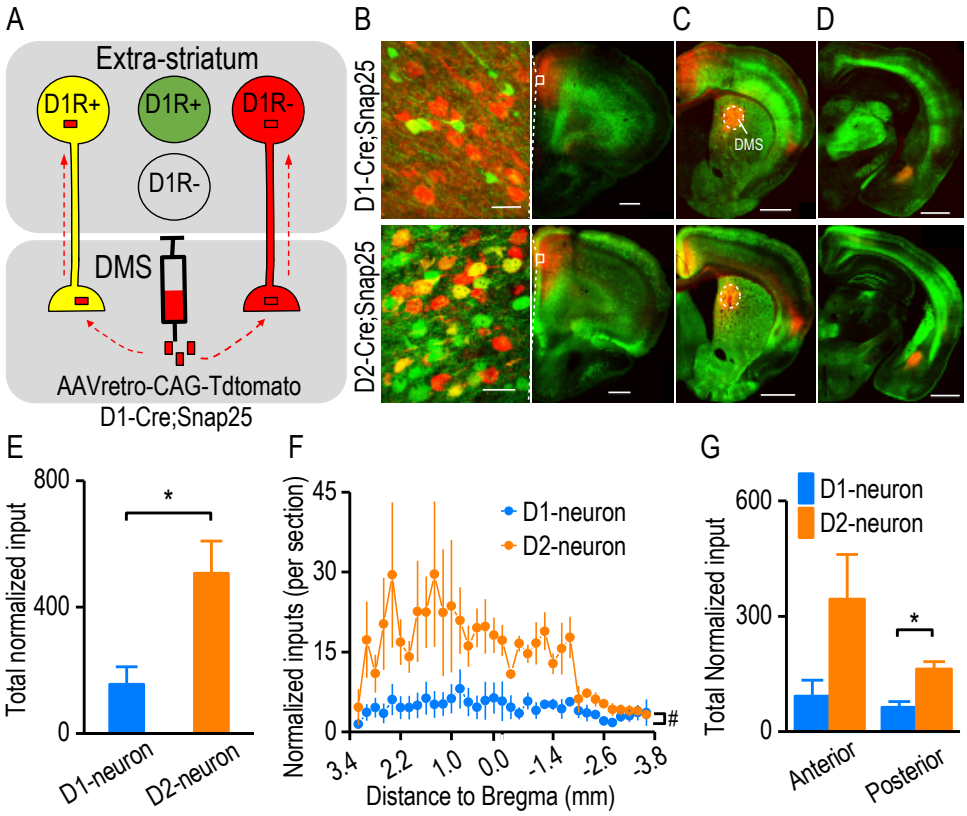
A
B
C
D
Extra-striatum
D1R+
D1R+
D1R-
D1R-
DMS
AAVretro-CAG-Tdtomato
D1-Cre;Snap25
D1-Cre;Snap25
D2-Cre;Snap25
DMS
E
F
G
Total normalized input
800
400
0
*
D1-neuron
D2-neuron
Normalized inputs (per section)
45
30
15
0
D1-neuron
D2-neuron
#
3.4
2.2
1.0
0.0
-1.4
-2.6
-3.8
Distance to Bregma (mm)
Total Normalized input
600
300
0
D1-neuron
D2-neuron
*
Anterior
Posterior

2.3.3. Suppression of glutamatergic transmission at distinct DMS synapses via pre- and postsynaptic D2Rs

D2R-mediated inhibition plays a critical role in modulating corticostriatal glutamatergic transmission. Although the mechanisms underlying this effect have not been fully elucidated, they may involve the activation of presynaptic D2Rs on the glutamatergic terminal (Bamford et al., 2004) and retrograde endocannabinoid (eCB) signaling via striatal postsynaptic D2Rs (Yin and Lovinger, 2006). To investigate the effect of presynaptic D2Rs on cortical inputs, we took advantage of the absence of postsynaptic D2R expression at D2→D1 synapses (Figure 2.5 A). We used paired-pulsed optical stimulation delivered at a frequency of 20 Hz (Bamford et al., 2004; Yin and Lovinger, 2006) to activate D2R-expressing afferents, and recorded light-evoked responses in DMS D1-MSNs of D2-Cre;Ai32 mice before and during the bath application of a D2R agonist, quinpirole (20 μM). We observed a significant inhibition of the first EPSC by quinpirole (Figure 2.5 B; 79.56 ± 3.78% of baseline; $t_{(8)} = 5.41$, $p < 0.001$). Moreover, this inhibition was accompanied by a significant increase in the paired-pulse ratio (PPR) (Figure 2.5 C; baseline, 0.27 ± 0.03; quinpirole, 0.39 ± 0.04; $t_{(8)} = -6.46$, $p < 0.001$), suggesting that quinpirole inhibited EPSCs by decreasing presynaptic glutamate release (Zucker and Regehr, 2002). We next tested whether the quinpirole-mediated inhibition required eCB signaling by treating DMS slices with AM251, a cannabinoid type 1 receptor (CB1R) antagonist. With 3 μM AM251 in the bath, quinpirole still inhibited EPSCs (Figure 2.5 D; EPSC 1 = 76.43 ± 5.91% of baseline; $t_{(6)} = 3.99$, $p < 0.01$). AM251 also failed to prevent the quinpirole-induced

increase in the PPR (Figure 2.5 E; baseline, 0.29 ± 0.03; quinpirole, 0.43 ± 0.04; $t_{(6)}$ = -8.75, $p < 0.001$). These results indicate that presynaptic D2R signaling suppresses glutamatergic transmission in an eCB-independent manner.

To determine the role of postsynaptic D2Rs on cortical inputs, we took advantage of the lack of presynaptic D2R expression at the D1→D2 synapse (Figure 2.5 F). We recorded D2-MSNs of D1-Cre;Ai32 mice, performed the same experiment as in Figure 2.5 A-E, and observed a similar inhibitory effect of quinpirole. The first EPSC amplitude was significantly reduced after quinpirole application (Figure 2.5 G; 72.18 ± 2.38% of baseline; $t_{(8)}$ = 11.67, $p < 0.001$), and PPR was significantly increased (Figure 2.5 H; baseline, 0.26 ± 0.04; quinpirole, 0.34 ± 0.05; $t_{(8)}$ = -4.73, $p < 0.01$). We next tested whether postsynaptic D2R-mediated inhibition required retrograde eCB signaling. In the presence of AM251, quinpirole failed to inhibit D1→D2 EPSCs (Figure 2.5 I; 99.7 ± 4.43% of baseline; $t_{(8)}$ = 0.07, $p > 0.05$) or to change PPR (Figure 2.5 J; baseline, 0.27 ± 0.05; quinpirole, 0.28 ± 0.05; $t_{(8)}$ = -1.64, $p > 0.05$), indicating that CB1R activation is necessary for postsynaptic D2R-mediated synaptic depression. Taken together, these results suggest that D2R-mediated inhibition of glutamatergic transmission in the DMS involves distinct pre- and postsynaptic mechanisms, and that postsynaptic D2R-mediated inhibition requires eCB signaling.

Figure 2.5 Suppression of glutamatergic transmission at different DMS synapses via pre- and postsynaptic D2Rs.
A, Illustration indicating whole-cell recordings of D2→D1 transmission in D2-Cre;Ai32 mice. D2Rs were selectively expressed at presynaptic terminals, but not in postsynaptic D1-MSNs. **B,** Activation of presynaptic D2Rs by bath application of quinpirole (Quin, 20 μM) suppressed the first of two EPSCs induced by paired-pulse (50-ms interval) stimulation of D2R-expressing inputs; *$p < 0.05$, paired t test; n=9 slices, 7 mice. The inset sample traces indicated the light-evoked paired-pulse EPSCs in the absence (1) and presence (2) of quinpirole. Scale bars: 20 ms, 100 pA. **C,** Time-course of the PPR (the second EPSC amplitude divided by the first EPSC amplitude) before and during quinpirole application; *$p < 0.05$, paired t test; n = 9 slices, 7 mice. **D,** Bath application of AM251 did not affect the quinpirole-induced suppression of the first EPSC; *$p < 0.05$, paired t test; n = 7 slices, 6 mice. **E,** Quinpirole-induced increases in the PPR were also observed in the presence of AM251; *$p < 0.05$, paired t test; n = 7 slices, 6 mice. **F,** Illustration showing whole-cell recordings of D1→D2 transmission in D1-Cre;Ai32 mice. D2Rs were selectively expressed in postsynaptic D2-MSNs, but not at presynaptic terminals. **G,** Activation of postsynaptic D2Rs by quinpirole suppressed the first of two EPSCs; *$p < 0.05$, paired t test; n = 9 slices, 4 mice. The inset sample traces indicate the two light-evoked EPSCs in the absence (1) and presence (2) of quinpirole. Scale bars: 20 ms, 50 pA. **H,** Time-course of the PPR before and during quinpirole application; *$p < 0.05$, paired t test; n = 9 slices, 4 mice. **I,** AM251 bath application abolished quinpirole-induced synaptic suppression; $p > 0.05$, paired t test; n = 9 slices, 5 mice. **J,** AM251 abolished quinpirole-induced increases in the PPR; $p > 0.05$, paired t test; n = 9 slices, 5 mice.

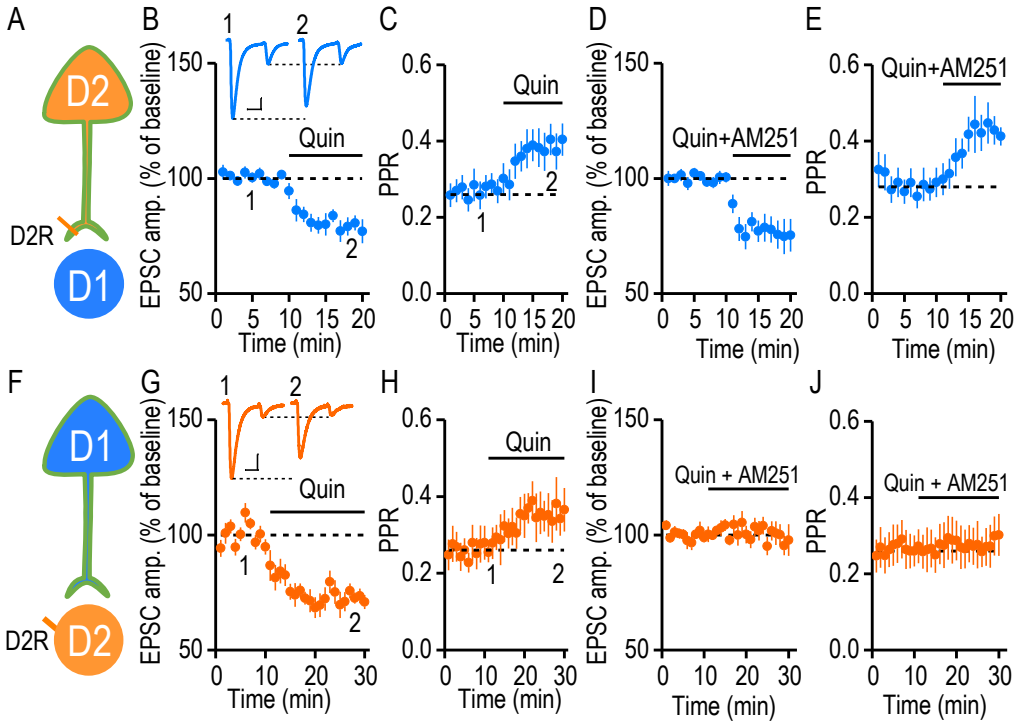
A
D2
D2R
D1
B
EPSC amp. (% of baseline)
150
100
50
1
2
Quin
0 5 10 15 20
Time (min)
C
PPR
0.6
0.4
0.2
0.0
Quin
0 5 10 15 20
Time (min)
D
EPSC amp. (% of baseline)
Quin+AM251
0 5 10 15 20
Time (min)
E
PPR
Quin+AM251
0 5 10 15 20
Time (min)
F
D1
D2R
D2
G
EPSC amp. (% of baseline)
Quin
0 10 20 30
Time (min)
H
PPR
Quin
0 10 20 30
Time (min)
I
EPSC amp. (% of baseline)
Quin + AM251
0 10 20 30
Time (min)
J
PPR
Quin + AM251
0 10 20 30
Time (min)

2.3.4. Excessive alcohol consumption causes a long-lasting potentiation of glutamatergic transmission at the DMS D2→D1 synapse

Altered dopaminergic transmission is the common mechanism underlying drug and alcohol abuse. To investigate how excessive alcohol intake alters D2→D1 and D1→D2 synaptic transmission, D2-Cre;Ai32 and D1-Cre;Ai32 mice were trained to consume 20% alcohol for 8 weeks using the intermittent-access two-bottle choice drinking procedure (Wang et al., 2015; Cheng et al., 2017; Cheng et al., 2018; Wei et al., 2018). As shown in Table 2.1, these mice consumed high levels of alcohol, and the drinking levels were identical between the two mouse lines (Table 2.1; $q = 0.58$, $p > 0.05$). The water control mice underwent the same treatment, but without alcohol exposure. Twenty-four hours after the last alcohol exposure, we prepared DMS slices and measured light-evoked AMPAR-mediated EPSCs in MSNs. We found that the amplitude of D2→D1 EPSCs was significantly higher in the alcohol-drinking group than in the water controls (Figure 2.6 A; $F_{(1,84)} = 10.01$, $p < 0.01$). Additionally, excessive alcohol intake produced a long-lasting (9 days) increase in AMPAR-EPSCs (Figure 2.6 A; $F_{(1,100)} = 7.93$, $p < 0.01$). In contrast, the amplitude of D1→D2 EPSCs was identical in both alcohol and water groups (Figure 2.6 B; $F_{(1,116)} = 0.57$, $p > 0.05$). Interestingly, we also discovered that excessive alcohol intake caused a long-lasting decrease in PPR at the D2→D1 synapse (Figure 2.6 C; 24-h withdrawal, $t_{(21)} = 2.432$, $p < 0.05$; 9-d withdrawal, $t_{(26)} = 2.648$, $p < 0.05$); this effect was not observed at the D1→D2 connection (Figure 2.6 D; $t_{(22)} = - 0.318$, $p > 0.05$). Since the PPR is inversely correlated with transmitter release probability (Zucker and Regehr, 2002), this reduction in PPR

indicated that the alcohol-induced enhancement of D2→D1 connectivity was mediated, at least in part, by an increased glutamate release. Collectively, these data demonstrate that excessive alcohol consumption persistently enhances glutamatergic transmission at the D2→D1 synapse of the DMS.

In the striatum, D2Rs are also expressed in cholinergic interneurons (CINs) and dopaminergic fibers (Kreitzer and Malenka, 2008; Oldenburg and Ding, 2011), leading to ChR2 expression by these cells in D2-Cre;Ai32 mice. Glutamate (Higley et al., 2011), acetylcholine, and dopamine might be released during light stimulation. However, we found that glutamatergic transmission from CINs to MSNs represented a small proportion of the overall D2→D1 transmission (Figure 2.7 A-C), suggesting that most D2→D1 synapses involved extra-striatal neurons. The light-evoked release of acetylcholine and dopamine was unlikely to influence the observed glutamatergic D2→D1 transmission (Figure 2.7 D-E).

Figure 2.6 Excessive alcohol consumption causes a long-lasting potentiation of glutamatergic D2→D1 transmission.

A, Excessive alcohol intake persistently increased the amplitude of AMPAR-mediated EPSCs at the D2→D1 connection. Whole-cell recordings were performed 24 h or 9 d after the last alcohol exposure. Left, illustration indicating that optical stimulation of ChR2-expressing D2R-expressing inputs in D2-Cre;Ai32 mice activated D2→D1 glutamatergic transmission. Middle, the representative traces of AMPAR-EPSCs evoked by a range of optical stimulation intensities in slices from alcohol-drinking mice (EtOH) and water controls. Scale bar: 10 ms, 100 pA. Right, input-output curves of optical AMPAR-EPSCs at the D2→D1 synapse from mice exposed to alcohol with 24 h withdrawal (EtOH_24 h W/D), alcohol with 9 d withdrawal (EtOH_9 d W/D), or water only; #$p < 0.01$, two-way RM ANOVA; *$p < 0.05$; **$p < 0.01$; ***$p < 0.001$ EtOH_24 h W/D versus water group at the same stimulation intensities; post hoc SNK test; n = 12 neurons, 6 mice (Water); 11 neurons, 5 mice (EtOH_24 h W/D); and 15 neurons, 5 mice (EtOH_9 d W/D). **B,** Excessive alcohol intake did not alter the amplitude of D1→D2 AMPAR-EPSCs. Left, illustration indicating that light stimulation of ChR2 expressed at presynaptic terminals of extra-striatal D1R-expressing neurons in D1-Cre;Ai32 mice triggered D1→D2 glutamatergic transmission. Middle, sample traces of AMPAR-EPSCs evoked by the indicated optical stimulation intensities in slices from alcohol- drinking mice and water controls. Scale bar: 10 ms, 80 pA. Right, the input-output curves of D1→D2 AMPAR-EPSCs from the indicated study groups; $p > 0.05$, versus same intensities in the water group, two-way RM ANOVA; n = 15 neurons, 7 mice (Water); 16 neurons, 7 mice (EtOH). **C,** Excessive alcohol intake increased the glutamate release probability at D2→D1 synapses. PPRs were calculated by comparing paired AMPAR-EPSCs induced by two optical stimuli, delivered at a 100-ms interval. Bar graph summarizing PPRs in the indicated groups; *$p < 0.05$, unpaired t test; n = 12 neurons, 4 mice (Water); 11 neurons, 6 mice (EtOH_24 h withdrawal); 16 neurons, 5 mice (EtOH_9 d withdrawal). The inset shows paired AMPAR responses in the water and alcohol groups. Scale bar: 20 ms, 50 pA. **D,** Excessive alcohol intake did not change the glutamate release probability at D1→D2 synapses. Bar graph comparing the corresponding mean PPRs in the indicated groups; $p > 0.05$, unpaired t test; n = 12 neurons, 5 mice per group. The inset shows paired AMPAR responses in the water and alcohol groups. Scale bar: 20 ms, 50 pA.

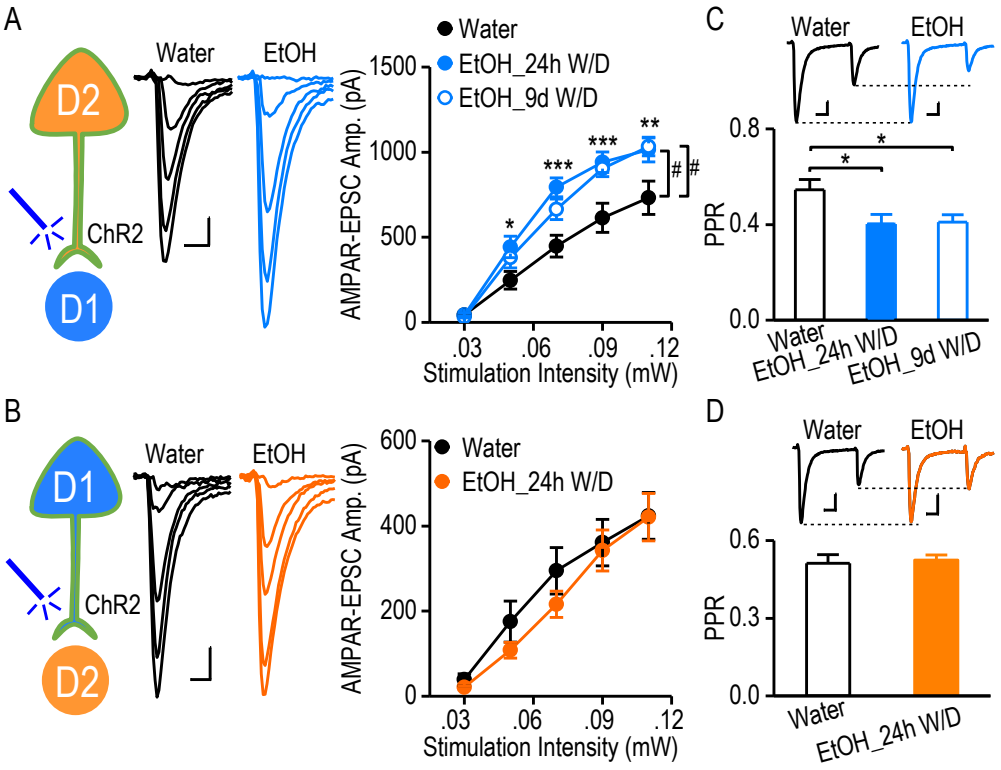
A
D2
D1
ChR2
Water
EtOH
Water
EtOH_24h W/D
EtOH_9d W/D
AMPAR-EPSC Amp. (pA)
1500
1000
500
0
.03
.06
.09
.12
Stimulation Intensity (mW)
*
***
***
**
#
#
C
Water
EtOH
0.8
0.4
0.0
PPR
*
*
Water
EtOH_24h W/D
EtOH_9d W/D
B
D1
D2
ChR2
Water
EtOH
Water
EtOH_24h W/D
AMPAR-EPSC Amp. (pA)
600
400
200
0
.03
.06
.09
.12
Stimulation Intensity (mW)
D
Water
EtOH
0.6
0.3
0.0
PPR
Water
EtOH_24h W/D

Figure 2.7 The effect of DMS D2R-expressing cholinergic interneurons and dopaminergic terminals on glutamatergic transmission at the D2-D1 synapse during light stimulation.

A, Schematic illustration showed light stimulation and recording arrangement in ChatCre;Ai32 mice. **B,** Left, sample traces of light-evoked CIN-mediated responses in MSNs in the absence (1) and presence (2) of glutamatergic transmission antagonists, DNQX (10 μM) and APV (50 μM). Scale bars: 40 ms, 5 pA. Right, the time course of light-evoked responses during bath application of DNQX and APV; $p < 0.05$, paired t test; n = 6 slices, 3 mice. **C,** Bar graph showed a significantly smaller glutamatergic transmission from CINs to MSNs than overall D2R-expressing neurons to D1-MSNs in the DMS; ***$p < 0.001$, unpaired t test; n = 8 neurons, 3 mice (CIN→MSN); 12 neurons, 6 mice (D2→D1). Grey bar graph indicated the data from Figure 2.1 G as reference. Note that light stimulation intensity was 20-fold stronger in recordings of CIN→MSN than that in D2→D1. **D-E,** No detectable impact of acetylcholine receptors and dopaminergic fibers on glutamatergic transmission at the D2→D1 connection during optical stimulation in the D2-Cre;Ai32 mice. The input-output relationship for AMPAR-EPSCs and PPR were measured in the absence and presence of a cocktail of antagonists of the D1R (SCH 23390, 10 μM), the D2R (sulpiride, 20 μM), the muscarinic acetylcholine receptor (scopolamine, 10 μM), and the nicotinic acetylcholine receptor (mecamylamine,10 μM; methyllycaconitine citrate, 50 nM). The antagonist cocktail did not significantly affect the input-output relationship for D2→D1 AMPAR-EPSCs (D; $F_{(1,84)} = 0.08$, $p > 0.05$; versus the same intensity in the group without antagonists, two-way RM ANOVA; n = 12 neurons, 6 mice [antagonists -]; 11 neurons, 4 mice [antagonists +]) or the PPRs (E; $t_{(22)} = 0.50$, $p > 0.05$, unpaired t test; n = 12 neurons, 4 mice per group). Grey line (D) and bar graph (E) indicated the data from water group in Figure 2.4 A and Figure 2.4 C as reference. PPR were evoked by two optical stimulations at a 100-ms interval.

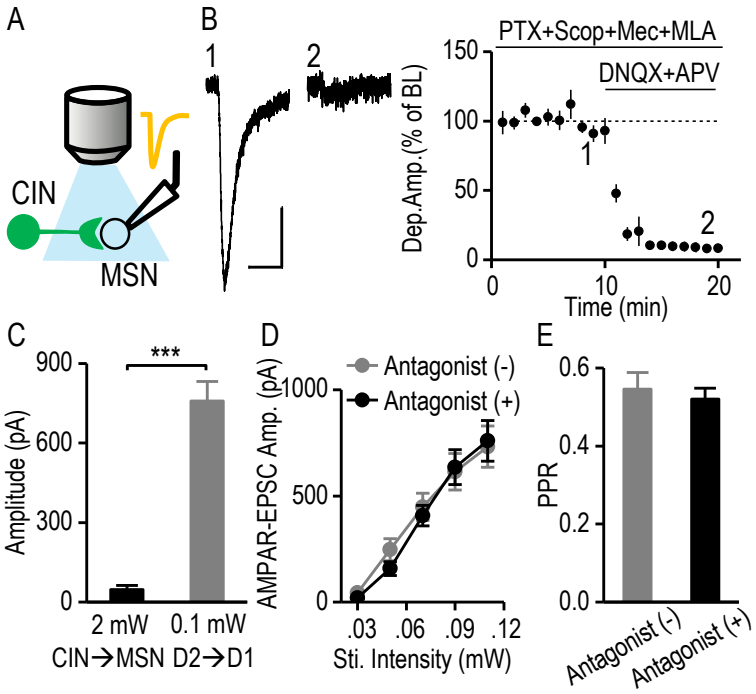
A
B
1
2
CIN
MSN
PTX+Scop+Mec+MLA
DNQX+APV
Dep.Amp.(% of BL)
150
100
50
0
0
10
20
Time (min)
C
D
E
***
900
600
300
0
Amplitude (pA)
2 mW
0.1 mW
CIN→MSN D2→D1
AMPAR-EPSC Amp. (pA)
1000
500
0
Antagonist (-)
Antagonist (+)
.03
.06
.09
.12
Sti. Intensity (mW)
PPR
0.6
0.4
0.2
0.0
Antagonist (-)
Antagonist (+)

2.3.5. The strong mPFC D2R-expressing input onto DMS D1-MSNs is potentiated by excessive alcohol consumption

The data shown in Figure 2.1 indicated that glutamatergic transmission from brain-wide D2R-expressing afferents onto D1-MSNs was stronger than that observed at the other tested connections. However, we also wished to investigate the strength of D2R-expressing afferents from the mPFC onto this neuronal type. Additionally, we recently found that excessive alcohol consumption increased AMPAR activity at the mPFC input to the DMS (Ma et al., 2017). To access the D2R-expressing mPFC input, a Cre-dependent Chronos-expressing AAV (Klapoetke et al., 2014) was infused into the mPFC of D2-Cre;Ai14 mice (Figure 2.8 A), which express Cre and tdTomato in D2-MSNs and in mPFC D2R-expressing neurons (Cheng et al., 2017; Wei et al., 2018). The expression of Chronos was indicated by the presence of GFP, which was restricted selectively to D2R-expressing (red) mPFC neurons (Figure 2.8 B). Infusion of AAV-Flex-Chronos-GFP caused intense green fluorescent labeling of mPFC D2R-expressing afferents in the DMS (Figure 2.8 C). DMS D2-MSNs were identified by the red fluorescence of tdTomato (Figure 2.8 C) and any non-fluorescent striatal MSNs were therefore considered as putative D1-MSNs. Whole-cell recordings were performed from these two types of MSN. Similar to the D2→D1 connection in D2-Cre;Ai32 mice, bath application of DNQX (10 μM) and an NMDAR antagonist (APV, 50 μM) completely abolished light-evoked activity at the mPFC D2R-expressing inputs onto both DMS D1-MSNs (Figure 2.8 D) and D2-MSNs (Figure 2.8 E), suggesting that they were glutamatergic. To compare the glutamatergic strength of D2→D1 and D2→D2

connections, we measured light-evoked AMPAR-EPSCs in D2-Cre;Ai14 mice. We found that the amplitudes of AMPAR-EPSCs were significantly higher in the D2→D1 group than in the D2→D2 group (Figure 2.8 F; $F_{(1,112)} = 4.95$, $p < 0.05$). These results indicate that mPFC D2R-expressing inputs distinctly control D1-MSNs and D2-MSNs, with a stronger glutamatergic connection between mPFC D2R-expressing neurons and DMS D1-MSNs.

Lastly, we explored the effect of excessive alcohol intake on AMPAR-mediated EPSCs at mPFC D2R-expressing inputs onto DMS D1- or D2-MSNs. D2-Cre;Ai14 mice with mPFC infusion of AAV-Flex-Chronos-GFP were trained to consume high levels of alcohol (Table 2.1), as described above. Twenty-four hours after the last alcohol exposure, we prepared DMS slices and measured light-evoked EPSCs in DMS D1-MSNs and D2-MSNs. We found that excessive alcohol intake selectively potentiated AMPAR-EPSCs at D2R-expressing mPFC inputs onto DMS D1-MSNs (Figure 2.8 G; $F_{(1,112)} = 8.36$, $p < 0.01$). In contrast, excessive alcohol intake did not alter EPSCs at D2R-expressing mPFC inputs onto DMS D2-MSNs (Figure 2.8 H; $F_{(1,112)} = 0.46$, $p > 0.05$).

We also investigated whether excessive alcohol intake altered presynaptic glutamate release. A marginally lower PPR was observed at the D2→D1 synapse of the mPFC-DMS pathway in alcohol-drinking mice, as compared with the water controls (Figure 2.8 I; $t_{(28)} = 1.77$, $p = 0.087$). However, the PPR at the D2→D2 synapse did not differ between the alcohol and water groups (Figure 2.8 I; $t_{(28)} = -0.22$, $p > 0.05$). These data suggest that excessive alcohol intake may increase the probability of glutamate release selectively at the mPFC D2R-expressing afferents onto D1-MSNs. In summary, these results suggest that excessive alcohol intake enhances AMPAR-mediated glutamate transmission selectively at the D2→D1 synapse within the mPFC-DMS pathway.

Figure 2.8 The strong mPFC D2R-expressing input onto DMS D1-MSNs is potentiated by excessive alcohol consumption.

A, Illustration depicting the infusion of AAV-Flex-Chronos-GFP into the mPFC of D2-Cre;Ai14 mice, resulting in selective expression of Chronos in mPFC D2R-expressing neurons, but not D1R-expressing neurons. The expressed Chronos (green) was trafficked down to the mPFC terminals within the DMS. Optical stimulation exclusively activated glutamatergic transmission from mPFC D2R-expressing inputs onto DMS D1-MSNs (D2→D1) or D2-MSNs (D2→D2). D2-MSNs were identified by their expression of tdTomato. The tdTomato-negative striatal neurons were considered as putative D1-MSNs. **B,** Representative images of the mPFC infusion site. Coronal sections were prepared 8 weeks after the viral infusion. The section was counterstained with NeuroTrace blue (NT-Blue). Infusion of AAV-Flex-Chronos-GFP caused intense green fluorescent labeling at the injection site (left). Scale bar: 500 μm. The boxed area is presented at higher magnification in the right-hand panels. All mPFC neurons were stained with NT-Blue (B1). D2-neurons expressed tdTomato (red), and the arrows indicate D2R-negative cells (B2). AAV-Flex-Chronos-GFP was selectively expressed in D2R-expressing neurons (B3, stars). Stars indicate the Chronos-expressing tdTomato-positive neurons. Arrows indicate that tdTomato-negative cells did not express Chronos. Scale bar: 10 μm. **C,** Sample images of Chronos-expressing mPFC fibers in the DMS (left). The striatal neurons from the indicated box are shown on the right. All neurons were blue-stained (C1). D2-MSNs (stars) expressed red tdTomato and putative D1-MSNs are indicated by arrows (C2). Green mPFC afferents innervated striatal neurons (C3). The merged image (C4) shows green fibers surrounded by both D2-MSNs (red and blue) and putative D1-MSNs (blue). Scale bar: 500 μm (left), and 7 μm (right). **D,** Verification of glutamatergic transmission at D2→D1 synapses. Illustration indicating the whole-cell recordings performed on D1-MSNs. Synaptic transmission was triggered by optical stimulation of Chronos-expressing D2R-expressing inputs from the mPFC. The light-evoked responses were completely abolished by bath application of the AMPAR antagonist, DNQX (10 μM), and the NMDAR antagonist, APV (50 μM); DNQX + APV: 4.00 ± 0.73% of baseline, $t_{(9)} = 131.27$, $p < 0.05$, paired t test; n = 10 slices, 8 mice. The inset sample traces indicate the light-evoked responses in D1-MSNs at baseline (1) and after infusion of DNQX and APV (2). Scale bars: 20 ms, 40 pA. **E,** Verification of glutamatergic transmission at D2→D2 synapses. Illustration showing that light-evoked responses were recorded from D2-MSNs. Bath application of DNQX and APV completely blocked these light-evoked responses; DNQX + APV: 5.43 ± 0.89% of baseline, $t_{(9)} = 106.82$, $p < 0.05$, paired t test; n = 10 slices, 8 mice. The inset sample traces indicate the light-evoked responses in D2-MSNs before (1) and after (2) infusion of DNQX and APV. Scale bars: 20 ms, 25 pA. Note that there was no ChR2 expression in the D2-MSNs of D2-Cre;Ai14 mice. Therefore, blockade of glutamatergic transmission completely abolished the light-evoked response, in contrast to the partial D2→D2 inhibition in D2-Cre;Ai32 mice. **F,** AMPAR-mediated EPSCs were significantly larger at the D2→D1 connection than at the D2→D2 synapse. Left, Representative traces of the responses evoked in DMS D1- and D2-MSNs by a range of stimulation intensities. Scale bars: 10 ms, 30 pA. Right, The corresponding input-output curves; $\#p < 0.05$; $*p < 0.05$; $**p < 0.01$ versus water group at the same stimulation intensities, two-way RM ANOVA followed by SNK test; n = 15 neurons, 5 mice per group. **G,** Excessive alcohol intake significantly increased the amplitude of AMPAR-mediated EPSCs from the mPFC D2-inputs onto D1-MSNs. The input-output curves of D2→D1 AMPAR-EPSCs were measured at a range of stimulation intensities in the water and alcohol (EtOH)-drinking groups; $\#p < 0.05$, two-way RM ANOVA; $*p < 0.05$; $**p < 0.01$; $***p < 0.001$ versus water group at the same stimulation intensities, post hoc SNK test; n = 15 neurons, 5 mice per group. **H,** Excessive alcohol intake did not alter the AMPAR-mediated D2-MSN response to mPFC D2-inputs. The input-output curves of D2→D2 AMPAR-EPSC were measured at the indicated stimulation intensities; $p > 0.05$, two-way RM ANOVA; n = 15 neurons, 5 mice per group. **I,** Excessive alcohol consumption caused a marginal reduction in PPR at the D2→D1 connection, but not at the D2→D2 connection. Bar graphs comparing PPRs in the indicated groups; $p = 0.087$, unpaired t test; n = 15 neurons, 5 mice per group (D2→D1); $p > 0.05$, unpaired t test; n = 15 neurons, 5 mice per group (D2→D2). Inset, representative AMPAR-EPSC traces induced by two optical stimuli delivered at a 100-ms interval in the water and EtOH groups. Scale bars: 30 ms, 30 pA (D2→D1); 30 ms, 15 pA (D2→D2).

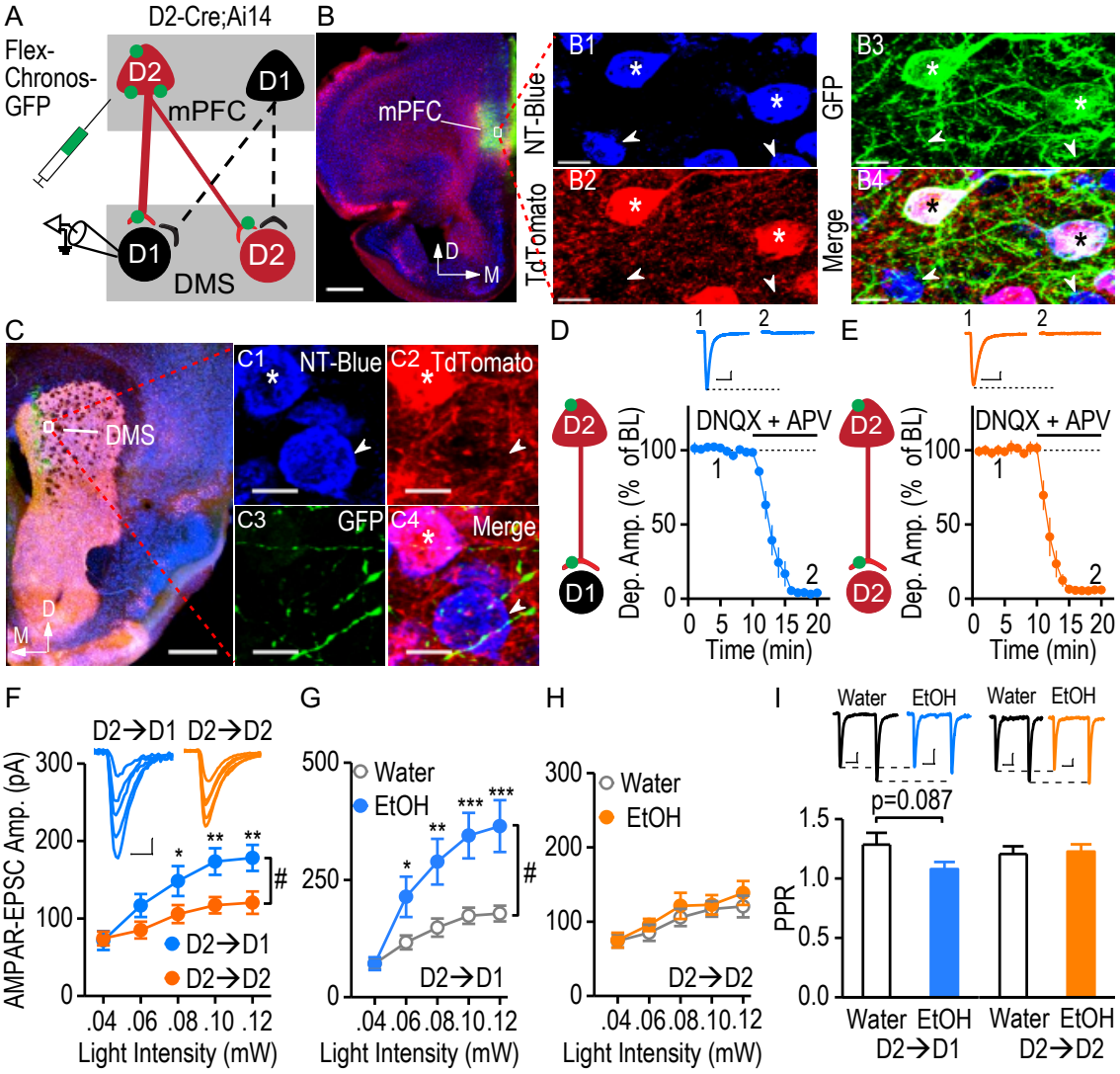
A
D2-Cre;Ai14
Flex-
Chronos-
GFP
D2
D1
mPFC
D1
D2
DMS
B
mPFC
D
M
B1
B2
NT-Blue
TdTomato
B3
B4
GFP
Merge
C
DMS
D
M
C1
NT-Blue
C2
TdTomato
C3
GFP
C4
Merge
D
E
D2
D1
DNQX + APV
Dep. Amp. (% of BL)
Time (min)
F
D2→D1
D2→D2
AMPAR-EPSC Amp. (pA)
Light Intensity (mW)
G
Water
EtOH
D2→D1
Light Intensity (mW)
H
Water
EtOH
D2→D2
Light Intensity (mW)
I
Water
EtOH
p=0.087
PPR
Water EtOH Water EtOH
D2→D1
D2→D2

Table 2.1 Comparison of levels of alcohol consumption in transgenic mice used.

Mouse lines	Alcohol intake (g/kg/24h)	
D2-Cre;Ai14	19.97 ± 3.24	n = 5
D1-Cre;Ai32	19.14 ± 2.31	n = 7
D2-Cre;Ai32	19.22 ± 1.88	n = 11

All mice were exposed to alcohol using the intermittent access to 20% alcohol 2-bottle-choice drinking procedure. The levels of alcohol intake were the averaged values of the last 3 drinking sessions. There was no significant difference in alcohol intake among mouse lines; $p > 0.05$, one-way ANOVA.

2.4. Discussion

The present study dissected glutamatergic afferents to the striatum based on their dopamine receptor expression, and it revealed that the glutamatergic connection between presynaptic D2R-expressing afferents and DMS D1-MSNs was stronger than that of the other three tested connections. This uneven synaptic strength may result in differential dopaminergic modulation of glutamatergic transmission. Additionally, we discovered that postsynaptic D2R-mediated suppression of glutamatergic transmission required eCB signaling, whereas presynaptic D2Rs mediated eCB-independent suppression. Our results contribute to the clarification of previous controversial findings relating to the role of the D2R in inhibitory presynaptic filtering of cortical inputs. Lastly, we found that excessive alcohol intake selectively strengthened glutamatergic transmission at the D2→D1 synapse, suggesting that this circuit may play a critical role in the pathogenesis of alcohol use disorder.

2.4.1. Glutamatergic connectivity at DMS synapses with distinct pre- and postsynaptic dopamine receptors

Dopamine is a key player in brain reward circuitry (Bamford et al., 2018). Investigations of cortical inputs onto MSNs have demonstrated that a major role of dopamine is to promote transient shifts in the balance between the direct and indirect striatal pathways of the basal ganglia during reward-driven behaviors (Kravitz et al., 2012; Bamford et al., 2018). Modulation of presynaptic filtering by dopamine may be critical in the determination of which cortical and thalamic signals are transduced by the appropriate excitatory striatal synapses during learning. Since D1Rs and D2Rs are major

dopamine receptors in the corticostriatal pathway, we employed D1-Cre;Ai32 and D2-Cre;Ai32 mice to dissect the circuitry into at least four types of synapse: D1→D1, D1→D2, D2→D1, and D2→D2.

In both brain-wide and mPFC studies, we found that glutamatergic D2→D1 transmission was stronger than that observed at the tested connection. It is known that in the dorsal striatum, D2Rs are more prevalent than D1Rs presynaptically at corticostriatal projections (Wang and Pickel, 2002; Dumartin et al., 2007; Bamford et al., 2018). This may explain our findings indicating that D2R-expressing inputs were stronger than D1R-expressing afferents in the DMS. However, our observation that the D2→D1 connection was stronger than the D2→D2 synapse indicated a difference at the postsynaptic site. Midbrain dopamine neurons predominantly fire at a low frequency, and such tonic activity builds up the basal level of dopamine in the striatum (Bamford et al., 2018). This tonic dopamine inhibits D2-MSNs via postsynaptic D2Rs. When the glutamatergic and dopaminergic inputs are activated at high frequency, eCB is preferentially generated in the D2-MSNs; this eCB suppresses presynaptic glutamate release onto D2-MSNs (Bamford et al., 2018). Additionally, at the behavioral level, the striatal circuit plays a dual role in the modulation of action initiated by the cortical inputs, by reinforcing the currently selected action via the direct pathway and suppressing potentially conflicting actions via the indirect pathway (Cui et al., 2013). Therefore, the intrinsically stronger D2→D1 circuit (as compared with the D2→D2 synapse) in the DMS may provide a mechanism for processing information through dopamine-dependent activation of the specific direct pathway in order to procure a reward. The current study only investigated

four types of dopamine receptor-based pathways. Although neurons expressing D1Rs or D2Rs were highly segregated in the cortical and striatal regions, some co-localization was observed (Cheng et al., 2017; Wei et al., 2018). Co-expressed D1Rs and D2Rs can form heterodimers, which contribute to addiction and schizophrenia (Perreault et al., 2014). Due to the limitations of our transgenic animals, the influence of this subpopulation on the corticostriatal pathway remains to be determined.

2.4.2. Alcohol-evoked circuit-specific plasticity

Accumulating evidence suggests that exposure to addictive substances, including alcohol, potentiates AMPAR-mediated responses in D1-MSNs, but not D2-MSNs (MacAskill et al., 2014; Wang et al., 2015; Cheng et al., 2017). Our current findings were consistent with this, with no alcohol-related changes observed in D2-MSNs. Importantly, D1-MSNs with inputs from extra-striatal neurons expressing D2Rs, such as mPFC D2-neurons, did exhibit marked alterations after repeated alcohol exposure. It is not fully clear why chronic alcohol exposure selectively potentiates the glutamatergic connectivity of D2→D1, while not affecting other synapses. Our observation of a decreased PPR indicated that this potentiation was mediated, at least in part, by an increase in presynaptic glutamate release. Presynaptic terminals are known to express D2Rs (Wang and Pickel, 2002), and their activation by tonic dopamine is reported to inhibit glutamate release (Kuei-Sen Hsu, 1995; Yin and Lovinger, 2006). The basal dopamine level is reported to decline gradually after a prolonged period of excessive alcohol drinking and withdrawal cycles (Barak et al., 2011; Trantham-Davidson and Chandler, 2015). The D2R is a high-affinity dopamine receptor that is classically

assumed to inhibit neuronal activity via $G\alpha_i$ protein or β-arrestin (Xing et al., 2016). Activation of D2R also blocks excitatory currents by recruiting Akt-GSK3 signaling (Li et al., 2016). The decreased basal dopamine level may reduce D2R-mediated suppression of D2→D1 signaling, which may consequently enhance glutamatergic transmission within this pathway and thus contribute to excessive drinking behavior.

2.4.3. D1-Cre and D2-Cre mouse lines

To achieve specific stimulation of extra-striatal inputs, we used D1-Cre and D2-Cre lines crossed with an optogenetic reporter mouse line. One limitation of this approach is that the representation of D1R-expressing neurons in the D1-Cre mouse and of D2R-expressing neurons in D2-Cre mouse might not be equally reliable. However, we compared the Cre efficiency of D1-Cre and D2-Cre mice, and the results suggested that these mouse lines showed equivalent levels of dopamine receptor expression. Thus, the observed difference in glutamatergic strength is highly likely to relate to intrinsic differences in the pathways, rather than to Cre line efficiency differences in D1-Cre and D2-Cre mice.

In conclusion, we demonstrated that inputs to the DMS can be classified in a cell type-specific manner and that the strengths of their glutamatergic connections with two types of MSN were not identical. The connection between corticostriatal D2R-expressing inputs and D1-MSNs was stronger than that of the other three tested connections and was selectively potentiated by excessive alcohol intake. The elucidation of this alcohol-evoked circuit-specific plasticity could contribute to the identification of new neuronal therapeutic targets for the treatment of alcohol use disorder.

2.5 Materials and methods

2.5.1. Reagents

AAV-Flex-Chronos-GFP, AAV-CAG-flex-GFP (Klapoetke et al., 2014), and retrograde AAVretro-CAG-tdTomato were purchased from the University of North Carolina Vector Core. All reagents were obtained from Sigma except DNQX (Abcam) and APV (R&D Systems).

2.5.2. Animals

Drd1a-Cre (D1-Cre) and *Drd2*-Cre (D2-Cre) mice were obtained from the Mutant Mouse Regional Resource Center. Ai32, Ai14, and Snap25 mice were purchased from the Jackson Laboratory. D1-Cre and D2-Cre mice were crossed with Ai32, Ai14, or Snap25 mice to obtain D1-Cre;Ai32, D2-Cre;Ai32, D1-Cre;Ai14, D2-Cre;Ai14, D1-Cre;Snap25, and D2-Cre;Snap25 mice. Mouse genotypes were determined by PCR analysis of Cre or the fluorescent protein in tail DNA (Cre for D1-Cre and D2-Cre mice; EYFP for Ai32 mice; tdTomato for Ai14 mice; GFP for Snap25 mice (Cheng et al., 2017; Wei et al., 2018)). Male mice (3-6 months-old) were used in this study. Mice were housed in a temperature- and humidity-controlled vivarium with a 12-h light/dark cycle (lights on at 11:00 P.M.). Food and water were available ad libitum. All animal care and experimental procedures were approved by the Texas A&M University Institutional Animal Care and Use Committee.

2.5.3. Stereotaxic infusion

Animals were anesthetized with 3-4% isoflurane at 1.0 L/min and mounted in a stereotaxic surgery frame. The head was leveled, and craniotomy was performed using

stereotaxic coordinates adapted from the mouse brain atlas (Franklin and Paxinos, 2007). AAV-Flex-Chronos-GFP (Figure 2.8) or AAV-CAG-Flex-GFP (Figure 2.2) was bilaterally infused at the mPFC of D1-Cre;Ai14 and D2-Cre;Ai14 mice (AP, +1.94 mm; ML, ± 0.25 mm; DV, -2.5 mm from the Bregma). AAVretro-CAG-Tdtomato was bilaterally infused into the DMS (AP1, +1.18 mm; ML1, ±1.3 mm; DV1, -2.9 mm; AP2, +0.38 mm; ML2, ±1.67 mm; DV2, -2.9 mm from the Bregma) of D1-/D2-Cre;Snap25 mice. A volume of 0.3 μL/site (mPFC) and 0.5 μL/site (DMS) of the virus was infused at a rate of 0.1 μL/min. The injectors were left in place for an additional 5-10 min before removal. The scalp incision was then sutured, and the animals were returned to their home cage for recovery.

2.5.4. Intermittent-access to 20% alcohol two-bottle-choice drinking procedure

To establish high levels of alcohol consumption in mice, we utilized the intermittent-access to 20% alcohol two-bottle-choice drinking procedure (Wang et al., 2015; Cheng et al., 2017; Cheng et al., 2018; Wei et al., 2018). D1-Cre;Ai32, D2-Cre;Ai32, and D2-Cre;Ai14 mice were given three 24-h sessions per week (Mondays, Wednesdays, and Fridays) of free access to two bottles containing water or 20% alcohol, with 24-h and 48-h withdrawal periods (Tuesdays, Thursdays, Saturdays, and Sundays). During the withdrawal periods, the mice had access to two bottles of water. The placement of the alcohol bottle was alternated for each drinking session to control for side preferences. Control animals were treated in the same manner, except that they were presented with water only. This procedure was followed for 8 weeks.

2.5.5. Electrophysiology

Slice preparation. Animals were euthanized and 250-μm coronal sections containing the DMS or mPFC (Figure 2.2) were prepared in an ice-cold cutting solution containing (in mM): 40 NaCl, 148.5 sucrose, 4 KCl, 1.25 NaH_2PO_4, 25 $NaHCO_3$, 0.5 $CaCl_2$, 7 $MgCl_2$, 10 glucose, 1 sodium ascorbate, 3 sodium pyruvate, and 3 myo-inositol saturated with 95% O_2 and 5% CO_2. Striatal slices from alcohol-drinking mice were prepared twenty-four hours or nine days after the last alcohol-drinking session. Slices were then incubated in a 1:1 mixture of the cutting solution and external solution at 32℃ for 45 min. The external solution was composed of the following (in mM): 125 NaCl, 4.5 KCl, 2.5 $CaCl_2$, 1.3 $MgCl_2$, 1.25 NaH_2PO_4, 25 $NaHCO_3$, 15 glucose, and 15 sucrose saturated with 95% O_2 and 5% CO_2. Slices were then maintained in the external solution at room temperature until use.

Whole-cell recordings. All recordings were conducted at 32°C and perfused with the external solution at a rate of 2-3 mL/min. Picrotoxin (100 μM) was included in the external solution of all recordings to block $GABA_A$ receptor-mediated transmission. Fluorescent axonal fibers and neurons were visualized using an epifluorescent microscope (Examiner A1, Zeiss). D1- and D2-MSNs of D2-Cre;Ai14 mice, mPFC neurons of D1-/D2-Cre;Ai14 mice were identified by fluorescence of tdTomato. A biophysical approach was used to distinguish D1- and D2-MSNs in D1-Cre;Ai32 or D2-Cre;Ai32 mice (see Figure 2.2 A-C for details). MSNs were clamped at -70 mV. The pipette solution contained (in mM): 119 $CsMeSO_4$, 8 tetraethylammonium chloride, 15 4-(2-hydroxyethyl) pipera-zine-1-ethanesulfonic acid (HEPES), 0.6 ethylene glycol

tetra-acetic acid (EGTA), 0.3 Na_3GTP, 4 MgATP, 5 QX-314, and 7 phosphocreatine, with an osmolarity of ~280 mOsm/L. The pH was adjusted to 7.3 with CsOH. For selective stimulation of inputs from channelrhodopsin-expressing fibers onto DMS neurons, 470-nm light was delivered through the objective lens for 2 ms. To generate input-output curves for AMPAR-mediated EPSCs, currents generated in response to stimulation at increasing intensities were recorded. The PPR was calculated using two EPSCs that were activated by paired two optical stimulation delivered at 50 or 100 ms apart. In recordings where Ca^{2+} was replaced with Sr^{2+}, AMPAR-mediated quantal events were collected during 50-500 ms after each stimulus (delivered once every 30 s) in an external solution containing APV (50 μM), 2.5 mM Sr^{2+}, and 0 Ca^{2+} (Ding et al., 2008; Mateo et al., 2017). Quantal events were analyzed using MiniAnalysis software (Synaptosoft) with detection parameters set at > 5 pA amplitude. For each cell, at least 30 trials were taken.

mPFC neurons were clamped at -60 mV with electrodes containing (in mM): 123 potassium gluconate, 10 HEPES, 0.2 EGTA, 8 NaCl, 2 MgATP, 0.3 NaGTP, pH 7.2-7.3, corresponding to an osmolarity of ~280 mOsm. mPFC cells with red fluorescence were recorded in the presence of DNQX (10 μM), APV (50 μM), and picrotoxin (100 μM) to block both excitatory and inhibitory synaptic transmission. A 500-ms current step was injected every minute to evoke firing. The baseline excitability was maintained for 5 min before D1 agonist or D2 agonist application for 10 min. Baseline firing was calculated from 1 to 5 minutes, and post-agonist (D1 or D2) firing was averaged from 11 to 15 minutes.

2.5.6. Histology and cell counting

Mice were intracardially perfused with 4% paraformaldehyde in phosphate-buffered saline. The brains were removed and post-fixed overnight in 4% paraformaldehyde at 4°C prior to dehydration in a 30% sucrose solution. The brains were cut into 50-μm coronal or sagittal sections using a cryostat. The sections (Figure 2.1 A, 2.1 B, 2.5 B, and 2.5 C) were stained with NeuroTrace Red or NeuroTrace Blue (1:100). Fluorescent images were acquired using a confocal microscope (FluoView 1200, Olympus, Tokyo, Japan) and analyzed using IMARIS 8.3.1 (Bitplane, Zürich, Switzerland), as previously reported (Cheng et al., 2017; Wei et al., 2018). Cell counting was performed in 12 double transgenic mice (Figure 2.4, D1-Cre;Snap25 and D2-Cre;Snap25; Figure 2.3, D1-Cre;Ai14 and D2-Cre;Ai14). In each brain region, a total of 33-35 brain sections were imaged from each mouse. Counting of green and red neurons were conducted using Imaris 8.3.1, which also calculated co-localization (Wei et al., 2018).

2.5.7. Statistical analysis

All data are expressed as the mean ± the standard error of the mean. Data were analyzed by two-tailed t test (unpaired or paired), one-way analysis of variance (ANOVA), or two-way ANOVA with repeated measures (two-way RM ANOVA), followed by the Student-Newman-Keuls (SNK) post hoc test. Differences were considered to be statistically significance if $p < 0.05$. Statistical analysis was conducted by SigmaPlot.

CHAPTER III

PERSISTENT REDUCTION OF ETHANOL-SEEKING BEHAVIOR BY OPTOGENETIC REVERSAL OF ETHANOL-EVOKED INPUT- AND CELL TYPE-SPECIFIC SYNAPTIC PLASTICITY IN THE DORSOMEDIAL STRIATUM

3.1. Overview

The reinforcement of drug- and ethanol-seeking and -taking behaviors is thought to require dopamine-dependent long-term synaptic plasticity in the striatum. The dorsomedial striatum (DMS) is essential for goal-directed actions and reinforcement of addictive behaviors. Although the involvement of dopamine D1 receptor-expressing medium spiny neurons (MSNs) in the DMS is increasingly being appreciated, it remains unclear how long-term potentiation (LTP) and depression (LTD) of cortical inputs onto DMS D1-MSNs mediate reinforcement behavior in addiction. Using triple transgenic D1-tdT;FosTRAP;Snap 25 mice in which D1-MSNs expressed tdT and activated neurons expressed eGFP after tamoxifen-induced Cre recombination, we discovered that more striatal D1-MSNs were activated during ethanol drinking than during water drinking only. Additionally, excessive ethanol intake selectively strengthened glutamatergic transmission from medial prefrontal cortical (mPFC) inputs onto DMS D1-MSNs. Notably, mimicking this ethanol-mediated mPFC→D1-MSN potentiation using *in vivo* dual-channel optogenetic self-stimulation of this synapse to induce LTP was sufficient to drive reinforcement of lever pressing in operant chambers. Conversely, time-locked delivery of a post-pre spike timing-dependent protocol that induced LTD at

this synapse persistently decreased ethanol-seeking behavior. In summary, our results demonstrate a causal link between synaptic plasticity and the reinforcement of ethanol-seeking behavior, providing a potential therapeutic strategy to restore normal function of dysregulated brain circuits in ethanol use disorder.

3.2. Introduction

Behavioral reinforcement induced by addictive substances depends on the activation of the mesolimbic dopamine system (Luscher and Malenka, 2011; Bamford et al., 2018; Luscher et al., 2020). Accumulating evidence suggests that this form of associative learning occurs through dopamine-dependent corticostriatal plasticity (Luscher and Malenka, 2011; Bamford et al., 2018; Luscher et al., 2020). The DMS, a brain region that is critically involved in drug and ethanol abuse, contains direct- and indirect-pathway MSNs (Gerfen and Surmeier, 2011; Cheng et al., 2017). Direct-pathway MSNs express D1Rs and positively control reward, whereas indirect-pathway MSNs express D2Rs and negatively control reward behaviors (Gerfen and Surmeier, 2011; Cheng et al., 2017). Excessive ethanol intake has been reported to increase glutamatergic activity selectively in DMS D1-MSNs, and thus reinforces this behavior (Wang et al., 2015; Cheng et al., 2017; Ma et al., 2018; Lu et al., 2019). In addition, intracranial self-stimulation of direct-pathway MSNs is sufficient to elicit reinforcement behavior in the absence of reward (White NM, 1998; Kravitz et al., 2012; Lalive et al., 2018). However, it remains unclear how excessive ethanol consumption differentially alters the plasticity of excitatory inputs, such as glutamatergic inputs from the mPFC onto DMS MSNs, and whether these changes are sufficient to drive reinforcement.

Ethanol-evoked corticostriatal plasticity shares similar mechanisms with LTP and LTD (Luscher and Malenka, 2011; Lovinger and Abrahao, 2018; Ma et al., 2018). Induction of *in vivo* LTD in DMS D1-MSNs using optogenetic high-frequency stimulation, combined with systemic administration of NMDA receptor (NMDAR) and D2R antagonists, was found to suppress ethanol-seeking and -taking behaviors (Ma et al., 2018; Roltsch Hellard et al., 2019). However, systemic administration of antagonists modulates neuronal activity throughout the brain, which may generate unexpected changes. Previous studies have shown that a post-pre spike timing-dependent protocol (STDP), i.e., depolarization of postsynaptic striatal neurons followed by excitation of presynaptic cortical inputs, could trigger LTD at corticostriatal synapses in D1-MSNs, but not D2-MSNs (Verena Pawlak, 2008; Wu et al., 2015). A dual-channel optogenetic approach facilitates the selective control of pre- and postsynaptic components simultaneously because they express two different channelrhodopsins that are activated by different wavelengths of light (Hooks et al., 2015; Ma et al., 2018; Roltsch Hellard et al., 2019). Thus, circuit-specific LTD can be induced at the mPFC inputs onto DMS D1-MSNs by using a combination of dual-channel optogenetics and STDP. This induction can be time-locked to lever presses for ethanol, which may exert potent and persistent inhibitory effects on ethanol-seeking or -taking.

In this study, we first identified mouse striatal neurons that were activated during home-cage ethanol intake using Fos-targeted recombination in active population (FosTRAP) technology (Allen et al., 2017; DeNardo et al., 2019). We discovered that excessive ethanol consumption preferentially engaged more D1-MSNs than did water

dinking only. Measurement of corticostriatal transmission showed that excessive ethanol consumption selectively potentiated glutamatergic mPFC inputs onto D1-MSNs, but not D2-MSNs. Notably, mimicking this ethanol-mediated mPFC→D1-MSN potentiation using *in vivo* optogenetic self-stimulation to induce LTP at this synapse reinforced operant behavior in rats. Conversely, time-locked delivery of an optogenetic LTD protocol at the mPFC→D1-MSN synapse led to a long-lasting decrease in ethanol-seeking behavior. These findings demonstrate a causal link between DMS corticostriatal synapse plasticity and reward-driven behaviors and facilitate the development and optimization of future circuit-based treatment strategies for ethanol use disorder.

3.3. Results

3.3.1. Excessive ethanol intake increases the proportion of the D1R-expressing neuronal ensemble in the dorsal striatum

To explore the striatal neurons associated with excessive ethanol drinking, we utilized the FosTRAP system, which allows identification of the neuronal ensembles engaged during a specific experience (Allen et al., 2017; DeNardo et al., 2019). Neuronal activation in the Fos-Cre;Snap25 mice employed in this study resulted in the translocation of Fos-driven CreER to the nucleus, where it catalyzed recombination and eGFP expression (Figure 3.1 A) To determine whether the activated neurons express D1Rs, we trained D1-tdT;Fos-Cre;Snap25 mice to consume high levels of ethanol using the intermittent-access to 20% ethanol 2-bottle choice for 8 weeks (Cheng et al., 2017; Ma et al., 2017; Cheng et al., 2018; Wei et al., 2018; Lu et al., 2019) (Figure 3.1 B; Table 3.1). After habituation to i.p. saline injection for three consecutive drinking

sessions, animals received the short-acting tamoxifen metabolite, 4-OHT, or saline i.p. 2 h before the last ethanol exposure (DeNardo et al., 2019) (Figure 3.1 B). Water controls underwent the same procedure, without ethanol exposure. The cells activated during ethanol drinking in the presence of 4-OHT were tagged by eGFP. Two weeks after 4-OHT injection, we sacrificed the mice and quantified eGFP-expressing cells (TRAPed cells) in the dorsal striatum (Figure 3.1 B). As expected, ethanol-drinking mice that received a saline injection on the TRAP day had very few eGFP-expressing cells, indicating minimal Cre-mediated recombination in the absence of 4-OHT (Figure 3.1 C, E). However, we found a marked increase in TRAPed cells in the dorsal striatum of mice exposed to ethanol and 4-OHT, as compared to water/4-OHT-treated controls (Figure 3.1 C, E; $t_{(7)} = -2.68$, $p < 0.05$), suggesting that ethanol consumption increases striatal neuronal activity.

Next, we examined the proportion of TRAPed D1-MSNs by quantifying the colocalization of tdT and eGFP in confocal images. We observed that 44% of TRAPed cells ($eGFP^+$) in the dorsal striatum were D1-MSNs (tdT^+) (Figure 3.1 D, F). This value was significantly higher than that observed in the water controls, where approximately 20% $eGFP^+$ cells were tdT^+ (Figure 3.1 F; $t_{(7)} = -2.68$, $p < 0.05$). Interestingly, we discovered a higher percentage of ethanol-drinking-associated D1-MSNs in the posterior part of the dorsal striatum (starting at 0.62 mm and ending at −1.34 mm relative to Bregma) than in the anterior part (starting at 1.7 mm and ending at 0.74 mm relative to Bregma) (Figure 3.1 G; $t_{(4)} = -3.85$, $p < 0.05$). These results indicate that as compared with water intake only, excessive ethanol consumption activates more D1-MSNs, with a greater number of these located in the posterior dorsal striatum than in the anterior dorsal striatum.

Figure 3.1 Excessive ethanol intake increased the D1R-expressing neuronal ensemble in the dorsal striatum.
A, The Fos-Cre;Snap25 mouse contains two transgenes, one encoding the tamoxifen-dependent recombinase CreER under the control of an activity-dependent immediate early gene Fos promoter (top), and one expressing eGFP in a Cre-dependent manner (middle). Fos-active neurons express CreER, which is translocated into the nucleus when 4-hydroxytamoxifen (4-OHT) is present; this leads to Cre-mediated recombination and eGFP expression in these neurons (bottom). **B,** Experimental timeline. Triple transgenic D1-tdT (tdT);Fos-Cre;Snap25 mice were trained to consume high levels of ethanol (EtOH) using the intermittent-access to 20% EtOH two-bottle choice (2BC) procedure for 8 weeks. Their water controls underwent the same procedure but without EtOH exposure. Both groups were habituated to receiving an intraperitoneal (i.p.) injection of saline for three consecutive drinking sessions. Saline or 4-OHT was injected 2 h before the last drinking session on the targeted recombination in active populations (TRAP) day to allow Fos-driven eGFP expression. Mice were separated into the three indicated experimental groups. Two weeks after the TRAP, mice were sacrificed for fluorescent imaging and cell counting. **C,** Representative coronal sections from the indicated groups. Left, no TRAP-eGFP neurons in the saline-injected group. Middle and right, increased expression of TRAP-eGFP was observed in EtOH/4-OHT-treated animals (right), as compared with Water/4-OHT-treated mice (middle). Scale bars: 500 μm. D, dorsal; L, lateral. **D,** High-magnification confocal images of the indicated part of the DMS of a D1-tdT;Fos-Cre;Snap25 mouse treated with EtOH and 4-OHT showing colocalization (arrow) of TRAP-eGFP (left), D1-tdT (middle), and a merged image (right). Scale bars: 20 μm. **E,** Bar graphs comparing the total numbers of dorsostriatal TRAP-eGFP cells in the indicated groups; $*p < 0.05$, unpaired t test; n = 64 sections, 4 mice (Water) and 80 sections, 5 mice (EtOH). **F,** Bar graphs showing greater colocalization of dorsostriatal TRAP-eGFP and D1-tdT in the EtOH group than in Water controls; $*p < 0.05$, unpaired t test; n = 64 sections, 4 mice (Water) and 80 sections, 5 mice (EtOH). **G,** Distribution of TRAP-eGFP and D1-tdT colocalization from the anterior to posterior dorsal striatum. A higher percentage colocalization of TRAP-eGFP and D1-tdT was observed in the posterior, as compared with anterior, region; $*p < 0.05$, paired t test; n = 30 sections, 5 mice (Anterior) and 50 sections, 5 mice (Posterior).

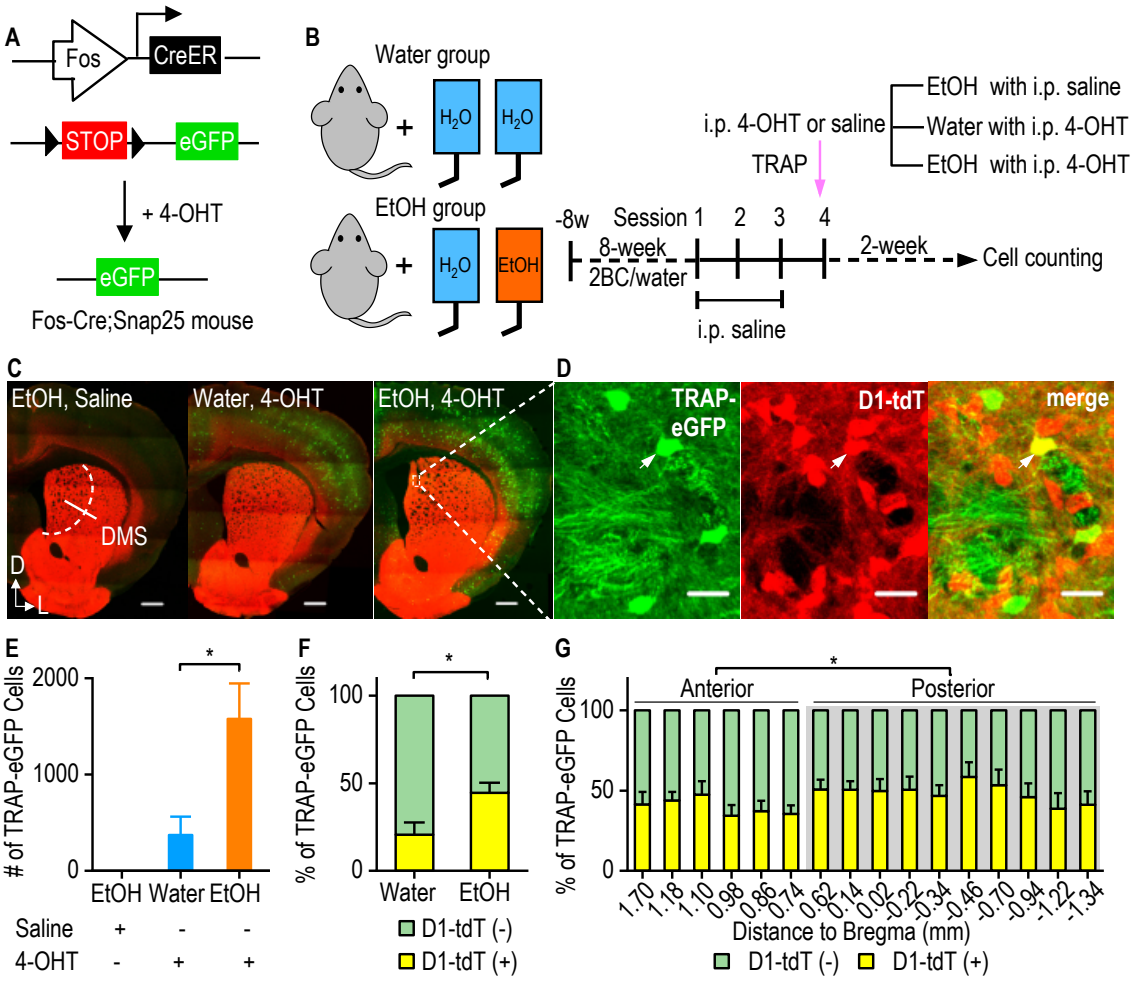
A
Fos
CreER
STOP
eGFP
+ 4-OHT
eGFP
Fos-Cre;Snap25 mouse
B
Water group
H2O
H2O
EtOH group
H2O
EtOH
i.p. 4-OHT or saline
TRAP
EtOH with i.p. saline
Water with i.p. 4-OHT
EtOH with i.p. 4-OHT
-8w
Session 1
2
3
4
8-week
2BC/water
2-week
Cell counting
i.p. saline
C
EtOH, Saline
Water, 4-OHT
EtOH, 4-OHT
DMS
D
L
D
TRAP-eGFP
D1-tdT
merge
E
# of TRAP-eGFP Cells
2000
1000
0
EtOH
Water
EtOH
Saline + - -
4-OHT - + +
F
% of TRAP-eGFP Cells
100
50
0
Water
EtOH
D1-tdT (-)
D1-tdT (+)
G
% of TRAP-eGFP Cells
Anterior
Posterior
100
50
0
1.70
1.18
1.10
0.98
0.86
0.74
0.62
0.14
0.02
-0.22
-0.34
-0.46
-0.70
-0.94
-1.22
-1.34
Distance to Bregma (mm)
D1-tdT (-)
D1-tdT (+)

3.3.2. Excessive ethanol consumption and withdrawal preferentially potentiate glutamatergic transmission at mPFC inputs onto D1-MSNs

We next explored the potential mechanisms underlying the increased percentage of D1-MSNs engaged during excessive ethanol intake. We previously reported that excessive ethanol intake potentiated glutamatergic neurotransmission from the mPFC onto striatal neurons in rats (Ma et al., 2017) and caused cell type-specific potentiation in mice (Wang et al., 2015; Cheng et al., 2017). This prompted us to reason that the observed increase in TRAPed D1-MSNs in ethanol-drinking mice, as compared with water controls, may result from ethanol-evoked glutamatergic plasticity that selectively affected corticostriatal inputs onto D1-MSNs, but not onto D2-MSNs. To assess how excessive ethanol consumption affected synaptic transmission in these two neuronal populations receiving mPFC inputs, we used D1-Cre;Ai14 and D2-Cre;Ai14 transgenic mice, which expressed tdT in D1-MSNs and D2-MSNs, respectively (Cheng et al., 2017; Lu et al., 2019). To facilitate selective stimulation of the mPFC input, we infused AAV-Chronos-GFP into this brain region (Figure 3.2 A), achieving intense fluorescent labeling of mPFC afferents in the DMS (Figure 3.2 B). The mice were then trained to consume 20% ethanol for 8 weeks using the intermittent-access two-bottle choice drinking procedure (Table 3.1). The water control mice underwent the same treatment, without ethanol exposure. Twenty-four hours after the last ethanol exposure, we prepared DMS slices, selectively activated mPFC inputs using 2-ms light at 470 nm light, and measured light-evoked AMPAR-mediated EPSCs in D1-MSNs and D2-MSNs.

We delivered a range of light intensities and compared the EPSCs observed in ethanol-drinking mice and their water controls. In D1-MSNs, the amplitude of AMPAR-mediated EPSCs was significantly higher in the ethanol-drinking group than in the water controls (Figure 3.2 C; $F_{(1,72)} = 4.86$, $p < 0.05$). In contrast, the amplitudes in D2-MSNs were identical in both groups (Figure 3.2 D; $F_{(1,72)} = 0.06$, $p > 0.05$). These results suggest that excessive ethanol intake potentiates AMPAR-mediated transmission selectively at mPFC inputs onto D1-MSNs in the DMS.

To examine whether excessive ethanol intake altered the probability of presynaptic glutamate release in an input- and cell type-specific manner, we measured the paired-pulse ratios of EPSCs. At the mPFC inputs onto D1-MSNs, we found that the paired-pulse ratio was significantly lower in ethanol-drinking mice than in the water controls (Figure 3.2 E; $t_{(16)} = 2.33$, $p < 0.05$). Conversely, this ratio did not differ in the D2-MSNs of the ethanol and water groups (Figure 3.2 F; $t_{(18)} = -0.28$, $p > 0.05$). Since the paired-pulse ratio is inversely correlated with transmitter release probability (Zucker and Regehr, 2002), these data suggest that excessive ethanol intake significantly increases glutamate release probability selectively at the mPFC afferents onto D1-MSNs.

The NMDAR is a well-established major ethanol target, and this receptor has been implicated in excessive ethanol consumption (Wang et al., 2007; Wang et al., 2010; Wang et al., 2011; Ben Hamida et al., 2013; Cheng et al., 2017; Lovinger and Abrahao, 2018). We next explored the effect of excessive ethanol intake on NMDAR-mediated EPSCs at mPFC inputs onto D1- and D2-MSNs. We used 0.05 mM Mg^{2+} and DNQX together to isolate the light-evoked NMDAR-mediated responses measured at a series of

stimulation intensities. We found that excessive ethanol intake selectively potentiated NMDAR-EPSCs in D1-MSNs (Figure 3.2 G; $F_{(1,71)} = 4.51$, $p < 0.05$), as compared with those observed in water controls. In contrast, excessive ethanol intake did not alter light-evoked NMDAR-mediated EPSCs in D2-MSNs (Figure 3.2 H; $F_{(1,80)} = 0.01$, $p > 0.05$). These results indicate that excessive ethanol intake selectively potentiates NMDAR-mediated transmission at mPFC inputs onto D1-MSNs in the DMS. Alterations in synaptic NMDAR subunits, and particularly potentiation of GluN2B-NMDAR activity, contribute to long-term changes in synaptic strength (Wang et al., 2007; Wang et al., 2011). To test ethanol-induced changes in NMDAR subunit composition, we evaluated the effect of excessive ethanol intake on the contribution of GluN2B subunits to NMDAR-mediated synaptic responses in the DMS. We observed that excessive ethanol consumption increased the GluN2B/NMDAR ratio in D1-MSNs at mPFC inputs (Figure 3.2 I; $t_{(16)} = -2.64$, $p < 0.05$), as compared with the water group. However, no difference was observed in the D2-MSN GluN2B/NMDAR ratio in the ethanol and water groups (Figure 3.2 J; $t_{(16)} = -0.96$, $p > 0.05$). These data reveal that excessive ethanol intake enhances GluN2B-NMDAR activity selectively at the mPFC inputs onto DMS D1-MSNs. Collectively, these results indicate that excessive ethanol consumption potentiates glutamatergic mPFC→D1-MSN transmission.

Figure 3.2 Excessive ethanol consumption preferentially potentiated glutamatergic transmission from mPFC inputs onto D1-MSNs.
D1Cre;Ai14 mice were trained to consume 20% ethanol for 8 weeks using the intermittent-access two-bottle choice drinking procedure, and DMS slices were prepared 24 h after the last ethanol exposure. **A,** Stereotaxic infusion of AAV-Chronos-GFP into the mPFC (left) of D1-Cre;Ai14 mice led to Chronos-GFP expression (green fluorescence; right; scale bar: 500 μm). The inset (arrowhead) shows a Chronos-GFP-expressing mPFC neuron at high magnification; scale bar: 5 μm. D, dorsal; L, lateral. **B,** Representative image from a D1-Cre;Ai14 mouse depicting the innervation of red D1-MSNs (inset) in the DMS by GFP-expressing afferents from the mPFC (green). **C and D,** Excessive ethanol (EtOH) intake potentiated AMPAR-EPSCs at mPFC inputs onto D1-MSNs, but not D2-MSNs. Left and middle, representative traces of AMPAR-EPSCs in D1-MSNs (C) or D2-MSNs (D) within DMS slices from the indicated mice; these were evoked using increasing optical stimulation intensities. Right, input-output curves for AMPAR-EPSCs; #$p < 0.05$ for the indicated comparison; *$p < 0.05$, **$p < 0.01$ versus the same stimulation intensity in the water group, two-way RM ANOVA followed by post hoc SNK test; n = 10, 4 per group. Scale bars: 10 ms, 150 pA (C) and 10 ms, 150 pA (D). **E and F,** Excessive EtOH intake significantly increased glutamate release at mPFC inputs onto D1-MSNs, but not D2-MSNs. Top, sample traces showing paired-pulse ratios (PPR; 100-ms interstimulus interval) measured in D1-MSNs (E) and D2-MSNs (F) from the indicated groups. Bottom, averaged data; *$p < 0.05$, unpaired t test; n = 9 neurons from 4 mice (9, 4) per group (E) and n = 10, 4 per group (F). Scale bars: 20 ms, 50 pA. **G and H,** Excessive EtOH consumption enhanced NMDAR-EPSC amplitudes at the mPFC inputs onto D1-MSNs, but not D2-MSNs. Left and middle, representative EPSC traces in D1-MSNs (G) or D2-MSNs (H) in DMS slices from the indicated mice. Right, the corresponding input-output curves; #$p < 0.05$ for the indicated comparison; *$p < 0.05$, ***$p < 0.001$ versus the same intensity in the water group, two-way RM ANOVA followed by SNK test; n = 11, 6 (Water, G); 11, 5 (Water, H); 9, 4 (EtOH, G) and 11, 3 (EtOH, H). Scale bars: 80 ms, 80 pA. **I and J,** Mice with excessive EtOH intake had higher GluN2B/NMDA ratios at mPFC inputs onto D1-MSNs, but not D2-MSNs. Left and middle, sample traces of NMDAR-EPSCs measured in D1-MSNs (I) or D2-MSNs (J) in the indicated treatment groups in the absence (NMDA) or presence (GluN2B) of Ro 25-6981 (0.5 μM). Right, summarized ratio data; *$p < 0.05$, unpaired t test; n = 9, 5 (Water) and 9, 4 (EtOH). Scale bars: 80 ms, 50 pA.

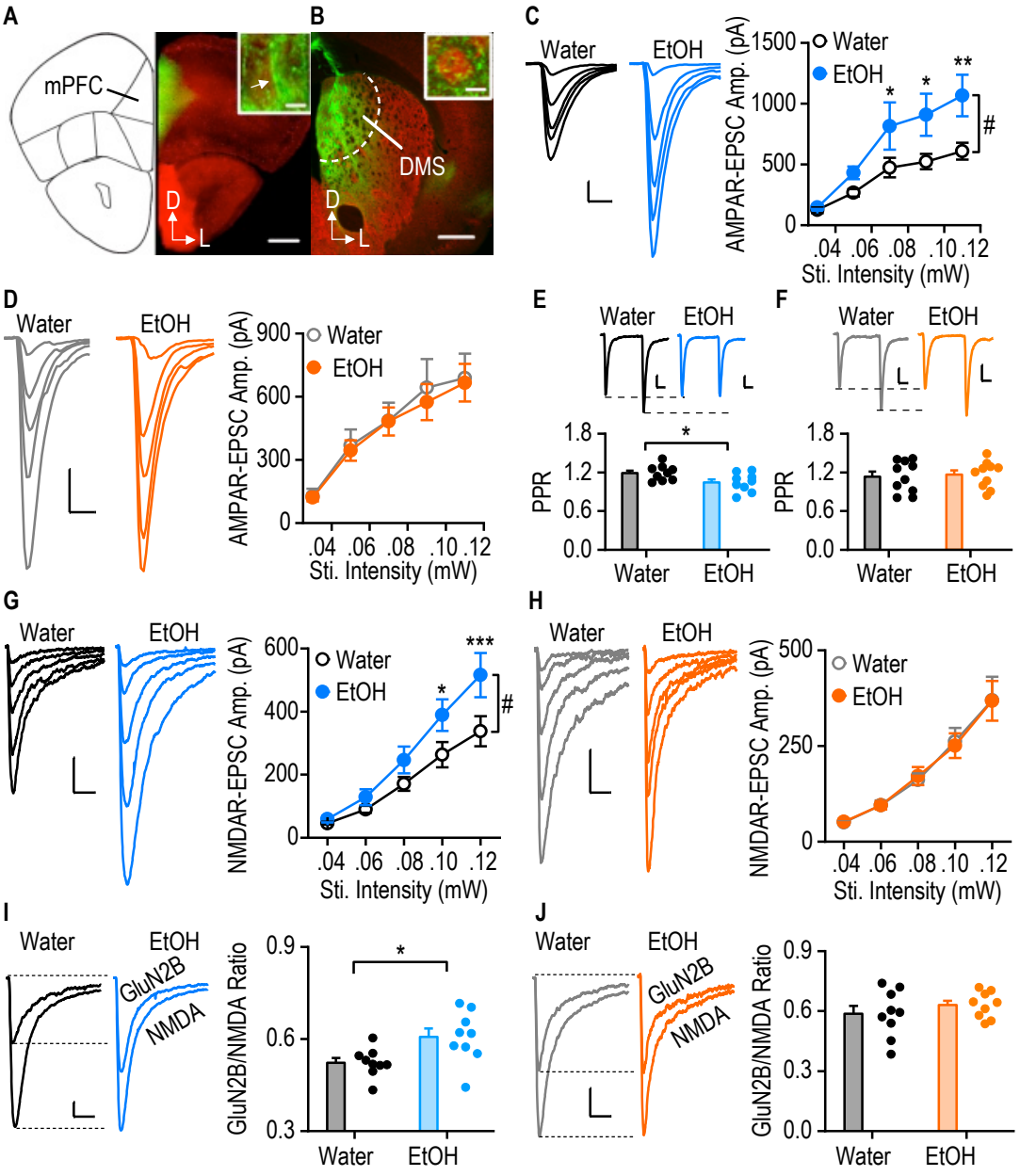
A
mPFC
D
L
B
DMS
D
L
C
Water
EtOH
AMPAR-EPSC Amp. (pA)
1500
1000
500
0
Water
EtOH
*
*
**
#
.04 .06 .08 .10 .12
Sti. Intensity (mW)
D
Water
EtOH
AMPAR-EPSC Amp. (pA)
900
600
300
0
Water
EtOH
.04 .06 .08 .10 .12
Sti. Intensity (mW)
E
Water
EtOH
L
L
PPR
1.8
1.2
0.6
0.0
*
Water
EtOH
F
Water
EtOH
L
L
PPR
1.8
1.2
0.6
0.0
Water
EtOH
G
Water
EtOH
NMDAR-EPSC Amp. (pA)
600
400
200
0
Water
EtOH
***
*
#
.04 .06 .08 .10 .12
Sti. Intensity (mW)
H
Water
EtOH
NMDAR-EPSC Amp. (pA)
500
250
0
Water
EtOH
.04 .06 .08 .10 .12
Sti. Intensity (mW)
I
Water
EtOH
GluN2B
NMDA
GluN2B/NMDA Ratio
0.9
0.6
0.3
*
Water
EtOH
J
Water
EtOH
GluN2B
NMDA
GluN2B/NMDA Ratio
0.9
0.6
0.3
0.0
Water
EtOH

3.3.3. *In vivo* self-stimulation of mPFC→D1-MSN synapses using an oLTP protocol reinforces active lever presses in rats

Corticostriatal plasticity is critical for drug-seeking behaviors (Bamford et al., 2018; Luscher et al., 2020). Having observed ethanol-evoked potentiation of mPFC→D1-MSN transmission, we next asked whether self-stimulation of this circuit was sufficient to drive reinforcement behavior. To test this possibility, we bilaterally infused AAV-Chronos-GFP into the mPFC, a Cre-inducible AAV expressing Chrimson (AAV-Flex-Chrimson-tdT) into the DMS, and a retrograde AAV encoding Cre (AAVretro-Cre-GFP) into the SNr in wild-type Long-Evans rats (Figure 3.3 A). Taking advantage of the direct pathway in which D1-MSNs project to the SNr, AAVretro-Cre-GFP underwent retrograde transport from the SNr to the DMS, where Cre recombinase drove selective Chrimson expression in D1-MSNs (Figure 3.3 B) (Ma et al., 2018). Chronos-expressing mPFC terminals in the DMS were activated by 470-nm light, and optogenetic postsynaptic depolarization in Chrimson-expressing D1-MSNs was induced by 590-nm light (Figure 3.3 A). Optical fibers were bilaterally implanted into the DMS for selective stimulation of mPFC→D1-MSN synapses (Figure 3.3 A, C). Rats were trained (30-min sessions on 12 consecutive days) to self-stimulate mPFC→D1-MSN synapses (Figure 3.3 D). Active lever presses triggered a cue light (500-ms pulses at 1 Hz for 10 s) above the lever. After a 5-s delay, oLTP was induced (2-s optogenetic high frequency stimulation of mPFC inputs at 50 Hz, paired with 2-s optogenetic postsynaptic depolarization of D1-MSNs (Ma et al., 2018)). A 20-s time-out followed all rewarded

lever presses, during which time lever presses had no consequences but were still recorded (Figure 3.3 D).

A direct comparison between active and inactive lever presses showed significant effects of levers and sessions (Figure 3.3 E, F; Lever: $F_{(1,66)} = 8.64$, $p < 0.05$; Sessions: $F_{(11,66)} = 2.48$, $p < 0.05$). During session 1 (no oLTP stimulation), the rats showed low levels of lever pressing, and there was no difference between active and inactive lever presses (Figure 3.3 E, F; $q = 0.98$, $p > 0.05$). During sessions 3 and 5-12, the active lever was pressed significantly more often than the inactive lever (Figure 3.3 E, F; $q = 3.55$, 3.30, 3.88, 3.48, 3.51, 5.72, 4.27, 4.42, 4.46 and $p < 0.05$, 0.01 as indicated).

Furthermore, more active lever presses were observed during these sessions than during session 1 (Figure 3.3 E, F; $q = 4.64$, 4.31, 5.36, 4.77, 4.64, 8.62, 6.07, 6.40, 6.47 and $p < 0.05$, 0.01, 0.001 as indicated). Analysis of preceding and succeeding inter-action intervals for three consecutive active lever presses showed that lever presses at intervals of < 60 s occurred more frequently in the final FR3 sessions than in the mock induction session (Figure 3.3 G), suggesting the establishment of action-outcome contingency after 12 training sessions (Matamales et al., 2020). The averaged inter-action intervals were significantly lower during the FR2 and FR3 sessions, as compared with the mock induction session (Figure 3.3 H; $F_{(3,14)} = 4.05$, $p < 0.029$. FR2 versus session 1: $q = 3.96$, $p < 0.05$; FR3 versus session 1: $q = 4.68$; $p < 0.05$). Consistent with the increase in active lever presses, the number of oLTP deliveries was significantly higher during the FR1 sessions, as compared to the mock induction session (Figure 3.3 I; $F_{(3,18)} = 3.92$, $p < 0.05$).

To ascertain whether optogenetic self-stimulation the mPFC→D1-MSN synapse caused glutamatergic potentiation at mPFC→D1-MSN synapses, we measured optically-evoked EPSCs in D1-MSNs from DMS slices prepared 24 h after the last training session. We found that the amplitude of AMPAR-EPSCs was significantly increased, as compared to neurons from control animals without oLTP induction (Figure 3.3 J; $F_{(1,128)} = 10.97$, $p < 0.01$). In addition, the higher AMPAR/NMDAR ratio in the oLTP group, as compared with controls, is likely attributable to oLTP induction (Figure 3.3 K; $t_{(26)} = 2.09$, $p < 0.05$). These *ex vivo* results confirmed that *in vivo* optogenetic self-stimulation of mPFC→D1-MSN synapses caused long-lasting synaptic potentiation.

Taken together, these results suggest that optogenetic self-stimulation of the mPFC→D1-MSN synapse induces oLTP and drives reinforcement of operant behavior.

Figure 3.3 *In vivo* optogenetic self-stimulation of mPFC→D1-MSN synapses to induce LTP reinforced of lever presses.
A, Schematic illustrating the dual-channel optogenetic approach used to achieve selective *in vivo* stimulation of mPFC inputs onto DMS D1-MSNs in wild-type Long-Evans (LE) rats. AAV-Chronos-GFP, AAV-Flex-Chrimson-tdT and AAVretro-Cre-GFP were infused into the mPFC, DMS, and SNr, respectively. The optical fiber was implanted in the DMS. Chronos and Chrimson were activated by 470- and 590-nm light, respectively. **B,** Representative sagittal image showing Chrimson-tdT expression (red) in D1-MSNs, which project to the SNr, and Chronos-GFP expression in mPFC fibers in the DMS. Three striatal neurons shown in the top right inset were stained with DAPI, and one of these expressed Chrimson-tdT (arrow). Scale bars: 500 μm, 5 μm (inset). A, anterior; D, dorsal. **C,** Coronal striatal section showing Chronos-GFP and Chrimson-tdT expression in the DMS and optical fiber track (dotted lines). D, dorsal; M, medial. Scale bar: 500 μm. **D,** Rats were trained in an operant self-administration chamber, where pressing the active lever resulted in optogenetic stimulation of mPFC→D1-MSN synapses to induce LTP. In the FR3 trial, active lever presses triggered a 10-s cue light; 5 s after this illuminated, a 2-s laser stimulation was delivered (2-s optogenetic high-frequency stimulation [oHFS] at 50 Hz with 2-s optogenetic postsynaptic depolarization [oPSD]). This was followed by a time-out period during which lever presses had no consequences. **E,** Example raster plot showing active lever presses during 30-min sessions, including the mock induction, and FR1, FR2, and FR3 trials involving self-stimulation of mPFC→D1-MSN synapses to induce oLTP. Each vertical line represents one lever press. **F,** Time-course of active and inactive lever presses over 12 consecutive daily self-stimulation sessions; #$p < 0.05$ for the indicated comparison; *$p < 0.05$, **$p < 0.01$ versus the inactive lever during the same session; ^$p < 0.05$, ^^$p < 0.01$, ^^^$p < 0.001$ versus session 1 (mock induction) for the active lever; two-way RM ANOVA followed by SNK test; n = 7 rats. **G,** Return maps of the inter-action interval (IAI) for active lever presses during mock induction (session 1) and the last FR3 session (session 12). Each data point represents the time delay to its preceding (x) and succeeding (y) behavioral element. Data are Log10 transformed. Dashed lines represent Log10(60) = 1.78. Note that there are more dots within the bottom left quadrant during FR3 than during mock induction; n = 7 rats. **H,** Bar graphs showing the average IAI in the indicated session, as compared with mock induction; *$p < 0.05$, one-way RM ANOVA followed by SNK test; n = 7 rats. **I,** The number of oLTP inductions delivered during the indicated session; *$p < 0.05$ versus mock induction, one-way RM ANOVA; n = 7 rats. **J,** *In vivo* self-induction of oLTP potentiated AMPAR-EPSCs in D1-MSNs. Left and middle, representative EPSC traces recorded 24 h after the last *in vivo* oLTP induction (oLTP) and in controls (no oLTP). Scale bars: 10 ms, 100 pA. Right, the input-output curves for AMPAR-EPSCs with (oLTP) and without (no oLTP) *in vivo* oLTP induction; ##$p < 0.05$ for the indicated comparison; **$p < 0.01$, ***$p < 0.001$ versus the same intensity in the no oLTP group, two-way RM ANOVA followed by SNK test; n = 18, 7 (oLTP) and 16, 6 (no oLTP). **K,** Sample traces and averaged data showing a significant increase in the AMPAR/NMDAR ratio in animals with oLTP induction; *$p < 0.05$, unpaired t test; n = 15, 7 (oLTP) and 13, 5 (no oLTP). Scale bars: 20 ms, 200 pA.

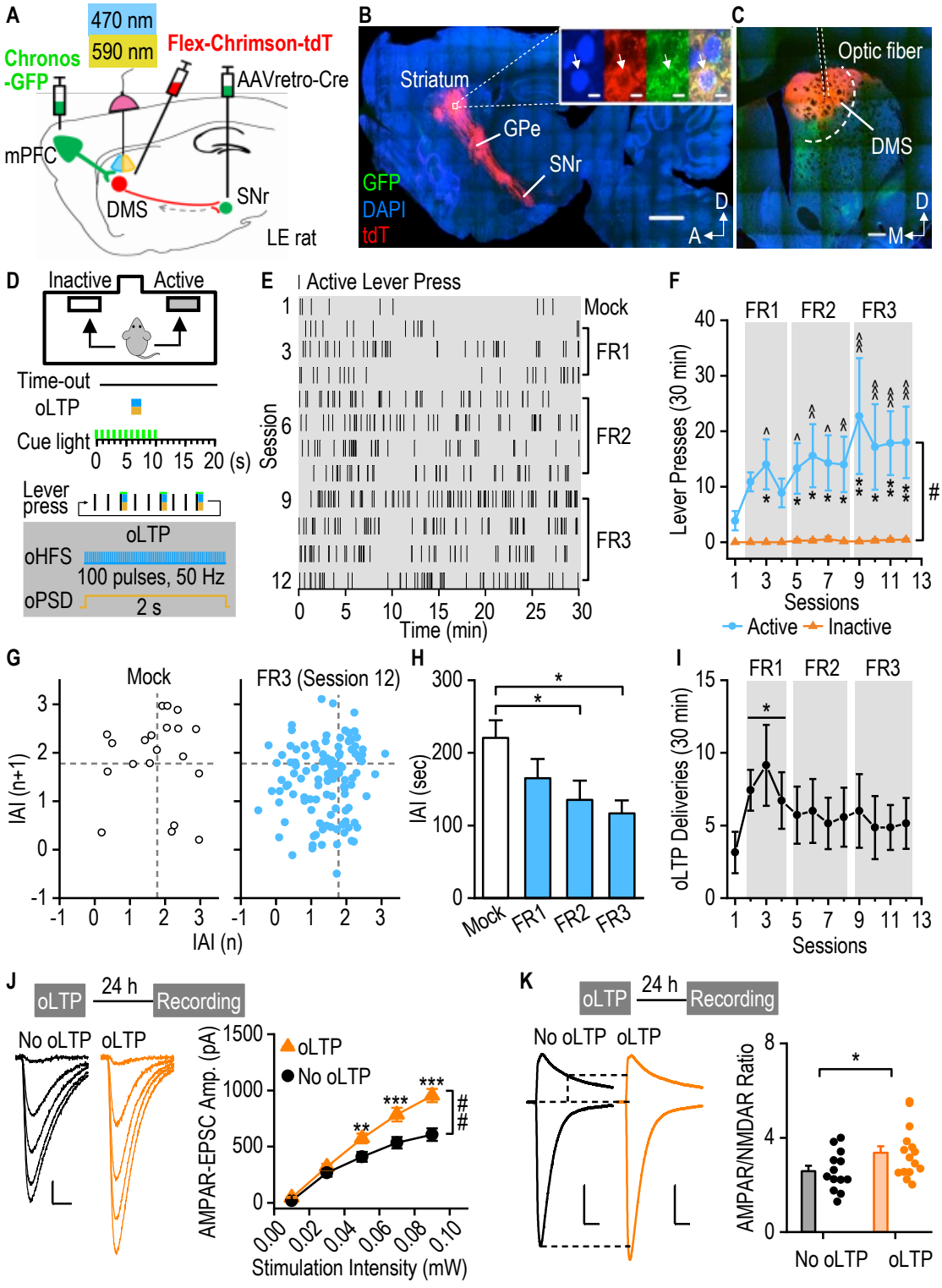
A
470 nm
590 nm
Chronos -GFP
Flex-Chrimson-tdT
AAVretro-Cre
mPFC
DMS
SNr
LE rat
B
Striatum
GPe
SNr
GFP
DAPI
tdT
C
Optic fiber
DMS
D
Inactive
Active
Time-out
oLTP
Cue light
0 5 10 15 20 (s)
Lever press
oLTP
oHFS
100 pulses, 50 Hz
oPSD
2 s
E
Active Lever Press
Mock
FR1
FR2
FR3
Session
Time (min)
F
FR1 FR2 FR3
Lever Presses (30 min)
Sessions
Active
Inactive
G
Mock
FR3 (Session 12)
IAI (n+1)
IAI (n)
H
IAI (sec)
Mock FR1 FR2 FR3
I
FR1 FR2 FR3
oLTP Deliveries (30 min)
Sessions
J
oLTP
24 h
Recording
No oLTP oLTP
AMPAR-EPSC Amp. (pA)
oLTP
No oLTP
Stimulation Intensity (mW)
K
oLTP
24 h
Recording
No oLTP oLTP
AMPAR/NMDAR Ratio
No oLTP oLTP

3.3.4. Time-locked *in vivo* stimulation of mPFC→D1-MSN synapses using an oLTD protocol produces a persistent reduction in rat ethanol-seeking behavior

The results described above suggested that excessive ethanol consumption was associated with a long-lasting strengthening of corticostriatal neurotransmission. Mimicking ethanol-induced potentiation of glutamatergic mPFC→D1-MSN synapses using self-induced oLTP also caused behavioral reinforcement. Given that ethanol-induced synaptic plasticity shares similar mechanisms with LTP and LTD, where LTP can be reversed by the induction of LTD (Luscher and Malenka, 2011; Lovinger and Abrahao, 2018; Ma et al., 2018), we reasoned that oLTD of mPFC→D1-MSNs would reverse synaptic strengthening and thus persistently attenuate ethanol-seeking and -taking behaviors in rats. We induced oLTD using a post-pre STDP protocol (Figure 3.4 A) employing 60 pairs of postsynaptic depolarization (590 nm, 2 ms) followed by presynaptic stimulation (470 nm, 2 ms) after 30 ms; these cycles were delivered every 10 s (Figure 3.4 A, Figure 3.3 A) (Shen et al., 2008; Verena Pawlak, 2008; Wu et al., 2015). This protocol induced a reliable LTD in DMS slices from ethanol naïve-rats (Figure 3.4 B; $t_{(4)} = 4.76$, $p < 0.05$). We also tested this protocol in slices from rats that were trained to self-administer ethanol in operant chambers. Surprisingly, the first post-pre STDP cycle did not induce LTD (Figure 3.4 C; $q = 0.44$, $p > 0.05$), while subsequent cycles induced a robust LTD (Figure 3.4 C; $F_{(3,14)} = 9.88$, $p < 0.001$ for three cycles; $q = 6.77$, $p < 0.01$ for the third cycle). This finding is consistent with a previous study showing that chronic ethanol exposure impaired LTD induction in D1-MSNs (Renteria et al., 2017). In contrast, presynaptic stimulation of mPFC fibers alone caused little suppression in

either ethanol-naïve (Figure 3.4 B; $t_{(2)} = -1.66$, $p > 0.05$) or ethanol-treated rats (Figure 3.4 C; $F_{(3,18)} = 1.35$, $p > 0.05$). Our *ex vivo* findings indicate that the post-pre STDP protocol successfully evokes oLTD in DMS slices.

We then asked whether *in vivo* delivery of this protocol altered ethanol-seeking and -taking behaviors in rats. To test this possibility, Chronos and Chrimson were expressed as described above, and optical fibers were separately implanted into the mPFC and the DMS. Animals were trained to self-administer 20% ethanol in operant chambers using a FR3 schedule. Once stable baseline active lever pressing was achieved during a mock induction session, time-locked post-pre STDP was delivered. For this study, we increased the frequency of light stimulation to 5 Hz and delivered a total of 900 post-pre pairs. During the *in vivo* oLTD-inducing sessions, three active lever presses (FR3) resulted in ethanol delivery and post-pre STDP (10 pairs at 5 Hz) (Figure 3.5 A). Rats underwent several 30-min time-locked oLTD induction sessions until an accumulative total of 900 pairs of post-pre stimulations had been delivered (Roltsch Hellard et al., 2019). This protocol induced a robust and reliable LTD in DMS slices from ethanol-native rats (Figure 3.4 D; $t_{(4)} = -7.80$, $p < 0.01$). In ethanol-drinking rats, we discovered that time-locked *in vivo* delivery of the post-pre STDP protocol significantly reduced active, but not inactive, lever presses (Figure 3.5 B, C; $F_{(1,10)} = 43.77$, $p < 0.05$). Specifically, active lever presses were reduced on day 2 after *in vivo* post-pre STDP, as compared to the baseline (Figure 3.5 B, C; $q = 6.17$, $p < 0.01$). This reduction was maintained for at least 10 days after optical stimulation (Figure 3.5 B, C; $q = 4.36, 4.66, 5.84, 4.29$ and $p < 0.05, 0.05, 0.01, 0.01$ for 4, 6, 8, 10 d, respectively). In

contrast, the number of inactive lever presses did not change after oLTD induction (Figure 3.5 C; q = 0.29, 0.15, 0.39, 0.20, 0.58 and p > 0.05, 0.05, 0.05, 0.05, 0.05 for 2, 4, 6, 8, 10 d, respectively).

Interestingly, we observed that during the 20-s ethanol delivery, there were additional active lever presses that did not result in reward delivery. We compared the numbers of effective active lever presses (prior to ethanol delivery) and ineffective active lever presses (during ethanol delivery). This analysis found that time-locked *in vivo* delivery of post-pre STDP specifically suppressed effective active lever presses (Figure 3.5 D; $F_{(1,10)}$ = 28.44, p < 0.05). Consistent with the effect of oLTD on total active lever presses, the suppression of effective active lever presses was also observed for 10 d (Figure 3.5 D; q = 5.78, 4.34, 4.31, 5.53, 4.23 and p < 0.01, 0.05, 0.05, 0.01, 0.01 for 2, 4, 6, 8, 10 d, respectively).

A reduced number of active lever presses could result from changes in the frequency of this behavior. To investigate this, we next analyzed the inter-action interval for active lever presses. Rats initially pressed the active lever rapidly to obtain an ethanol reward during mock induction, while delivery of the post-pre STDP significantly and persistently increased the inter-action interval for all active lever presses (Figure 3.5 E; $F_{(5,10)}$ = 6.12, p < 0.05; q = 6.71, 3.23, 6.51 and p < 0.01, 0.05, 0.01 for 2, 4, 8 d, respectively), and for effective active lever presses (Figure 3.6 A; $F_{(5,10)}$ = 3.85, p < 0.05). Additionally, return maps of the inter-action interval for all active lever presses showed that the post-pre STDP changed the action-outcome contingency (Figure 3.5 F).

Together, these results suggest that *in vivo* delivery of the post-pre STDP protocol time-locked to ethanol delivery causes a long-lasting reduction in effective active lever presses, and that this reduction is associated with an increased interval between presses.

Ethanol was delivered following three effective active lever presses (Figure 3.6 B; $t_{(2)} = -0.58$, $p > 0.05$). The STDP-associated reduction in effective active lever presses led to a long-lasting decrease in ethanol delivery (Figure 3.5 G; $F_{(5,10)} = 5.84$, $p < 0.05$; $q = 6.91, 6.07, 5.00, 4.10, 3.83$ and $p < 0.01, 0.05, 0.05, 0.05, 0.05$ for 2, 4, 6, 8, 10 d, respectively).

After ethanol was delivered, rats were expected to enter the magazine to collect the ethanol reward. To our surprise, the time-locked *in vivo* delivery of the post-pre STDP protocol affected neither total magazine entries (Figure 3.6 C; $t_{(2)} = 1.22$, $p > 0.05$) nor effective magazine entries during ethanol delivery (Figure 3.5 H; $t_{(2)} = 1.31$, $p > 0.05$). Similarly, delivery of the STDP protocol had no effect on the inter-action interval for total magazine entries (Figure 3.6 D; $F_{(5,10)} = 1.84$, $p > 0.05$) or for effective magazine entries during ethanol delivery (Figure 3.5 I; $F_{(5,10)} = 0.44$, $p > 0.05$). Return maps also suggested that rats showed indistinguishable magazine entry performance before and after the STDP (Figure 3.5 J).

However, consistent with the reduced number of ethanol deliveries, the time-locked *in vivo* delivery of the post-pre STDP protocol significantly reduced the number of collections; this was defined as the number of ethanol deliveries with at least one magazine entry (Figure 3.5 K; $F_{(5,10)} = 4.11$, $p < 0.05$). The stimulation also caused a long-lasting decrease in ethanol intake (Figure 3.5 L; $F_{(5,10)} = 7.61$, $p < 0.05$; $q = 6.49$, 6.24, 6.55, 7.53, 6.55 and $p < 0.01$, 0.01, 0.01, 0.01, 0.01 for 2, 4, 6, 8, 10 d, respectively).

Collectively, these results suggested that the time-locked *in vivo* delivery of the post-pre STDP protocol to mPFC→D1-MSN synapses persistently attenuated operant ethanol-seeking behaviors in rats.

Figure 3.4 Post-pre STDP stimulation of mPFC→D1-MSN synapses induced LTD in DMS slices.

A, Schematic illustration of the post-pre STDP protocol for LTD induction at mPFC→D1-MSNs using dual-channel optogenetics. D1-MSNs were depolarized by 590-nm light, followed by presynaptic stimulation by 470-nm light after 30 ms. Sixty such pairs were delivered every 10 s. **B,** Time-course (left) and bar graphs (right) showing that delivery of 60 post-pre STDP stimulation pairs, but not presynaptic stimulation only (Pre-only), induced LTD of field excitatory postsynaptic potentials/population spikes (fEPSP/PS) in DMS slices from ethanol-naïve rats; $^{**}p < 0.01$, paired t test; n = 5 slices, 3 rats (Post-Pre) and 3 slices, 2 rats (Pre-only). **C,** Time-course (left) and bar graphs (right) showing that multiple deliveries of the post-pre STDP protocol induced LTD of fEPSP/PS in DMS slices from ethanol-drinking rats; $^{*}p < 0.05$, $^{**}p < 0.01$ versus BL, one-way RM ANOVA followed by SNK test; n = 6 slices, 4 rats (Post-Pre) and 7 slices, 5 rats (Pre-only). **D,** Delivery of 900 post-pre STDP stimulation pairs (5 Hz) induced LTD in DMS slices from ethanol-naïve rats; $^{**}p < 0.01$, paired t test; n = 5 slices, 3 rats. Scale bars: 2 ms, 0.1 mV (B-D).

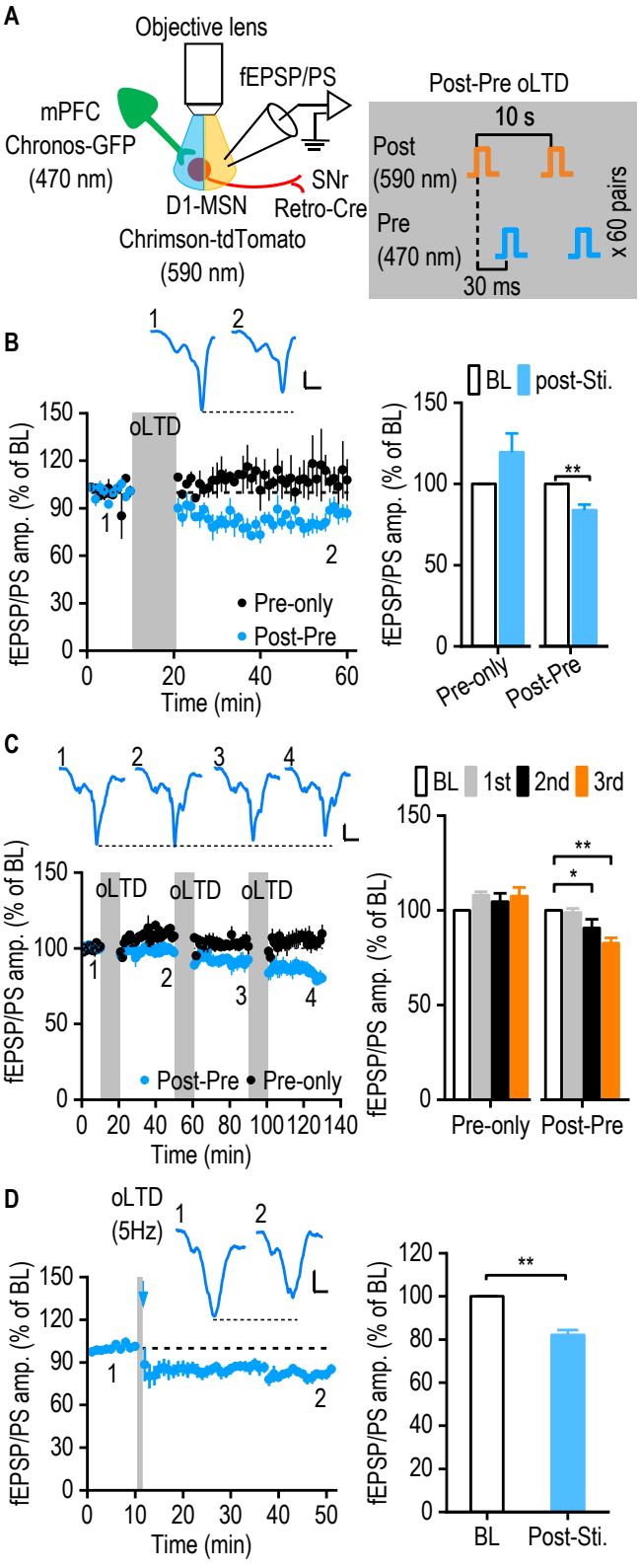
A
Objective lens
fEPSP/PS
mPFC
Chronos-GFP
(470 nm)
SNr
D1-MSN
Retro-Cre
Chrimson-tdTomato
(590 nm)
Post-Pre oLTD
10 s
Post
(590 nm)
Pre
(470 nm)
30 ms
x 60 pairs
B
oLTD
fEPSP/PS amp. (% of BL)
Pre-only
Post-Pre
Time (min)
BL
post-Sti.
**
C
oLTD
oLTD
oLTD
BL
1st
2nd
3rd
*
D
oLTD
(5Hz)
Post-Sti.

Figure 3.5 *In vivo* optogenetic induction of mPFC→D1-MSN LTD time-locked to active lever presses for ethanol persistently reduced ethanol-seeking behavior. **A,** Schematic of the training protocol and *in vivo* oLTD induction in Long-Evans (LE) rats. Optical fibers were separately implanted in the mPFC and DMS. Chronos-expressing mPFC neurons and Chrimson-expressing D1-MSNs were activated by 470- and 590-nm light, respectively. Rats were trained to self-administer 20% ethanol (EtOH) in an operant setting using a 30-min FR3 schedule. Once a stable baseline performance had been attained during mock induction (BL), light stimulation was delivered via the implanted optical fibers at the same time as EtOH delivery. In the post-pre STDP protocol employed to induce oLTD, postsynaptic D1-MSN depolarization preceded presynaptic stimulation by 30 ms. Three active lever presses triggered both EtOH delivery and post-pre STDP stimulation (10 pairs, 5 Hz). After 900 stimulation pairs had been delivered, post-oLTD operant self-administration of ethanol was measured for 10 d. **B,** Example raster plot of active lever presses during 30-min self-administration of 20% EtOH at BL (mock), during time-locked oLTD induction, and on the indicated days post-oLTD induction. Each vertical line represents one lever press. **C,** Time-locked delivery of the *in vivo* oLTD-inducing protocol and EtOH produced a long-lasting reduction in active lever presses, but not in inactive lever presses; #$p < 0.05$ for the indicated comparison; *$p < 0.05$, **$p < 0.01$, ***$p < 0.001$ versus inactive lever presses on the same day; ^$p < 0.05$, ^^$p < 0.01$ versus active lever presses during mock induction (BL); two-way RM ANOVA followed by SNK test. **D,** *In vivo* oLTD stimulation significantly reduced effective active lever presses, prior to ethanol delivery, but not ineffective active lever presses during ethanol delivery; #$p < 0.05$ for the indicated comparison; *$p < 0.05$, **$p < 0.01$, ***$p < 0.001$ versus active lever presses during ethanol delivery on the same day; ^$p < 0.05$, ^^$p < 0.01$ versus active lever presses prior to ethanol delivery during mock induction (BL); two-way RM ANOVA followed by SNK test. **E,** The time-locked *in vivo* oLTD induction and EtOH delivery produced a sustained increase in the inter-action interval (IAI) for active lever presses; *$p < 0.05$, **$p < 0.01$ versus mock induction (BL); one-way RM ANOVA followed by SNK test. **F,** Return maps of IAI for active lever presses during mock induction (left) and on day 2 post-stimulation (right). Each dot represents the time delay to its preceding (x) and succeeding (y) behavioral element. Data are Log10 transformed. Dashed lines represent Log10(60) = 1.78. Note that there are fewer dots within the bottom left quadrant on day 2 post-oLTD, as compared with mock induction. **G,** Time-locked *in vivo* oLTD induction caused a long-lasting reduction in ethanol delivery; *$p < 0.05$, **$p < 0.01$ versus mock induction (BL); one-way RM ANOVA followed by SNK test. **H and I,** No significant change in either effective magazine entries (H) or the IAI for effective magazine entries (I) was observed following *in vivo* oLTD induction during ethanol delivery. **J,** Return maps of IAI for magazine entries identified no significant difference between the numbers of dots within the bottom left quadrants during mock induction (left) and on day 2 post-oLTD (right). **K and L,** Delivery of *in vivo* oLTD time-locked to active lever presses caused a sustained decrease in EtOH collections (the number of EtOH delivery with at least one magazine entry) (K) and EtOH intake (L); *$p < 0.05$, **$p < 0.01$ versus mock induction (BL); one-way RM ANOVA followed by SNK test. n = 3 rats (C-L).

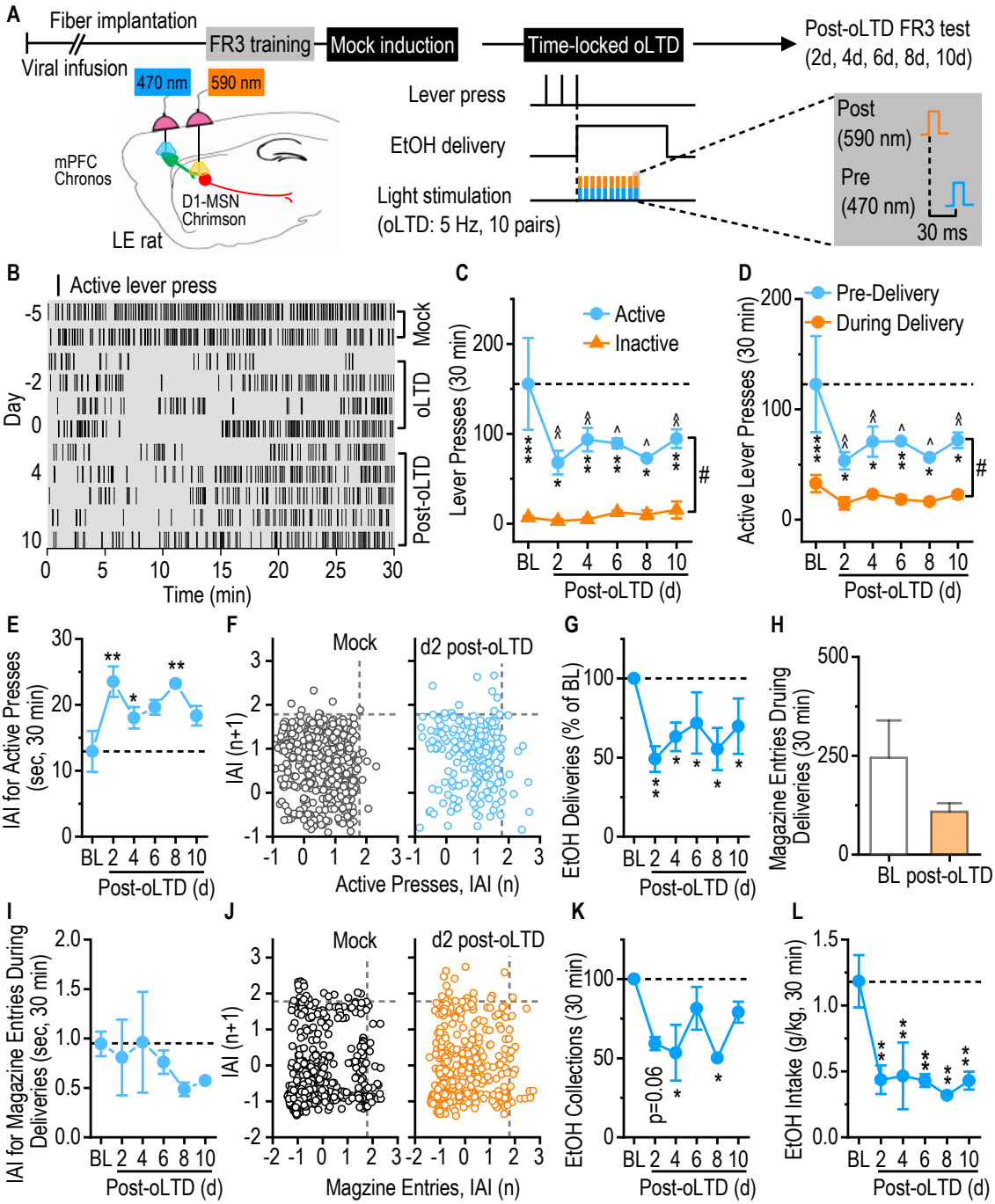
A
Fiber implantation
Viral infusion
FR3 training
Mock induction
Time-locked oLTD
Post-oLTD FR3 test
(2d, 4d, 6d, 8d, 10d)
470 nm
590 nm
mPFC
Chronos
D1-MSN
Chrimson
LE rat
Lever press
EtOH delivery
Light stimulation
(oLTD: 5 Hz, 10 pairs)
Post
(590 nm)
Pre
(470 nm)
30 ms
B
Active lever press
Day
Mock
oLTD
Post-oLTD
Time (min)
C
Active
Inactive
Lever Presses (30 min)
Post-oLTD (d)
D
Pre-Delivery
During Delivery
Active Lever Presses (30 min)
Post-oLTD (d)
E
IAI for Active Presses (sec, 30 min)
Post-oLTD (d)
F
Mock
d2 post-oLTD
IAI (n+1)
Active Presses, IAI (n)
G
EtOH Deliveries (% of BL)
Post-oLTD (d)
H
Magazine Entries Druing Deliveries (30 min)
BL post-oLTD
I
IAI for Magazine Entries During Deliveries (sec, 30 min)
Post-oLTD (d)
J
Mock
d2 post-oLTD
IAI (n+1)
Magzine Entries, IAI (n)
K
EtOH Collections (30 min)
p=0.06
Post-oLTD (d)
L
EtOH Intake (g/kg, 30 min)
Post-oLTD (d)

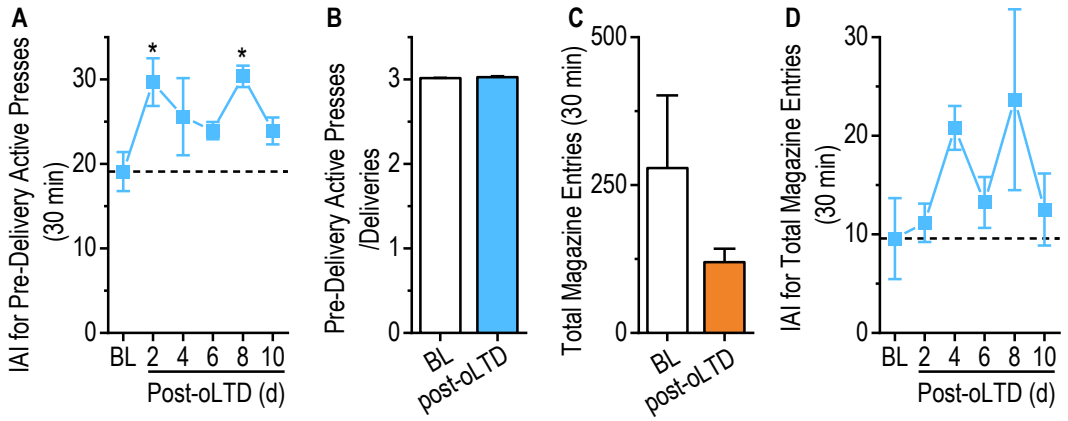

Figure 3.6 *In vivo* optogenetic induction of mPFC→D1-MSN LTD time-locked to active lever presses for ethanol persistently reduced the active lever presses but not magazine entries.

A, Light stimulation for oLTD induction produced a long-lasting increase in the inter-action interval (IAI) for active lever presses prior to ethanol delivery; *$p < 0.05$ versus mock induction (BL); one-way RM ANOVA followed by SNK test. **B,** The ratio of active lever presses prior to ethanol delivery did not differ before (BL) and after oLTD induction. **C and D,** Light stimulation for *in vivo* oLTD induction produced no significant changes in total magazine entries (C) or the IAI for total magazine entries (D). n = 3 rats (A-D).

3.3.5. Time-locked *in vivo* stimulation of mPFC→D1-MSN synapses using the oLTD protocol produces a persistent reduction of glutamatergic transmission in DMS slices

Lastly, to ascertain the effects of *in vivo* post-pre STDP on glutamatergic transmission, we prepared DMS slices form rats expressing Chrimson-tdT in D1-MSNs two days after the last light stimulation. We used whole-cell recording to measure corticostriatal EPSCs from both Chrimson-tdT-positive and -negative striatal neurons underneath the optical fiber (Figure 3.7 A, B). We found that the *in vivo* delivery of the post-pre STDP protocol caused an increase in paired-pulsed ratio in D1-MSNs (Chrimson-tdT positive); this indicated that these neurons had a reduced probability of glutamate release, as compared to neurons from control animals without the STDP stimulation (Figure 3.7 C; $t_{(35)} = -4.14$, $p < 0.05$). In contrast, we did not observe any changes in the paired-pulse ratio of putative D2-MSNs (Chrimson-tdT negative) after the STDP stimulation, as compared to neurons from control rats (Figure 3.8; $t_{(26)} = -0.70$, $p > 0.05$). To further investigate the properties of mPFC→D1-MSN synapses after the STDP stimulation, we measured the Sr^{2+}-induced asynchronous EPSCs (aEPSCs) evoked by optical stimulation of the mPFC input. Replacement of Ca^{2+} in the recording solution by Sr^{2+} caused asynchronous exocytosis of vesicles during light stimulation (Ding et al., 2008; Renteria et al., 2018; Lu et al., 2019). In the STDP group, we observed a significant decrease in the frequency of asynchronous release onto D1-MSNs, as compared to that observed in neurons from the control group without oLTD induction (Figure 3.7 D, E; $t_{(29)} = 2.52$, $p < 0.05$); this reflected a decrease in release

probability. In contrast, there were no significant differences between the aEPSC amplitude of the STDP and control groups (Figure 3.7 D, F; $t_{(29)} = -0.83$, $p > 0.05$); this suggested that the *in vivo* STDP stimulation did not affect vesicle size or postsynaptic AMPAR components at mPFC→D1-MSNs (Ding et al., 2008). Taken together, these findings indicate that *in vivo* time-locked delivery of the post-pre STDP protocol induces oLTD of glutamatergic mPFC→ DMS D1-MSN transmission, associated with reduced glutamate release.

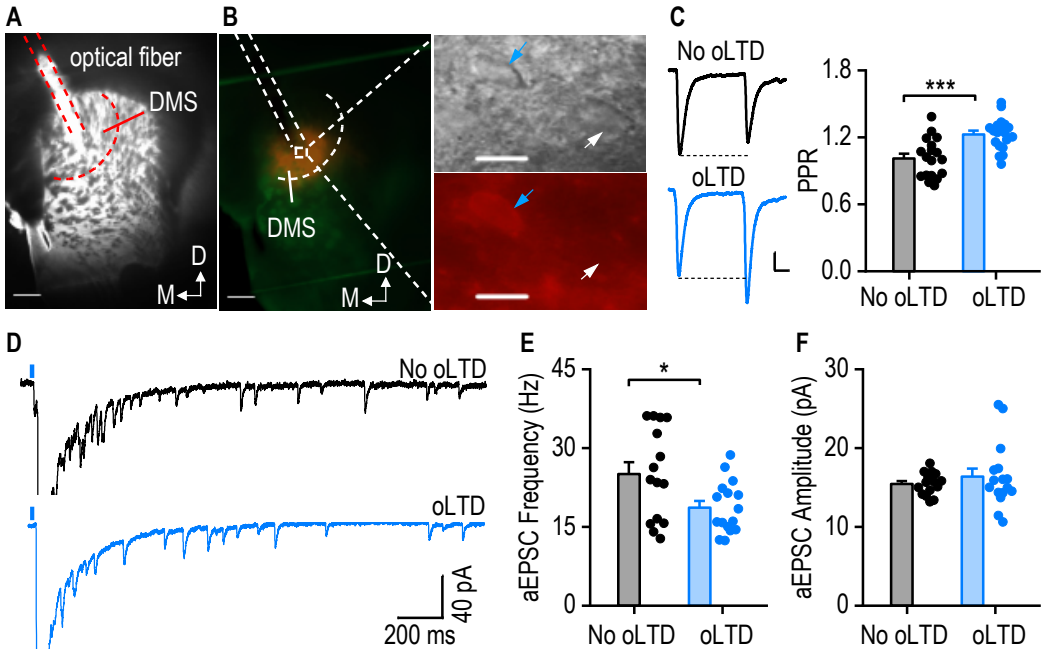

Figure 3.7 *In vivo* optogenetic induction of mPFC→D1-MSN LTD time-locked to active lever presses for ethanol persistently reduced glutamatergic transmission in DMS D1-MSNs.

A and B, Representative differential interference contrast (A) and fluorescent images (B) of a striatal slice showing the optical fiber track, Chronos-GFP, and Chrimson-tdT expression in the DMS. Whole-cell recording was performed in the area receiving light stimulation during oLTD induction (boxed area of B, left). Higher magnification images of a Chrimson-expressing D1-MSN (blue arrow) and a Chrimson-negative neuron (white arrow) (B, right). Scale bars: 500 µm (A, B left), 10 µm (B right). D, dorsal; M, medial. **C,** Sample traces (left) and averaged data (right) showing an increased PPR in Chrimson-expressing D1-MSNs recorded 2 days after the last *in vivo* oLTD induction; ***$p < 0.001$, unpaired t test; n = 18, 5 (No oLTD) and 19, 5 (oLTD). Scale bars: 20 ms, 50 pA. **D,** Sample traces of Sr^{2+}-induced aEPSCs recorded at Chrimson-expressing D1-MSNs. The EPSCs were evoked by 2-ms 470-nm light in the presence of 2.5 mM Sr^{2+}. E and F, Bar graphs summarizing aEPSC frequency (E) and amplitude (F) at mPFC inputs onto Chrimson-expressing D1-MSNs; *$p < 0.05$, unpaired t test; n = 15, 5 (No oLTD) and 16, 5 (oLTD).

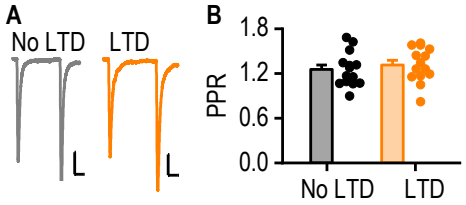

Figure 3.8 *In vivo* optogenetic induction of mPFC→D1-MSN LTD time-locked to active lever presses for ethanol did not alter the PPR in Chrimson-negative DMS neurons on day 2 post-stimulation.
Sample traces (A) and averaged data (B) showing no change in the PPR in Chrimson-negative neurons 2 days after the last time-locked *in vivo* oLTD induction; n = 14 neurons, 5 rats per group. Scale bars: 20 ms, 50 pA.

Table 3.1 Ethanol consumption by transgenic mice

Mouse line	Ethanol intake (g/kg/24 h)	
D1-Cre;Ai14	21.63 ± 2.17	n = 5
D2-Cre;Ai14	22.18 ± 0.30	n = 4
D1-tdT;Fos-Cre;Snap25	20.51 ± 2.09	n = 5

All mice were exposed to 20% ethanol using the intermittent access two-bottle choice drinking procedure. There was no significant difference in ethanol intake among the mouse lines; $p > 0.05$, one-way ANOVA.

3.4. Discussion

The present study revealed that more D1-MSNs within the dorsal striatum were activated in mice engaged in excessive ethanol consumption than in those consuming water only. We found that cycles of ethanol consumption and withdrawal potentiated both AMPAR- and GluN2B-NMDAR-mediated synaptic transmission selectively at mPFC inputs onto D1-MSNs. This potentiation was accompanied by an increase in glutamate release. Mimicking this ethanol-evoked mPFC→D1-MSN potentiation via self-stimulation of this synapse using optogenetic LTP induction was sufficient to elicit reinforcement of operant behaviors. Importantly, reversal of this synaptic plasticity via *in vivo* LTD induction produced a long-lasting reduction in ethanol-seeking behavior. The present study has elucidated the detailed mechanisms involved in ethanol-mediated circuit-specific plasticity in the DMS, which may contribute to excessive ethanol consumption.

3.4.1. Ethanol-induced D1R-expressing neuronal ensembles in the dorsal striatum

Using the recently developed FosTRAP technology (Allen et al., 2017; DeNardo et al., 2019), we found that a higher percentage of DMS D1R-expressing neurons were activated in mice engaged in excessive ethanol consumption, as compared to those drinking water only. These data are consistent with previous studies showing that excessive ethanol consumption is associated with elevated D1-MSN activity, while inhibition of D1-MSNs reduces ethanol intake (Cheng et al., 2017; Ma et al., 2018). Surprisingly, we observed that the majority of neurons TRAPed during ethanol-drinking sessions did not colocalize with the D1-MSN reporter. Because the vast majority of

striatal neurons are MSNs (Kreitzer and Malenka, 2008; Cheng et al., 2017) and a previous transgenic mouse model suggested less than 5% overlap of DMS D1-MSNs and D2-MSNs (Cheng et al., 2017), those D1R-negative ensembles were likely to be D2-MSNs. Our data appear to be inconsistent with the predominant current model of basal ganglia function, which postulates that there should be more activity in the direct pathway circuit than in the indirect pathway circuit during reward-driven behaviors (DeLong, 1990; Kreitzer and Malenka, 2008). However, it is consistent with other models proposing that the coordinated activation of both D1-MSNs and D2-MSNs is important for action selection, by reinforcing the current action via the direct pathway and suppressing potentially conflicting actions via the indirect pathway (Chan et al., 2005; Brown, 2007; Bromberg-Martin et al., 2010; Hikida et al., 2010; Cui et al., 2013). Additionally, we observed that 80% of TRAPed striatal cells in the water-drinking group were putative D2-MSNs, with a significant decrease in this proportion in ethanol-drinking mice. This observation is supported by our recent report that GABAergic activity was exclusively increased in D2-MSNs following cycles of excessive ethanol consumption and withdrawal (Cheng et al., 2017). Given the negative role of D2-MSNs in the regulation of ethanol consumption (Cheng et al., 2017; Roltsch Hellard et al., 2019), our findings indicate that under physiological conditions, D2-MSNs were highly activated to suppress actions, but this activity was inhibited during the addictive ethanol-drinking behaviors. Taken together, both increased activation of D1-MSNs and decreased activation of D2-MSNs were associated with a reinforcement of pathological excessive ethanol consumption.

Interestingly, we also found a higher percentage of the D1R-expresing neuronal ensemble in the posterior dorsal striatum than in the anterior region. The anterior dorsal striatum has been shown to be important for visual cues (Williams and Eskandar, 2006) and sensory-guided learning and behavior (Lee et al., 2019). The posterior striatum is critical for selective instrumental and Pavlovian reward learning (Yin et al., 2005a; Corbit and Janak, 2010; Shiflett et al., 2010). Considering that our animals were trained to excessively consume 20% ethanol using intermittent-access two-bottle choice for 8 weeks, our data suggested that the posterior striatum may play an important role in chronic excessive ethanol consumption.

3.4.2. Manipulation of ethanol-evoked circuit-specific plasticity

Ethanol induces abnormal learning and memory, and this involves modulation of striatal synaptic plasticity (Abrahao et al., 2017; Ma et al., 2018). Chronic ethanol exposure has been found to facilitate corticostriatal LTP and dampen endocannabinoid-mediated LTD at corticostriatal synapse (Wang et al., 2012a; Ma et al., 2018). Using optogenetic and transgenic tools, we observed ethanol-induced circuit-specific potentiation at mPFC inputs onto D1-MSNs. This enhanced synaptic strength was due to both stronger postsynaptic AMPAR- and GluN2B-containing NMDAR-mediated responses, and an enhanced probability of presynaptic transmitter release. This is consistent with other studies showing that addictive substances, including ethanol, potentiated glutamatergic responses in D1-MSNs, but not D2-MSNs (MacAskill et al., 2014; Wang et al., 2015; Cheng et al., 2017; Cheng et al., 2018; Ma et al., 2018).

A leading addiction hypothesis posits that drugs of abuse reinforce addictive behaviors because they increase the concentration of dopamine in the brain (Pascoli et al., 2015; Volkow and Morales, 2015; Bamford et al., 2018). The behavioral importance of dopamine has been confirmed using optogenetic self-stimulation of mesolimbic dopamine neurons to mimic the reinforcement of addictive drugs (Pascoli et al., 2015; Pascoli et al., 2018). In addition to reinforcing behavior, self-stimulation of dopamine neurons selectively elicited a synaptic potentiation in D1-MSNs that was indistinguishable from cocaine-induced plasticity (Pascoli et al., 2012; Pascoli et al., 2014; Pascoli et al., 2015). Dopamine-dependent corticostriatal plasticity has been considered to be the mechanism underlying drug-induced reinforcement (MacAskill et al., 2014; Pascoli et al., 2015; Bamford et al., 2018). The observation that cocaine self-administration occluded optogenetic self-stimulation of dopamine neurons supports the importance of this system (Pascoli et al., 2015). However, much less is known about whether corticostriatal plasticity is sufficient to drive the reinforcement of behavior. To circumvent issues of non-specificity, we trained rats to self-stimulate the corticostriatal synapse via a well-established dual-channel optogenetic LTP-inducing protocol that employed presynaptic high-frequency stimulation paired with postsynaptic depolarization (Ma et al., 2018); this was used to mimic ethanol-evoked potentiation. We repeatedly paired a specific action (active lever press) with *in vivo* stimulation of mPFC→D1-MSN synapses to induce LTP and observed reinforcement in operant behavior. Additionally, a reduction in the inter-action intervals between active lever presses suggested that LTP induction at mPFC→D1-MSNs had a positive effect on the

initial acquisition of instrumental contingency (Matamales et al., 2020). Lastly, the induction of LTP was confirmed by post-induction electrophysiological recording. Taken together, these results support the idea that corticostriatal synaptic plasticity is sufficient for reinforcement learning.

Deep brain stimulation techniques are entering widespread use for the investigation and treatment of neurological and neuropsychiatric disorders (Peterchev et al., 2012; Creed et al., 2015). We recently reported that optogenetic inhibition of D1-MSNs in the DMS, or of their axonal terminals in the SNr, transiently reduced lever presses for ethanol without altering locomotor activity (Roltsch Hellard et al., 2019). Moreover, *in vivo* induction of LTD in DMS D1-MSNs using optogenetic high-frequency stimulation, combined with systemic administration of glutamatergic NMDAR and D2R antagonists, persistently suppressed ethanol-seeking behavior (Ma et al., 2018). However, systemically administered NMDAR and D2R antagonists can influence neurons in both diseased and healthy brain regions. Additionally, our previous studies induced oLTD outside the operant chambers, which occurred in the absence of the context of alcohol-seeking or -taking behavior (Ma et al., 2018; Roltsch Hellard et al., 2019). There is evidence showing that the state of the brain during the stimulation can change the outcome of the intervention (Silvanto et al., 2008; Mansouri et al., 2018). Previous studies (Verena Pawlak, 2008; Wu et al., 2015) have shown that endocannabinoid-mediated LTD can be induced specifically in D1-MSNs in slices using STDP without the inclusion of NMDAR and D2R antagonists. The present study took advantage of *in vivo* dual-channel optogenetics to induce LTD when rats engaged in

ethanol-seeking behavior. We discovered that optogenetic delivery of a post-pre STDP LTD-inducing protocol reduced operant self-administration of ethanol for 10 d. Whole-cell recording in DMS slices prepared from rats 2 d after light stimulation showed that glutamate release was reduced, suggesting persistent expression of *in vivo* LTD. Interestingly, we found that oLTD induction at the mPFC→D1-MSN synapse reduced ethanol-seeking behavior more effectively than it did ethanol-taking (magazine entry) behavior. It has been reported that brain circuits controlling drug-seeking behaviors are dissociable from those regulating drug-taking behaviors (Luscher et al., 2020).

Acquisition of goal-directed drug-seeking depends on the DMS and on afferents from the mPFC and orbitofrontal cortex (Luscher et al., 2020). This view is supported by the observation that optogenetic inhibition of the corticostriatal pathway decreases ethanol-seeking behaviors (Ma et al., 2018; Roltsch Hellard et al., 2019). Although drug-taking behaviors also depend on the plasticity of projections from the mPFC and orbitofrontal cortex to the DMS (Luscher et al., 2020), some evidence suggests that there is more activity in orbitofrontal cortex-DMS connections and less engagement of mPFC-ventrolateral striatum circuitry in compulsive methamphetamine taking (Hu et al., 2019). Additionally, the oLTD induction in the present study was time-locked to pressing of the active lever, which may have increased the sensitivity of this ethanol-seeking behavior to the oLTD-mediated suppression.

In summary, the present study demonstrated that excessive ethanol consumption potentiated glutamatergic mPFC→D1-MSN neurotransmission. Notably, we showed that this corticostriatal plasticity was sufficient to elicit reinforcement behavior.

Additionally, reversal of this potentiation reduced ethanol-seeking behavior. These findings are expected to facilitate the development and optimization of future circuit-based therapeutics for ethanol use disorder.

3.5. Materials and methods

3.5.1. Reagents

AAV8-Syn-Chronos-GFP and AAV8-Syn-Flex-Chrimson-tdTomato (tdT) were purchased from the University of North Carolina Vector Core. Retrograde AAVretro-Cre-GFP (pENN.AAV.hSyn.HI.eGFP-Cre.WPRE.SV40) was obtained from Addgene. NBQX and APV were purchased from R&D Systems. Ro 25-6981 was obtained from Tocris Bioscience. Picrotoxin, strontium, 4-hydroxytamoxifen (4-OHT), and other reagents were purchased from Sigma.

3.5.2. Animals

Drd1a-Cre (D1-Cre) and Drd2-Cre (D2-Cre) mice were obtained from the Mutant Mouse Regional Resource Centers (Wang et al., 2015; Cheng et al., 2017; Cheng et al., 2018; Wei et al., 2018; Lu et al., 2019). Drd1a-tdT (Ade et al., 2011), Ai14 (Madisen et al., 2010), Snap25 (Madisen et al., 2015), and Fos-iCreER (TRAP2) mice (Allen et al., 2017; DeNardo et al., 2019) were purchased from the Jackson Laboratory. Long-Evans rats were obtained from Harlan Laboratories. TRAP2 mice were crossed with Snap25 and D1-tdT mice to obtain the D1-tdT;Fos-Cre;Snap25 mice (Figure 3.1). D1-Cre and D2-Cre mice were crossed with Ai14 to obtain D1-Cre;Ai14 and D2-Cre;Ai14 mice (Figure 3.2). Mouse genotypes were determined by PCR analysis of Cre or the fluorescent protein gene in tail DNA (Cre for D1-Cre and D2-Cre mice; tdT for

D1-tdT and Ai14 mice; GFP for Snap25 mice) (Wang et al., 2015; Cheng et al., 2017; Cheng et al., 2018; Wei et al., 2018; Lu et al., 2019). Male 2-3-month-old mice and Long-Evans rats were used in Figures 3.2-3.5; male and female mice were used in Figure 3.1. Animals were housed in a temperature- and humidity-controlled vivarium with a 12-h light/dark cycle (lights on at 11:00 P.M.). All behavior experiments were conducted in their dark cycle. Food and water were available ad libitum. All animal care and experimental procedures were approved by the Texas A&M University Institutional Animal Care and Use Committee.

3.5.3. Intermittent-access to 20% ethanol two-bottle-choice drinking procedure

To establish high levels of ethanol consumption in mice, we utilized the intermittent-access to 20% ethanol two-bottle-choice drinking procedure (Wang et al., 2015; Cheng et al., 2017; Cheng et al., 2018; Wei et al., 2018). D1-tdT;Fos-Cre;Snap25 mice, D1-Cre;Ai14, and D2-Cre;Ai14 mice were given free access to two bottles containing water or 20% ethanol for three 24-h sessions (Mondays, Wednesdays, and Fridays), with 24-h or 48-h withdrawal periods (Tuesdays, Thursdays, Saturdays, and Sundays) each week. During the withdrawal periods, the mice had unlimited access to water bottles. The placement of the ethanol bottle was alternated for each drinking session to control for side preferences. Control animals were treated in the same manner, except that they were presented with water only. This procedure was followed for 8 weeks.

3.5.4. Capturing neuronal ensembles and drug preparation

After 8 weeks of two-bottle choice training, D1-tdT;Fos-Cre;Snap25 mice were habituated to intraperitoneal (i.p.) injection of saline for three consecutive ethanol-drinking sessions. On the fourth ethanol-drinking session (TRAPing day), animals were i.p. injected with either 50 mg/kg 4-OHT or saline under infrared light 2 h before ethanol exposure. Animals were then returned to their home-cage until the time of sacrifice, which was 2 weeks after TRAPing. 4-OHT was prepared as described in previous studies (Allen et al., 2017; DeNardo et al., 2019). Briefly, a 20-mg/mL stock solution was prepared by shaking 4-OHT powder in 200 proof ethanol at 37°C until the 4-OHT had dissolved. The stock solution was protected from light and stored as aliquots at -20°C for several weeks. Before each use, the 4-OHT stock was shaken at 37°C to ensure that it was dissolved. An equal volume of a 1:4 mixture of castor oil:sunflower seed oil was added to give a final concentration of 10 mg/mL 4-OHT, and the ethanol was evaporated by centrifugation under a vacuum. The final 4-OHT in oil was stored at 4°C for a maximum of 12 h before use.

3.5.5. Confocal imaging and cell counting

Animals were perfused intracardially with 4% paraformaldehyde in phosphate-buffered saline. The brains were removed and post-fixed overnight in 4% paraformaldehyde in phosphate-buffered saline at 4°C prior to dehydration in 30% sucrose solution. The brains were cut into 50-µm coronal or sagittal sections using a cryostat. Fluorescent images were acquired using a confocal microscope (FluoView 1200, Olympus, Tokyo, Japan) and analyzed using IMARIS 8.3.1 (Bitplane, Zürich,

Switzerland), as previously reported (Cheng et al., 2017; Wei et al., 2018; Lu et al., 2019). Cell counting was performed in 11 D1-tdT;Fos-Cre;Snap25 mice. In each brain region, a total of 33-35 brain sections were imaged from each mouse. Imaris 8.3.1 was used to count green and red neurons, and to calculate co-localization. Brain regions were subdivided using the Paxinos Mouse Brain Atlas (Franklin and Paxinos, 2007).

3.5.6. Stereotaxic virus infusion

The stereotaxic virus infusion procedure was conducted as described previously (Ma et al., 2018; Lu et al., 2019; Roltsch Hellard et al., 2019). Where required for the experimental design, AAV-Chronos-GFP was bilaterally infused into the mPFC (AP: +1.94 mm, ML: ±0.25 mm, DV: -2.5 mm from the Bregma) of D1-Cre;Ai14 and D2-Cre;Ai14 mice (Figure 3.2). In rats, AAV-Chronos-GFP was infused into the mPFC (AP1: +3.2 mm, ML1: ±0.65 mm, DV1: -4.0 mm; AP2: +2.6 mm, ML2: ±0.65 mm, DV2: -4.0 mm from the Bregma), AAV-Flex-Chrimson-tdT was infused into the DMS (AP1: +1.2 mm, ML1: ±1.9 mm, DV1: -4.7 mm; AP2: + 0.36 mm, ML2: ±2.3 mm, DV2: -4.7 mm from the Bregma), and AAVretro-Cre-GFP was infused into the substantia nigra pars reticulata (SNr) (AP1: -4.92 mm, ML1: ±2.3 mm, DV1: -8.3 mm; AP2: -5.5 mm, ML2: ±2.0 mm, DV2: -8.6 mm from the Bregma). Animals were anesthetized with 3 4% isoflurane at 1.0 L/min and mounted in a stereotaxic surgery frame. The head was leveled and craniotomy was performed using stereotaxic coordinates adapted from the mouse brain atlas (Franklin and Paxinos, 2007). A volume of 0.5 μL/site (mice) or 1 μL/site (rats) of virus was infused at a rate of 0.08 μL/min. At the end of the infusion, the injectors remained at the injection site for an additional 10-15

min before removal to allow for virus diffusion. The scalp incision was then sutured, and the animals were returned to their home cage for recovery.

3.5.7. Slice electrophysiology

Slice preparation. Slices were prepared and electrophysiological recordings were conducted as described previously (Cheng et al., 2017; Huang et al., 2017; Ma et al., 2017; Ma et al., 2018; Lu et al., 2019; Roltsch Hellard et al., 2019). Briefly, coronal sections containing the striatum (250 μm) were cut in an ice-cold cutting solution containing (in mM): 40 NaCl, 148.5 sucrose, 4 KCl, 1.25 NaH_2PO_4, 25 $NaHCO_3$, 0.5 $CaCl_2$, 7 $MgCl_2$, 10 glucose, 1 sodium ascorbate, 3 sodium pyruvate, and 3 myo-inositol. The solution was saturated with 95% O_2 and 5% CO_2. Slices were then incubated in a 1:1 mixture of the cutting solution and external solution at 32°C for 45 min. The external solution was composed of the following (in mM): 125 NaCl, 4.5 KCl, 2.5 $CaCl_2$, 1.3 $MgCl_2$, 1.25 NaH_2PO_4, 25 $NaHCO_3$, 15 glucose, and 15 sucrose. The external solution was saturated with 95% O_2 and 5% CO_2. Slices were then maintained in the external solution at room temperature until use. Striatal slices were prepared from ethanol-drinking mice 24 h after the last ethanol-drinking session (Figure 3.2), 24 h after the last self-stimulation to induce optogenetic LTP (oLTP) in rats (Figure 3.3), and 2 d after the last time-locked optogenetic LTD (oLTD) induction in rats (Figure 3.7).

Whole-cell recordings. Individual slices were transferred to a recording chamber and continuously perfused with the external solution at a rate of 2-3 mL/min at 32°C. Picrotoxin (100 μM) was included in the external solution of all recordings to block $GABA_A$ receptor-mediated transmission. Fluorescent axonal fibers and neurons

were visualized using an epifluorescent microscope (Examiner A1, Zeiss). Prior to patching onto a cell, the presence of tdT expression was used to verify the cell type, as well as GFP expression for mPFC terminal expression of Chronos. MSNs were clamped at -70 mV. We used a Cs-based intracellular solution containing (in mM): 119 $CsMeSO_4$, 8 tetraethylammonium chloride, 15 4-(2-hydroxyethyl) piperazine-1-ethanesulfonic acid (HEPES), 0.6 ethylene glycol tetraacetic acid (EGTA), 0.3 Na_3GTP, 4 MgATP, 5 QX-314, and 7 phosphocreatine, with an osmolarity of ~280 mOsm/L. The pH was adjusted to 7.3 with CsOH.

For selective stimulation of inputs from channelrhodopsin-expressing fibers onto DMS neurons, 470-nm light was delivered through the objective lens for 2 ms. To generate input-output curves for AMPAR- and NMDAR-mediated EPSCs, light-evoked currents were recorded at 5 different stimulation intensities. NMDAR-EPSCs were measured in the presence of 0.05 mM Mg^{2+} and 10 μM NBQX. Paired-pulse ratios were calculated by dividing the second light-evoked EPSC by the first, with a 100-ms interval between the two. The proportion of NMDARs containing the GluN2B subunit (GluN2B/NMDAR ratio) was measured using the GluN2B antagonist, Ro 25-6981 (0.5 μM). GluN2B-EPSCs were obtained by digital subtraction of NMDAR-EPSCs observed in the presence of Ro 25-6981 from those observed in the absence of this antagonist. The GluN2B/NMDAR ratio was determined by the peak amplitude of GluN2B-EPSCs divided by the peak amplitude of NMDAR-EPSCs. To obtain AMPAR/NMDAR ratios, we initially clamped neurons at -70 mV and measured five EPSCs; neurons were then clamped to +40 mV, and five additional EPSCs were recorded. AMPAR values were

calculated by averaging the current traces recorded at -70 mV and measuring the amplitude of the averaged peak. The +40 mV traces were also averaged, and the NMDAR current was determined 30 ms after the peak AMPAR current, when the contribution of the AMPAR component was minimal (Maroteaux and Mameli, 2012; Ma et al., 2018). The AMPAR/NMDAR ratio was calculated by dividing the peak amplitude of AMPAR-EPSCs by that of NMDAR-EPSCs. Evoked EPSC data were analyzed using Clampfit 10.5. To record asynchronous release, 2.5 mM Ca^{2+} was replaced with 2.5 mM strontium (Sr^{2+}) in the recording solution. AMPAR-mediated quantal events were collected between 50 ms and 500 ms after each stimulus (delivered once every 30 s) in an external solution containing APV (50 μM), 2.5 mM Sr^{2+}, and 0 Ca^{2+} (Ding et al., 2008; Lu et al., 2019). Quantal events were analyzed using MiniAnalysis software (Synaptosoft) with a detection parameter of > 5 pA amplitude. For each cell, at least 30 trials were conducted.

Field recording. For LTD experiments, extracellular field recordings were conducted as described previously (Ma et al., 2017; Ma et al., 2018; Roltsch Hellard et al., 2019). Specifically, the recording used a patch pipette filled with 1 M NaCl, which was placed within the DMS. Field excitatory postsynaptic potentials/population spikes (fEPSP/PS) were evoked by optical stimulation (2 ms, 470 nm) through the objective lens at 0.05 Hz. After a stable baseline had been established for 10 min, post-pre-STDP stimulation was delivered through the objective lens to induce LTD. Postsynaptic depolarization preceded presynaptic stimulation by 30 ms, and either 60 pairs (0.1 Hz) or 900 pairs (5 Hz) were delivered. fEPSP/PS were continuously measured for another 40

min. For the LTD analysis, the peak amplitude of each fEPSP/PS was measured and normalized to the mean peak amplitude of all fEPSP/PS during the 10-min baseline. The magnitude of fEPSP/PS potentiation was calculated using the mean peak amplitude of responses measured 30-40 min post LTP induction.

3.5.8. Optical fiber implantation

The optical fiber implantation was conducted as described previously (Ma et al., 2018; Roltsch Hellard et al., 2019). Animals were anesthetized with isoflurane and then placed in a stereotaxic frame. An incision was made, and optical fiber implants (300-μm diameter optical fiber secured to a 2.5-mm stainless steel ferrule) were lowered into the mPFC (AP: 2.6 mm; ML: ±0.0 mm; DV: -3.5 mm from Bregma) and/or bilateral DMS (AP: +0.78 mm; ML: ±2.93 mm; DV: -4.65 mm from Bregma) at a 10-degree angle. Four metal screws were fixed into the skull to support the implants, which were further secured with dental cement (Henry Schein). Meloxicam was administered for pain management. Rats were monitored for one week or until they resumed normal activity.

3.5.9. Operant self-administration of ethanol

Long-Evans rats were trained to self-administer 20% ethanol in operant chambers using a fixed ratio 3 (FR3) schedule, as described previously (Huang et al., 2017; Ma et al., 2018; Roltsch Hellard et al., 2019). Each chamber contained two levers: pressing an active lever three times resulted in delivery of 0.1 mL of 20% ethanol; presses of the inactive lever were recorded but did not result in a programmed event. The ethanol solution was delivered via a stainless steel dipper that rested within an ethanol reservoir. When rats pressed the active lever three times, the dipper (filled with ethanol)

was raised into the magazine port for 20 s before returning to the reservoir. The weight of the ethanol reservoir was measured before and after the operant session. During ethanol delivery, the magazine port was illuminated to provide a cue for reward availability. Once a stable baseline of active lever presses was achieved, the animals underwent *in vivo* oLTD induction (described below). Following the induction, the operant behavior of some rats was continuously monitored for 10 d, while other rats were euthanized for electrophysiology recording 2 d after LTD induction. Ethanol-seeking behavior was quantified using the number of active lever presses, while ethanol-taking was determined as the difference in ethanol reservoir weight before and after the 30-min operant session.

3.5.10. *In vivo* dual-channel optogenetic stimulation

Self-stimulation of mPFC→D1-MSN synapses for oLTP induction. Rats were food-restricted the night before the mock and first training session. Each session lasted 30 min. The optical fiber from each hemisphere of the rat was connected to the laser via fiber-optic patch cords (Doric Lenses or Thorlab), a 1x2 intensity division fiberoptic rotary joint (FRJ_1x2i_FC-2FC; Doric Lenses), and FC/PC fiber cables (Thorlabs), allowing free movement during operant behavior. Bilateral optical stimulation was administered by the laser at wavelengths of 473 nm and 590 nm (Ma et al., 2018; Roltsch Hellard et al., 2019). Each light pulse was 2 ms, with 8 mW power at the fiber tip. The rats learned to self-stimulate corticostriatal synapses in the operant chamber for 12 consecutive days. Active (laser-paired) and inactive levers were present on one wall of the chamber, and a cue light was located above each lever. On day 1, rats were

habituated in the operant chamber and then a 30-min baseline was collected with the patch cord attached but no laser stimulation delivery (mock induction). On day 2, rats that pressed the active lever received 100 pulses of 473-nm light at 50 Hz, with constant 590-nm light for 2 s, to induce oLTP. Presses of the inactive lever were recorded, but did not result in any light delivery. During the first 3 sessions (days 2-4), a single press of the active lever (FR1) resulted in the illumination of a cue light for 10 s. After a delay of 5 s, the 2-s oLTP was delivered. A FR2 schedule was used on days 5-8 and FR3 was used on days 9 12.

oLTD induction time-locked to active lever presses for ethanol. Rats were trained to self-administer 20% ethanol in the operant chamber using the FR3 schedule. The optical fibers from the mPFC and bilateral DMS of the rat were separately connected to the 473-nm and 590-nm laser via fiber optic patch cords (Doric Lenses), a separate light path 2x2 fiberoptic rotary joint (FRJ_2x2_2FC-2FC; Doric Lenses), and FC/PC fiber cables (Thorlabs). Light stimulation at 473 nm was used to activate mPFC neurons, while 590-nm light was utilized to depolarize D1-MSNs. Once a stable baseline of active lever presses had been attained during mock induction, the LTD-inducing protocol was delivered at the same time as ethanol during 30-min operant sessions. In these sessions, three presses of the active lever by the rat (FR3) triggered delivery of post-pre stimulations (10 pairs at 5 Hz), where 590-nm light preceded 473-nm light by 30 ms and each light pulse lasted 2 ms, with 8 mW power at the fiber tip.

3.5.11. Statistical analysis

All data are expressed as the mean ± the standard error of the mean. Data were analyzed by two-tailed t test (unpaired or paired), one- or two-way ANOVA with repeated measurement, followed by the Student-Newman-Keuls (SNK) post hoc test. Significance was determined if $p < 0.05$. Statistical analysis was conducted by the SigmaPlot program. Graphs were constructed using the OriginPro program.

CHAPTER IV

WHOLE-BRAIN MAPPING OF DIRECT INPUTS TO DOPAMINE D1 AND D2 RECEPTOR-EXPRESSING MEDIUM SPINY NEURONS IN THE POSTERIOR DORSOMEDIAL STRIATUM

4.1. Overview

The posterior dorsomedial striatum (pDMS), which is mainly composed of medium spiny neurons (MSNs) expressing either dopamine D1 receptors (D1Rs) or D2Rs, is crucial for goal-directed actions and drug-seeking behavior. Activation of these two MSN types produces opposing effects on addictive behaviors. However, it remains unclear whether pDMS D1- or D2-MSNs receive afferent inputs from different brain regions or whether the extra-striatal afferents express distinct dopamine receptors. To assess whether these afferents also contained D1Rs or D2Rs, we generated double transgenic mice, in which D1R- and D2R-expressing neurons were fluorescently labeled. We utilized rabies virus-mediated retrograde tracing in these mice to perform whole-brain mapping of direct inputs to D1-MSNs or D2-MSNs in the pDMS. We found that D1-MSNs preferentially received inputs from the secondary motor, secondary visual, and cingulate cortices, whereas D2-MSNs received inputs from the primary motor and primary sensory cortices, and the thalamus. We also discovered that while the bed nucleus of the stria terminalis (BNST) and central nucleus of the amygdala are not the major inputs to pDMS MSNs, these regions contained abundant D2R-expressing, but few D1R-expressing, neurons in a triple transgenic mouse model. Remarkably, although

limited D1R or D2R expression was observed in extra-striatal neurons that projected to D1- or D2-MSNs, we found that cortical structures preferentially contained D1R-expressing neurons that projected to D1- or D2-MSNs, while the thalamus, substantia nigra pars compacta, and BNST had more D2R-expressing cells that projected to D2-MSNs. Taken together, these findings provide a foundation for future understanding of the pDMS circuit and its role in action selection and reward-based behaviors.

4.2. Introduction

The basal ganglia has critical roles in movement control and action selection (Balleine et al., 2009). The striatum, which provides the primary input to the basal ganglia, receives and integrates information from cortical, thalamic, and limbic structures before passing this to the basal ganglia for an appropriate action (Bamford et al., 2018). Growing evidence indicates that the dorsomedial striatum (DMS) is involved in the control of goal-directed actions and drug-seeking behaviors (Volkow et al., 2006; Wang et al., 2010; Ma et al., 2018). Two distinct subtypes of medium spiny neuron (MSN) make up as much as 95% of neurons within the DMS (Gerfen and Surmeier, 2011; Cheng et al., 2017). One type of MSN expresses dopamine D1 receptors (D1Rs) and projects to the substantia nigra pars reticulata (SNr), forming the direct pathway (Kreitzer and Malenka, 2008; Gerfen and Surmeier, 2011). The other type of MSN expresses dopamine D2 receptors (D2Rs) and projects to the external globus pallidus (GPe), forming the indirect pathway (Kreitzer and Malenka, 2008; Gerfen and Surmeier, 2011). Activation of D1R-expressing MSNs (D1-MSNs) or D2R-expressing MSNs (D2-MSNs) produces opposing effects on movement and reward-related behaviors (Gerfen

and Surmeier, 2011; Cheng et al., 2017; Luscher et al., 2020). Thus, many learned responses require the coordinated activation of the direct pathway and inhibition of the indirect pathway in the DMS. Importantly, recent studies have found that the posterior region of the DMS (pDMS) is likely to play a greater role in goal-directed behavior than the anterior DMS (aDMS) (Yin and Knowlton, 2004; Yin et al., 2005a; Regier et al., 2015). While the aDMS is important for sensory-guided learning (Williams and Eskandar, 2006; Lee et al., 2019), the pDMS is necessary for the integration of action-outcome associations and expression of goal-directed learning (Yin and Knowlton, 2004; Yin et al., 2005a; Yin et al., 2005b; Corbit and Janak, 2010; Shiflett et al., 2010). In addition to these differences in behavioral function, a recent anatomical study also found different cortical inputs to the aDMS and pDMS (Hunnicutt et al., 2016). While the aDMS mainly received inputs from the orbital, prelimbic, infralimbic, and anterior cingulate cortices, the pDMS primarily received inputs from the motor, orbital, cingulate, and visual cortices (Hunnicutt et al., 2016). While the innervation of D1-MSNs and D2-MSNs in the aDMS has been studied using the rabies virus-mediated retrograde monosynaptic tracing system (Wall et al., 2013), it remains unclear whether D1- and D2-MSNs in the pDMS receive distinct inputs from other brain areas.

In addition to receiving excitatory glutamatergic inputs from the cortex, thalamus, and amygdala, DMS D1- and D2-MSNs are modulated by dopaminergic inputs from the substantia nigra pars compacta (SNc) (Bamford et al., 2018). Dopamine can alter MSN activity by acting on their postsynaptic D1Rs or D2Rs (Gerfen and Surmeier, 2011; Cheng et al., 2017; Luscher et al., 2020), as well as by acting on

presynaptic receptors (Wang and Pickel, 2002; Dumartin et al., 2007; Lu et al., 2019). Electron microscopy studies have provided evidence that cortical fibers in the dorsal striatal contain both D1Rs and D2Rs (Wang and Pickel, 2002; Dumartin et al., 2007), although D1R immunoreactivity was observed less frequently (Dumartin et al., 2007). A recent study also showed that cortical neurons that projected to the DMS preferentially expressed D2Rs, rather than D1Rs (Lu et al., 2019). However, these studies could not determine which specific DMS neuron types received the D1R- or D2R-expressing inputs.

In this study, we assessed D1R and D2R expression patterns in extra-striatal neurons by generating cell-type-specific Cre-expressing double transgenic mice, in which D1R- and D2R-expressing cells were labeled by a fluorescent protein. To map direct inputs to D1- or D2-MSNs, we utilized the rabies virus-mediated monosynaptic tracing approach; this allowed us to label neurons anywhere in the brain that projected monosynaptically to D1- or D2-MSNs (Wall et al., 2013; Ogawa and Watabe-Uchida, 2018). We discovered that neurons in the orbital frontal, secondary motor, visual cortex, and cingulate cortices preferentially targeted pDMS D1-MSNs. In contrast, neurons in the thalamus, primary motor cortex, and primary sensory cortex preferentially projected to pDMS D2-MSNs. Furthermore, our triple transgenic mouse models showed that the bed nucleus of the stria terminalis (BNST) and the central nucleus of the amygdala (CeA) contained abundant D2R-expressing neurons, but few D1R-expressing cells. Lastly, we found that while the number of D1R- or D2R-expressing neurons that projected to pDMS MSNs was low, they exhibited distinct distribution across different

brain regions. These findings lay a foundation for an improved understanding of how the pDMS organizes information from multiple upstream brain regions to determine an action.

4.3. Results

4.3.1. Identification of distinct whole-brain extra-striatal inputs to D1-MSNs and D2-MSNs in the pDMS

To compare afferent inputs onto pDMS D1- and D2-MSNs, we employed rabies-mediated monosynaptic retrograde tracing in D1-Cre;Snap25 and D2-Cre;Snap25 mice, in which D1-MSNs or D2-MSNs selectively expressed Cre (and thus GFP), respectively (Madisen et al., 2015; Wei et al., 2018; Lu et al., 2019). In these mouse lines, the pDMS was injected with Cre-dependent AAVs that expressed TVA-mCherry and RG (Figure 4.1 A). TVA facilitated neuronal infection by the pseudotyped rabies virus, while RG facilitated retrograde monosynaptic spread of the rabies virus from infected neurons (Wall et al., 2013; Ogawa and Watabe-Uchida, 2018). Three weeks after the infusion of these vectors, we injected the glycoprotein-deleted pseudotyped rabies virus, EnvA-SADΔG-mCherry, at the same pDMS location using an angled injection tract (Figure 4.1 B), to prevent coincident infection (Wall et al., 2013). This strategy of selectively expressing TVA and RG in Cre-expressing D1-MSNs in D1-Cre;Snap25 mice or D2-MSNs in the D2-Cre;Snap25 mice meant that the rabies virus infected these neurons and spread to neurons with monosynaptic inputs to them (Figure 4.1 C). One week after the rabies virus infusions, serial coronal 50-µm sections of the whole brain were prepared, and every fourth section was imaged using confocal laser-scanning microscopy. We

observed intense GFP expression in the striatum and at D1-MSN projection targets, including the GPe (Figure 4.1 Div), entopeduncular nucleus (Figure 4.1 Dv), and SNr (Figure 4.1 Dvii), and at D2-MSN projection targets such as the GPe (Figure 4.1 Dxi). We also observed a large number of mCherry-positive extra-striatal neurons with monosynaptic connections to D1-MSNs (Figure 4.1 Di–Dvii) or D2-MSNs (Figure 4.1 Dviii–Dxiv); these were located in the cortex (Figure 4.1 Di–Dxiv), BNST (Figure 4.1 Diii and Dx), GPe (Figure 4.1 Div and Dxi), amygdala (Figure 4.1 Dv and Dxii), thalamus (Figure 4.1 Dvi and Dxiii), and the midbrain (Figure 4.1 Dvii and Dxiv).

These rabies-labeled afferent (mCherry-positive) neurons in both hemispheres were counted relative to brain region boundaries. The total number of extra-striatal mCherry-positive neurons did not differ significantly between D1-Cre;Snap25 and D2-Cre;Snap25 mice (Figure 4.1 E; $t_{(11)} = -0.55$, $p > 0.05$). Since both AAV8-Flex-TVA-mCherry and the rabies virus expressed mCherry, this did not allow for selective visualization of starter cells, which expressed the rabies virus and AAV8-Flex-RG. Thus, labeled neuron counts from any given brain region were normalized to the total inputs to the pDMS detected within each animal. This approach was used to account for any inter-animal differences in viral infusion. This analysis identified significant differences in the extent of inputs from distinct brain regions (Figure 4.1 F; $F_{(5,55)} = 627.19$, $p < 0.001$). Specifically, the majority of inputs onto pDMS D1-MSNs and D2-MSNs arose from the cortex (Figure 4.1 F; $q = 54.22$, 60.72, 62.5, 63.38, and 63.05, $p < 0.001$ for cortex versus thalamus, basal ganglia, amygdala, midbrain and others), and thalamus (Figure 4.1 F; $q = 6.50$, 8.28, 9.16, and 8.83, $p < 0.001$ for thalamus versus

basal ganglia, amygdala, midbrain and others). Interestingly, the cortical neurons innervated significantly more D1-MSNs than D2-MSNs, whereas thalamic neurons connected with significantly more D2-MSNs than D1-MSNs (Figure 4.1 F; cortical neurons: $q = 4.56$, $p < 0.01$; thalamic neurons: $q = 3.51$, $p < 0.05$).

Both the cortex and thalamus contain many sub-regions. Within the cortex, the most prominent inputs to D1-MSNs (expressed as a percentage of total inputs) were from the orbital frontal cortex (6.62 ± 1.45%), primary (6.17 ± 1.31%) and secondary (21.93 ± 1.47%) motor cortices, primary sensory cortex (10.53 ± 1.25%), and cingulate cortex (18.59 ± 1.27%) (Figure 4.2). For D2-MSNs, the equivalent percentages were 5.20 ± 0.93%, 8.40 ± 0.94%, 17.13 ± 0.42%, 15.31 ± 1.52%, and 11.66 ± 1.10% of total D2-MSN inputs, respectively (Figure 4.2). Within the thalamus, the parafascicular nucleus, mediodorsal thalamic nucleus, and central thalamic nucleus gave rise to the majority of thalamostriatal inputs to D1- and D2-MSNs (Figure 4.2; 2.75% ± 0.77%, 2.21% ± 0.40%, and 1.28% ± 0.21% of total D1-MSN inputs, respectively; and 2.97% ± 1.10%, 2.29% ± 0.31%, and 3.10% ± 0.86% of total D2-MSN inputs, respectively). These data suggest that pDMS MSNs receive inputs primarily from the cortex and thalamus, which preferentially project to D1-MSNs and D2-MSNs, respectively.

Previous studies have demonstrated that the striatum plays a critical role in sorting sensory, motor, and reward information arriving from two major excitatory sources: the cortex and thalamus (Lovinger, 2010; Bamford et al., 2018). Differential activation of the direct and indirect pathways subsequently results in the selection and execution of appropriate responses. Therefore, we next analyzed whether there were

cortical or thalamic subregions that preferentially targeted D1-MSNs or D2-MSNs. Although many cortical structures provided similar proportions of the inputs to D1-MSNs and D2-MSNs, we identified some cortical regions that showed a considerable bias in their synaptic input to a specific cell type. The secondary motor, cingulate, and secondary visual cortices provided significantly higher proportions of the inputs to D1-MSNs, as compared with D2-MSNs (Figure 4.1 D; Figure 4.2; $q = 9.13$, $p < 0.001$; $q = 13.19$, $p < 0.001$; $q = 2.95$, $p < 0.05$, respectively). This trend was also observed in the orbital frontal cortex (Figure 4.2; $q = 2.71$, $p < 0.001$). In contrast, the primary motor and primary sensory cortices provided more inputs to D2-MSNs than to D1-MSNs (Figure 4.1 D; Figure 4.2; $q = 4.24$, $p < 0.05$; $q = 9.10$, $p < 0.001$, respectively). The other major source of glutamatergic input to the striatum, the thalamostriatal projections, also showed some biased connectivity. Both the central and ventromedial thalamic nuclei provided significantly higher proportions of inputs to D2-MSNs than to D1-MSNs (Figure 4.1 D; Figure 4.2; $q = 3.47$, $p < 0.05$; $q = 3.15$, $p < 0.05$, respectively). In addition to these cortical and thalamic inputs, the amygdala provides glutamatergic inputs to the DMS. The present study found similar proportions of synaptic inputs to D1-MSNs and D2-MSNs from the central, basal, and lateral amygdala (Figure 4.1 D; Figure 4.2; $q = 0.09$, $p > 0.05$; $q = 0.51$; $p > 0.05$; $q = 0.08$; $p > 0.05$, respectively).

We also compared the projections from the SNc, a known dopaminergic input to the DMS, to D1- and D2-MSNs (Surmeier et al., 2009). Consistent with previous report (Wall et al., 2013), we found that a relatively small proportion of the total inputs were from the SNc, and there was no significant difference between the percentages of these

inputs to D1-MSNs and D2-MSNs (Figure 4.1 D; Figure 4.2; $q = 0.04$, $p > 0.05$). Lastly, we compared the GABAergic inputs from the GPe to the DMS (Lee et al., 2004; Hernandez et al., 2015) and found significantly greater D2-MSN innervation (Figure 4.1 D; Figure 4.2; $q = 3.04$, $p < 0.05$).

Taken together, these observations demonstrated input specificity onto two MSN subtypes in the pDMS. We discovered that the secondary motor, secondary visual, and cingulate cortices preferentially targeted D1-MSNs, whereas inputs from the thalamus, primary motor cortex, and primary sensory cortex preferentially projected to D2-MSNs. Consequently, the cortex and thalamus preferentially project to pDMS D1-MSNs and D2-MSNs, respectively.

Figure 4.1 Rabies virus-mediated retrograde monosynaptic whole-brain tracing of neurons projecting to D1-MSNs and D2-MSNs in the pDMS.
A and **B**, The experimental design used to trace neurons with afferent inputs to D1-MSNs in the pDMS. The design shows how we employed D1-Cre;Snap25 transgenic mice, in which D1-MSNs selectively expressed Cre and GFP (green). Please note that the same approach was repeated in D2-Cre;Snap25 and D1-tdTomato;D2Cre mice, where we traced afferent inputs to D2-MSNs. Selective rabies infection of D1-MSNs was achieved by injecting the pDMS of these mice with Cre-dependent helper viruses expressing an avian membrane EnvA receptor protein (TVA) and rabies glycoprotein (RG) (AAV-Flex-TVA-mCherry and AAV-Flex-RG) three weeks before injection of a modified rabies virus (EnvA-SADΔG-mCherry) into the same area at a 10-degree angle. **C**, One week after rabies injection, the rabies virus had specifically infected TVA-expressing D1-MSNs, and spread retrogradely from RG-expressing D1-MSNs to neurons with monosynaptic connections with them. Note that extra-striatal neurons with monosynaptic connections to RG-expressing D1-MSNs expressed rabies-derived mCherry (red). mCherry-expressing neurons that also contained D1Rs and thus expressed Cre-driven GFP (green) appeared yellow. Extra-striatal neurons that expressed D1Rs but did not make any connections with RG-expressing D1-MSNs were labeled green. **D**, Representative confocal images of rabies virus-labeled mCherry-expressing neurons (red) that project to D1-MSNs (i–vii) or D2-MSNs (viii–xiv) throughout the brain in the D1-Cre;Snap25 or D2-Cre;Snap25 mice, respectively. Rows 2 and 4 show enlarged images of the boxed areas in rows 1 and 3, respectively. Note that there were extensive mCherry-positive neurons in the cortex (i–xiv), BNST (iii, x), GPe (iv, xi), amygdala (v, xii), thalamus (vi, xiii), and midbrain (vii, xiv). M2, secondary motor cortex; Cg, cingulate cortex; PrL, prelimbic cortex; S1, primary sensory cortex; M1, primary motor cortex; BNST, bed nucleus of the stria terminalis; GPe, globus pallidus external; AD, anterior dorsal thalamus; AV, anterior ventral thalamus; BLA, basolateral amygdala; CeA, central amygdala; EP, entopeduncular nucleus; Pf, parafascicular thalamic nucleus; SNc, substantia nigra pars compacta; SNr, substantia nigra pars reticulata; inj. site, injection site. Scale bars: 500 μm (rows 1 and 3), 200 μm (rows 2 and 4). **E**, There was no significant difference between the total number of extra-striatal neurons with projections to D1-MSNs or D2-MSNs; unpaired t test. **F**, Extra-striatal inputs onto D1-MSNs (blue) versus D2-MSNs (orange); $*p < 0.05$, $**p < 0.05$, $***p < 0.001$; two-way RM ANOVA followed by SNK test for the indicated comparisons; n = 5 mice for D1-MSNs (D1-Cre;Snap25 mice) and 8 mice for D2-MSNs (4 D2-Cre;Snap25 mice and 4 D1-tdTomato;D2-Cre mice) (**E** and **F**).

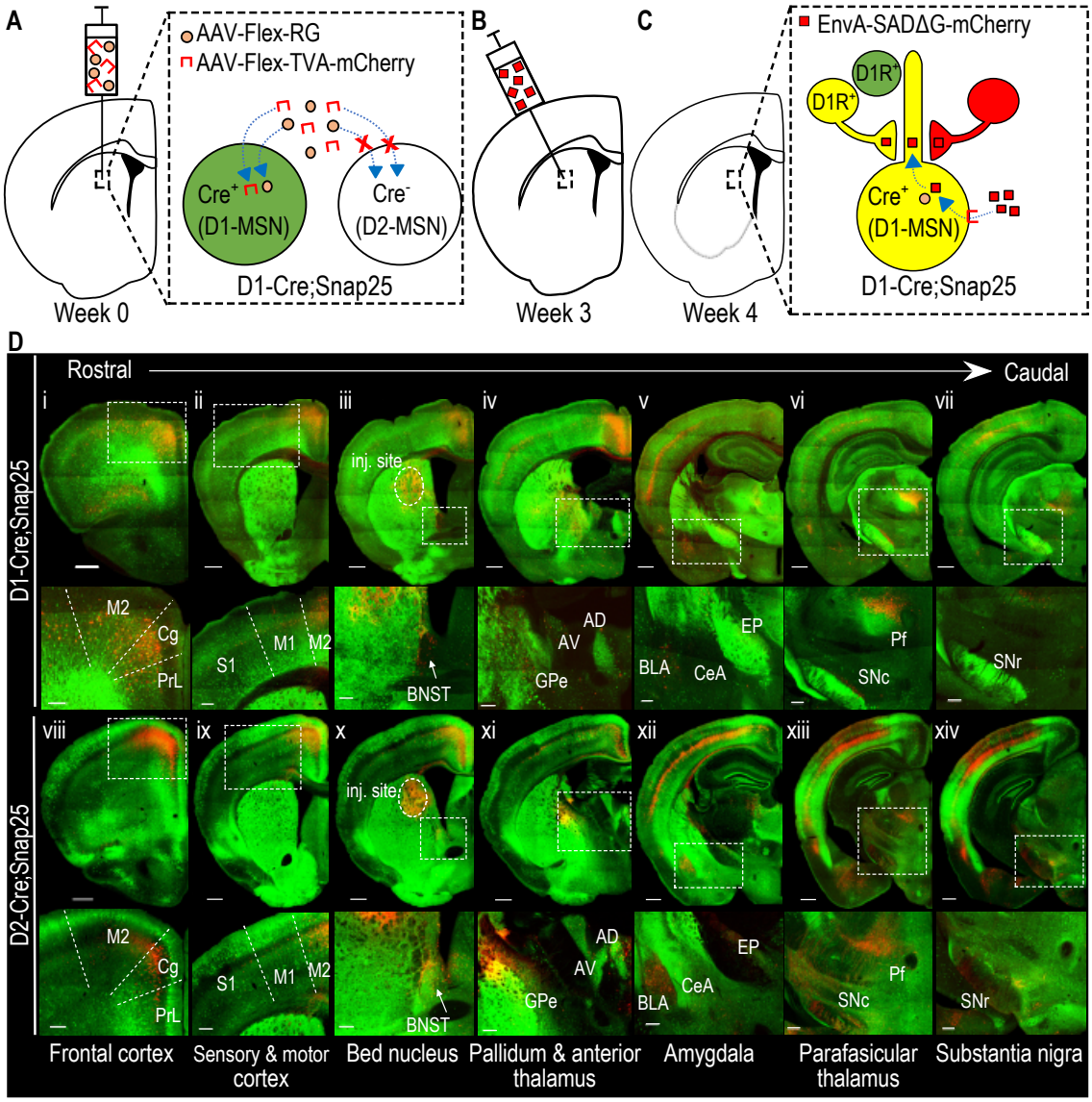
A
AAV-Flex-RG
AAV-Flex-TVA-mCherry
Cre+ (D1-MSN)
Cre- (D2-MSN)
D1-Cre;Snap25
Week 0
B
Week 3
C
EnvA-SADΔG-mCherry
D1R-
D1R+
Cre+ (D1-MSN)
D1-Cre;Snap25
Week 4
D
Rostral
Caudal
D1-Cre;Snap25
D2-Cre;Snap25
inj. site
M2
Cg
PrL
S1
M1
M2
BNST
AD
AV
GPe
BLA
CeA
EP
Pf
SNc
SNr
Frontal cortex
Sensory & motor cortex
Bed nucleus
Pallidum & anterior thalamus
Amygdala
Parafasicular thalamus
Substantia nigra
E
Total extra-striatal inputs
p = 0.59
D1-MSN
D2-MSN
F
% of total inputs
Cortex
Thalamus
Basal ganglia
Amygdala
Midbrain
Others

Figure 4.2 Summary of brain-wide monosynaptic inputs to pDMS D1-MSNs and D2-MSNs.
The majority of direct synaptic inputs to the pDMS arose in the cortex and thalamus. Analysis of the normalized distribution of rabies virus-labeled neurons showed that the orbital frontal cortex, secondary motor cortex, cingulate cortex, and secondary visual cortex preferentially projected to D1-MSNs versus D2-MSNs. The primary motor cortex, primary sensory cortex, central thalamic nucleus, ventromedial thalamic nucleus, and globus pallidus preferentially innervated D2-MSNs versus D1-MSNs. The extra-striatal inputs onto D1-MSNs (blue) or D2-MSNs (orange) are expressed as a percentage of the total inputs to these cell types; $*p < 0.05$, two-way RM ANOVA followed by SNK test; n = 5 mice for D1-MSNs (D1-Cre;Snap25 mice) and 8 mice for D2-MSNs (4 D2-Cre;Snap25 mice and 4 D1-tdTomato;D2-Cre mice).

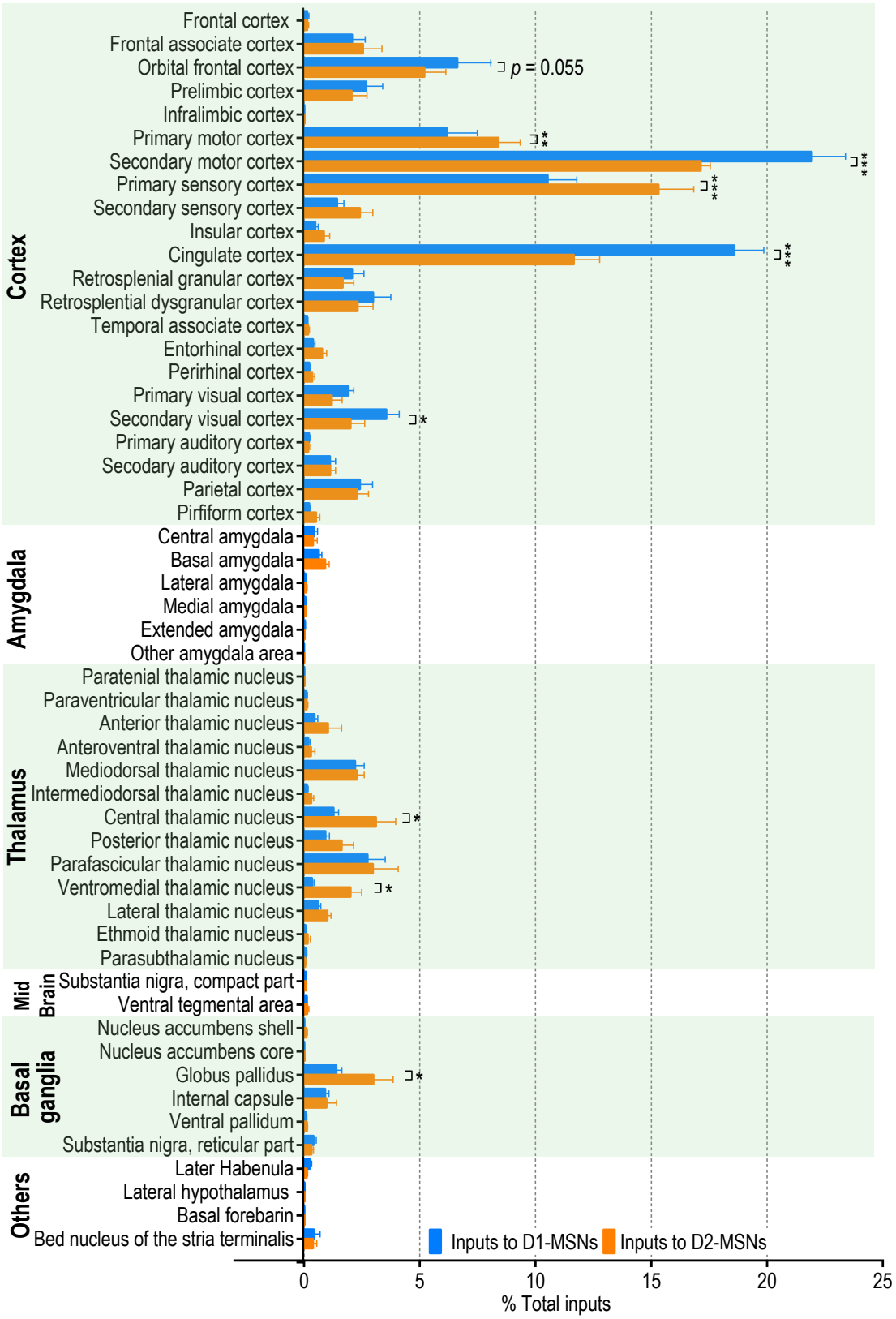
Cortex
Frontal cortex
Frontal associate cortex
Orbital frontal cortex
p = 0.055
Prelimbic cortex
Infralimbic cortex
Primary motor cortex
Secondary motor cortex
Primary sensory cortex
Secondary sensory cortex
Insular cortex
Cingulate cortex
Retrosplenial granular cortex
Retrosplential dysgranular cortex
Temporal associate cortex
Entorhinal cortex
Perirhinal cortex
Primary visual cortex
Secondary visual cortex
Primary auditory cortex
Secodary auditory cortex
Parietal cortex
Pirfiform cortex
Amygdala
Central amygdala
Basal amygdala
Lateral amygdala
Medial amygdala
Extended amygdala
Other amygdala area
Thalamus
Paratenial thalamic nucleus
Paraventricular thalamic nucleus
Anterior thalamic nucleus
Anteroventral thalamic nucleus
Mediodorsal thalamic nucleus
Intermediodorsal thalamic nucleus
Central thalamic nucleus
Posterior thalamic nucleus
Parafascicular thalamic nucleus
Ventromedial thalamic nucleus
Lateral thalamic nucleus
Ethmoid thalamic nucleus
Parasubthalamic nucleus
Mid Brain
Substantia nigra, compact part
Ventral tegmental area
Basal ganglia
Nucleus accumbens shell
Nucleus accumbens core
Globus pallidus
Internal capsule
Ventral pallidum
Substantia nigra, reticular part
Others
Later Habenula
Lateral hypothalamus
Basal forebarin
Bed nucleus of the stria terminalis
Inputs to D1-MSNs
Inputs to D2-MSNs
0
5
10
15
20
25
% Total inputs

4.3.2. Preferential expression of D2Rs versus D1Rs in the BNST and CeA

There is increasing evidence that the BNST and CeA play crucial roles in many neuropsychiatric disorders that include fear formation, anxiety, or reward-related impulsivity (Davis et al., 2010; Kim et al., 2018). Dopaminergic afferents from the ventral tegmental area innervate the amygdala and BNST, but the detailed D1R- and D2R-expression patterns remain unclear. Therefore, we crossed D1-tdTomato transgenic mice, which expressed tdTomato under the control of the D1R gene, with D2-Cre;Snap25 mice. We counted neurons expressing D1Rs (tdTomato-positive) and D2Rs (GFP-positive) in coronal sections containing the BNST and CeA of these D1-tdTomato;D2-Cre;Snap25 transgenic mice. Strong expression of GFP and tdTomato was observed in the striatum (Figure 4.3 A; Figure 4.3 B). However, while strong GFP expression was present in the BNST area, tdTomato expression was barely detectable (Figure 4.3 A; Figure 4.3 B). For each mouse, we examined six BNST sections from Bregma AP +0.26 to -0.34 mm (Figure 4.3 C). The average number of D1R-expressing neurons (41) was significantly lower than the average number of D2R-expressing neurons (215) (Figure 4.3 D; $t_{(34)} = -3.28$, $p < 0.01$).

Our previous study showed relatively high D1R expression and weak D2R expression in the basolateral amygdala (Wei et al., 2018). Interestingly, using the same transgenic animals, the present study identified high D2R expression levels in the CeA (Figure 4.3 E; Figure 4.3 F). We examined six CeA sections from Bregma AP -0.82 to -1.46 mm (Figure 4.3 G). An average of 82 D1R-expressing neurons was observed, and this value was significantly lower than the average number of D2R-expressing neurons (439) (Figure 4.3 H; $t_{(34)} = -7.42$, $p < 0.001$). These results indicate that D2Rs are preferentially expressed in the BNST and CeA.

Figure 4.3 The BNST and CeA preferentially express D2Rs versus D1Rs.
A, Representative fluorescent image of a coronal section of the BNST from a D1-tdTomato;D2-Cre;Snap25 mouse. The atlas skeleton (left) shows the BNST location at +0.26 mm relative to Bregma. **B,** Representative dual-channel higher magnification fluorescent images of the boxed region of panel A showing abundant GFP-expressing (D2R-positive) neurons (left), a few tdTomato-expressing (D1R-positive) neurons (middle), and some colocalization (right). The bottom panels show an enlarged image of the boxed region from the top panels. Str, striatum; aca, anterior commissure area; acp, posterior commissure area. **C,** Schematic representation of the BNST starting at +0.26 mm and ending at -0.34 mm relative to Bregma. **D,** Bar graph summarizing the numbers of D1R- and D2R-expressing neurons in the BNST; $^{**}p < 0.01$, unpaired t test; n = 18 sections from three mice. **E,** Representative fluorescent image of a coronal section of the CeA from a D1-tdTomato;D2-Cre;Snap25 mouse. The atlas skeleton (left) shows the location of the CeA at -1.22 mm relative to Bregma. **F,** Representative dual-channel higher magnification fluorescent images of the boxed region of panel E showing abundant GFP-expressing D2R-positive neurons (left), a few tdTomato-expressing D1R-positive neurons (middle), and some colocalization (right). The bottom panels show enlarged images of the boxed region of the top panels. GPe, globus pallidus external; tDS; tail of the striatum; BLA, basolateral amygdala. **G,** Schematic representation of the CeA starting at -0.82 mm and ending at -1.46 mm relative to Bregma. **H,** Bar graph depicting the higher average number of D2R-expressing neurons than D1R-expressing neurons in the CeA; $^{***}p < 0.001$, unpaired t test; n = 18 sections from three mice. Scale bars: 1 mm (**A**, **E**); 250 μm (**B**, **F**, top panels); 20 μm (**B**, **F**, bottom panels).

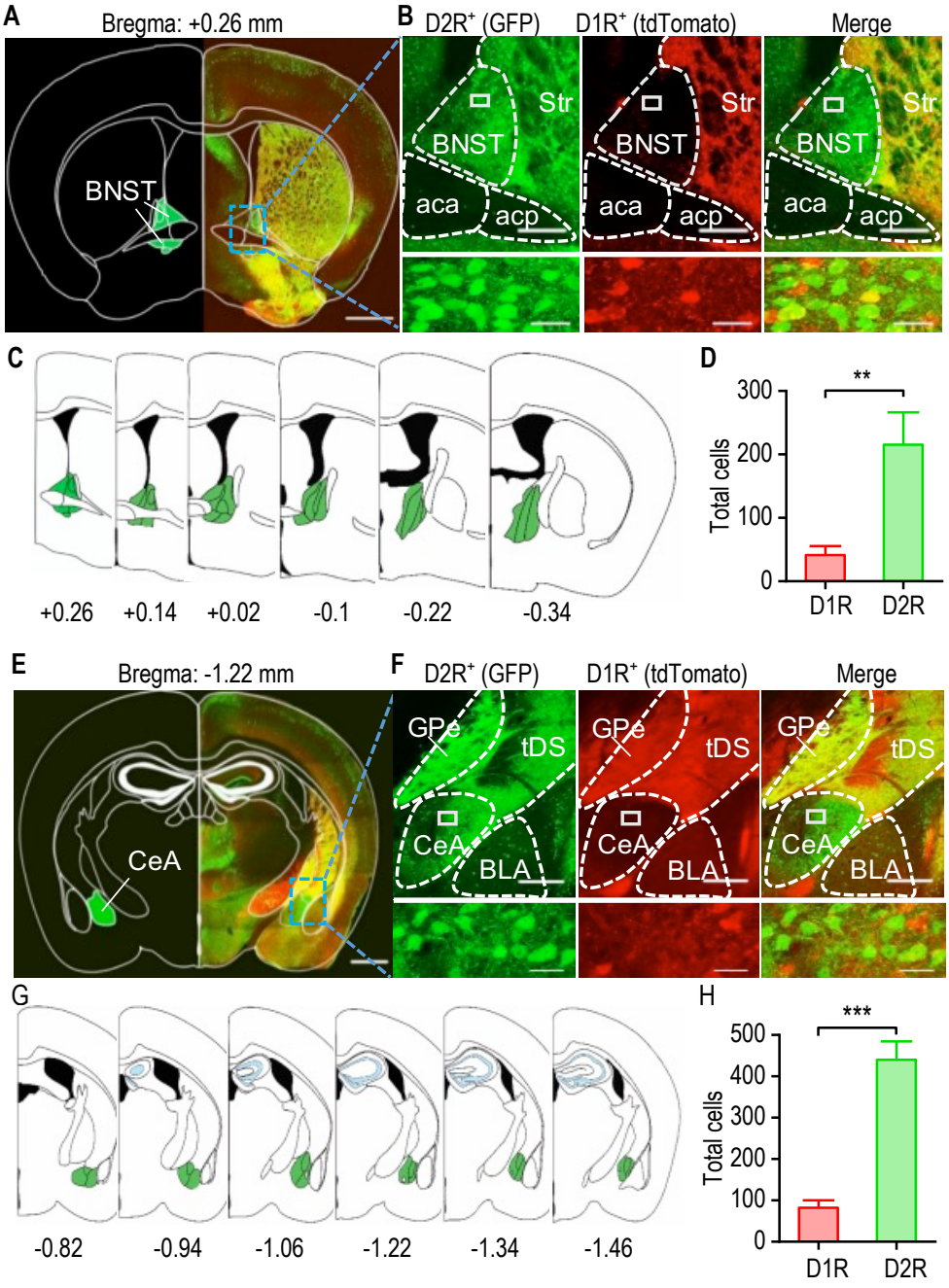
A
Bregma: +0.26 mm
BNST
B
D2R+ (GFP)
D1R+ (tdTomato)
Merge
Str
BNST
aca
acp
C
+0.26
+0.14
+0.02
-0.1
-0.22
-0.34
D
**
Total cells
300
200
100
0
D1R
D2R
E
Bregma: -1.22 mm
CeA
F
D2R+ (GFP)
D1R+ (tdTomato)
Merge
GPe
tDS
CeA
BLA
G
-0.82
-0.94
-1.06
-1.22
-1.34
-1.46
H
***
Total cells
500
400
300
200
100
0
D1R
D2R

4.3.3. Whole-brain mapping of D1R- or D2R-expressing inputs to pDMS MSN subtypes

The above results (Figure 4.3) and recent transgenic models have revealed a tight segregation of D1Rs and D2Rs in some reward structures, including the orbitofrontal cortex, prefrontal cortex, and amygdala (Wei et al., 2018). In addition to the differential innervation of D1-MSNs and D2-MSNs, it is essential to note that previous anatomical studies indicated that cortical fibers in the dorsal striatum contained abundant D2Rs, but few D1Rs (Wang and Pickel, 2002; Dumartin et al., 2007). In addition, we recently discovered that DMS-projecting extra-striatal neurons preferentially expressed D2Rs, rather than D1Rs (Lu et al., 2019). We thus asked whether extra-striatal D1R- or D2R-expressing inputs showed biased projections to D1-MSNs or D2-MSNs in the pDMS. To test this, we measured the overlap between neurons that projected to D1-MSNs or D2-MSNs in the pDMS, and extra-striatal neurons that expressed D1Rs or D2Rs. To explore the anatomical connections between extra-striatal D1R-expressing inputs and D1-MSNs (D1→D1), and between D2R-expressing inputs and D2-MSNs (D2→D2), we analyzed the numbers of neurons that were both GFP-positive and tdTomato-positive in D1-Cre;Snap25 and in D2-Cre;Snap25 mice following EnvA-SADΔG-mCherry injection.

D1R- or D2R-expressing neurons were selectively labeled with GFP (Figure 4.4 A, Figure 4.4 B, Figure 4.4 D; left and middle) and the EnvA-SADΔG-mCherry rabies virus infected D1-MSNs or D2-MSNs before spreading to neurons with direct inputs to these cells (Figure 4.4 A, Figure 4.4 B, Figure 4.4 D; left and middle). As a result, neurons that projected to D1-MSNs or D2-MSNs were labeled red (mCherry) in these

mice. To probe the connections between extra-striatal D1R-expressing inputs and D2-MSNs (D1→D2), we employed D1-tdTomato;D2-Cre mice, in which extra-striatal D1R-expressing neurons and pDMS D1-MSNs were both labeled red (tdTomato) (Figure 4.4 C, Figure 4.4 D; right). These mice did not express GFP in D2-MSNs as GFP was subsequently used in the rabies virus. Injection of AAV8-Flex-TVA-mCherry and AAV8-Flex-RG into the pDMS, followed by EnvA-SADΔG-GFP, led to the infection of Cre-positive D2-MSNs and extra-striatal inputs to D2-MSNs by rabies virus; these expressed GFP and were thus labeled green (Figure 4.4 C, Figure 4.4 D; right). Note that pDMS-projecting neurons that contained D1Rs (or D2Rs) showed co-expression of mCherry (or tdTomato) and GFP and were thus yellow (Figure 4.4 D).

To our surprise, the majority of extra-striatal neurons that projected to D1-MSNs or D2-MSNs did not express D1Rs or D2Rs. Specifically, the D1R was expressed by 2.6 ± 0.5% of the rabies virus-labeled neurons that projected to D1-MSNs in D1-Cre;Snap25 mice (D1→D1), and the D2R were expressed by 5.4 ± 0.9% of the inputs to D2-MSNs in D2-Cre;Snap25 mice (D2→D2). The D1R was expressed by 0.8 ± 0.4% of the inputs to D2-MSNs in D1-tdTomato;D2-Cre mice (D1→D2). However, analysis of these findings showed that there were significantly more D2→D2 connections than either D1→D1 or D1→D2 connections (Figure 4.4 E; $q = 4.34$, $p < 0.05$; $q = 6.73$, $p < 0.01$, respectively). This was consistent with previous anatomical studies showing greater D2R expression, as compared with D1R expression, at presynaptic terminals in the dorsal striatum (Wang and Pickel, 2002; Dumartin et al., 2007; Lu et al., 2019).

Interestingly, although the number of extra-striatal D1R- or D2R-expressing neurons that projected to D1-MSNs or D2-MSNs was low, these neurons showed distinct distribution patterns across the brain. We normalized D1R- or D2R-expressing inputs from individual brain regions to the total number of extra-striatal D1R- or D2R-expressing inputs. D1→D1, D2→D2, and D1→D2 connections were observed in cortical and thalamic structures, but not in the amygdala (Figure 4.4 F; $F_{(2,20)} = 60.22$, $p < 0.001$). Cortical regions had higher percentages of D1→D1 and D1→D2 connections, as compared with D2→D2 (Figure 4.4 F; $q = 5.44$, $p < 0.001$; $q = 5.36$, $p < 0.01$; respectively), while the thalamus had a higher percentage of D2→D2 than of D1→D1 or D1→D2 (Figure 4.4 F; $q = 2.93$, $p < 0.05$; $q = 4.44$, $p < 0.05$; respectively). In the SNc, lateral habenula, and BNST, a higher percentage of the connections were D2→D2, as compared with D1→D1 or D1→D2 (Figure 4.4 G; SNc: $q = 4.55$, $p < 0.01$; $q = 4.52$, $p < 0.01$; lateral habenula: $q = 2.87$, $p = 0.052$, D2→D2 vs. D1→D1; BNST: $q = 3.50$, $p < 0.05$; $q = 4.25$, $p < 0.05$; respectively).

We also analyzed the distribution of D1→D1, D2→D2, and D1→D2 in sub-regions of the cortex, amygdala, and thalamus that provided the most inputs to the pDMS. Analysis of ten cortical regions found a significantly higher percentage of D1→D2 than of D1→D1 projections from the frontal associate cortex (Figure 4.5 A; $q = 2.87$, $p < 0.05$). D1→D2 was also detected more frequently than D2→D2 from the cingulate cortex, and D1→D1 was detected more frequently than D2→D2 from the secondary motor cortex, although these differences did not achieve statistical significance (Figure 4.5 A; $q = 3.13$, $p = 0.074$; $q = 2.46$, $p = 0.085$, respectively). The

basolateral amygdala and CeA contained similar percentages of D1→D1, D2→D2, and D1→D2 connections (Figure 4.5 B; $F_{(1,10)} = 0.62$, $p > 0.05$). The data presented in Figure 4.5 C showed that a significantly higher percentage of D2→D2 than of D1→D1 or D1→D2 projections arose from the mediodorsal thalamic nucleus ($q = 10.33$, $p < 0.001$; $q = 14.05$, $p < 0.001$), central thalamic nucleus ($q = 8.26$, $p < 0.001$; $q = 10.18$, $p < 0.001$), and ventromedial thalamic nucleus ($q = 4.91$, $p < 0.001$; $q = 5.19$, $p < 0.001$). A higher percentage of D1→D1 than of D1→D2 was observed in the parafascicular thalamic nucleus (Figure 4.5 C; $q = 3.53$, $p < 0.05$). Together, these results suggest that while the number of D1R- or D2R-expressing neurons with projections to pDMS MSNs was low, they exhibited distinct brain distribution.

Figure 4.4 Rabies virus-mediated retrograde monosynaptic whole-brain labeling of D1R- and D2R-expressing neurons projecting to D1-MSNs and D2-MSNs in the pDMS.

A-C, Schematic showing the experimental approach used to label extra-striatal D1R- or D2R-expressing neurons with projections to pDMS D1-MSNs or D2-MSNs. D1-Cre;Snap25 mice were employed to identify D1→D1 connections (A), D2-Cre;Snap25 mice for D2→D2 connections (B), and D1-tdTomato;D2-Cre mice for D1→D2 connections (C). D1-Cre;Snap25 and D2-Cre;Snap25 mice expressed GFP in D1R- and D2R-expressing neurons, respectively (A and B). In D1-tdTomato;D2-Cre mice, D1R-expressing neurons were labeled red (C). Injection of Cre-dependent helper viruses (AAV-Flex-TVA-mCherry and AAV-Flex-RG) into the pDMS induced selective expression of TVA and RG in Cre-expressing D1-MSNs (A), D2-MSNs (B), and D2-MSNs (C). Three weeks after helper virus infusion, injection of EnvA-SADΔG-mCherry into the same site of the D1-Cre;Snap25 (A) and D2-Cre;Snap25 (B) mice, and of EnvA-SADΔG-GFP into the same site of D1-tdTomato;D2-Cre mice (C) caused selective rabies infection and expression of mCherry by D1-MSNs (A) or D2-MSNs (B), and expression of rabies-GFP by D2-MSNs (C). Retrograde spread of rabies virus then occurred from D1-MSNs (A) or D2-MSNs (B, C) to extra-striatal presynaptic neurons. This facilitated identification of D1→D1 (A), D2→D2 (B), and D1→D2 (C) connections, as indicated. **D,** Representative confocal images of the cortex in the indicated mice following injection of either EnvA-SADΔG-mCherry or EnvA-SADΔG-GFP. White arrows indicate colocalization of D1→D1 (left), D2→D2 (middle), and D1→D2 (right). Scale bars: 10 μm. **E,** The relative levels of the indicated connections, where D1→D1 is expressed as a percentage of the total number of D1-MSN inputs, and D2→D2 or D1→D2 is expressed as a percentage of the total number of D2-MSN inputs; $*p < 0.05$, $**p < 0.01$ for the indicated comparisons, one-way ANOVA followed by SNK test. **F,** Bar graph comparing D1R- and D2R-expressing inputs from the cortex, amygdala, and thalamus onto MSNs. D1R- or D2R-expressing inputs from the indicated brain regions were normalized to the total extra-striatal D1R- or D2R-expressing inputs, as appropriate. Note that the cortex exhibited high percentages of D1→D1 and D1→D2 connections, whereas the thalamus showed a high percentage of D2→D2 connections; $***p < 0.001$, $*p < 0.05$, two-way RM ANOVA followed by SNK test. **G,** Bar graph comparing D1R- and D2R-expressing inputs from the SNc, lateral habenula (LHb), and BNST onto MSNs. D1R- or D2R-expressing inputs from these brain regions were normalized to the total extra-striatal D1R- or D2R-expressing inputs; $**p < 0.01$, $*p < 0.05$, two-way RM ANOVA followed by SNK test. n = 5 (D1→D1), 4 (D2→D2), 4 (D1→D2) mice (**E**-**G**).

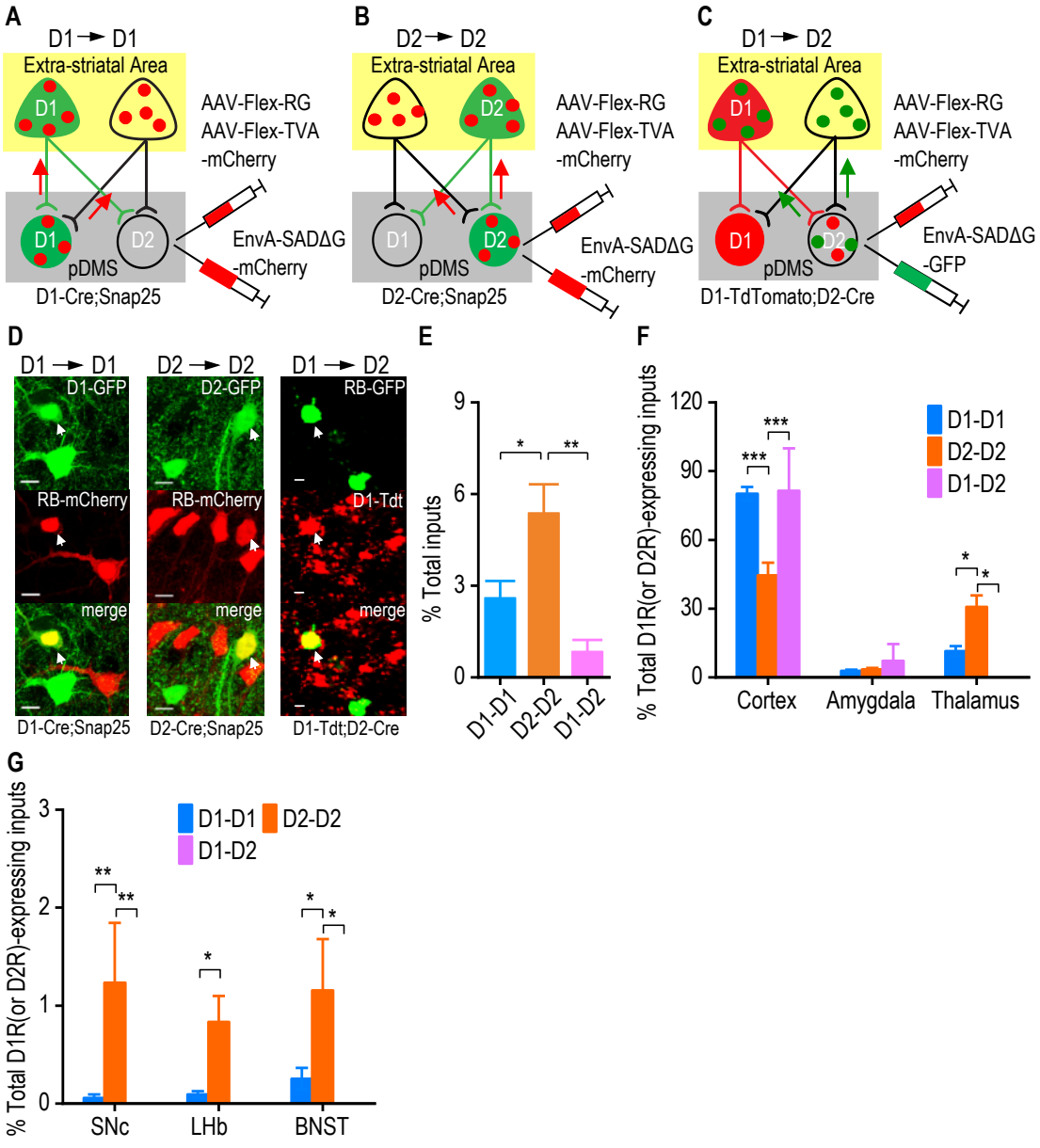
A
D1 → D1
Extra-striatal Area
D1
D1
D2
pDMS
D1-Cre;Snap25
AAV-Flex-RG
AAV-Flex-TVA
-mCherry
EnvA-SADΔG
-mCherry
B
D2 → D2
Extra-striatal Area
D2
D1
D2
pDMS
D2-Cre;Snap25
AAV-Flex-RG
AAV-Flex-TVA
-mCherry
EnvA-SADΔG
-mCherry
C
D1 → D2
Extra-striatal Area
D1
D1
D2
pDMS
D1-TdTomato;D2-Cre
AAV-Flex-RG
AAV-Flex-TVA
-mCherry
EnvA-SADΔG
-GFP
D
D1 → D1
D1-GFP
RB-mCherry
merge
D1-Cre;Snap25
D2 → D2
D2-GFP
RB-mCherry
merge
D2-Cre;Snap25
D1 → D2
RB-GFP
D1-Tdt
merge
D1-Tdt;D2-Cre
E
% Total inputs
9
6
3
0
*
**
D1-D1
D2-D2
D1-D2
F
% Total D1R(or D2R)-expressing inputs
120
90
60
30
0
***
***
*
*
D1-D1
D2-D2
D1-D2
Cortex
Amygdala
Thalamus
G
% Total D1R(or D2R)-expressing inputs
3
2
1
0
**
**
*
*
*
D1-D1
D2-D2
D1-D2
SNc
LHb
BNST

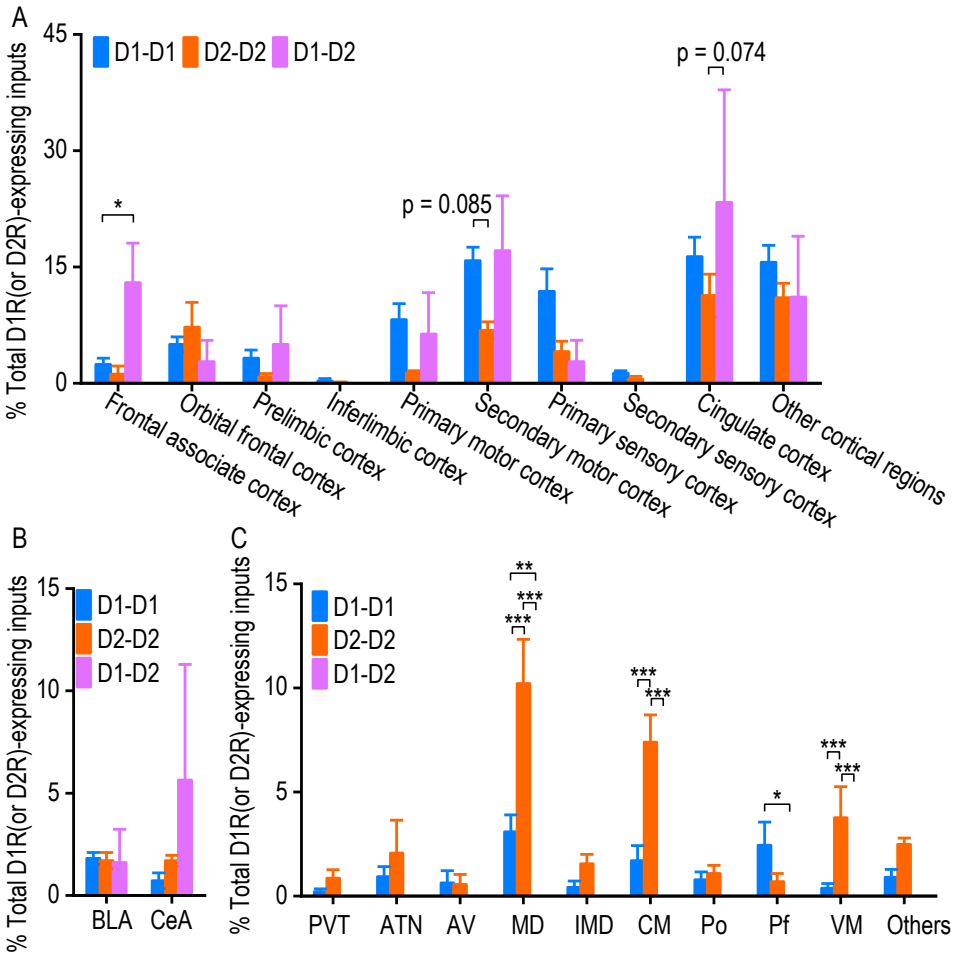

Figure 4.5 Distribution of extra-striatal D1R- or D2R-expressing inputs onto MSNs from the cortex, amygdala, and thalamus.

D1R- or D2R-expressing inputs from the indicated brain regions were normalized to the total extra-striatal D1R- or D2R-expressing inputs, as appropriate. **A**, Bar graph of cortical inputs, segregated into ten major sub-regions, indicating that the frontal associate cortex had a high proportion of D1→D2 connections; **p* <0.05, two-way RM ANOVA followed by SNK test. No significant differences were found in the proportions of connection types between the BLA or CeA and the pDMS. **C**, No significant differences were found in the proportions of connection types between the paraventricular thalamic nucleus (PVT), anterior thalamic nucleus (ATN), anteroventral thalamic nucleus (AV), intermediodorsal thalamic nucleus (IMD), or posterior thalamic nucleus (Po) and the pDMS. However, the mediodorsal thalamic nucleus (MD), central thalamic nucleus (CM), and ventromedial thalamic nucleus (VM) were found to have high percentages of D2→D2 connections, while the parafascicular thalamic nucleus (Pf) had a high percentage of D1→D1 connections; ****p* <0.001, ***p* <0.01, **p* <0.05, two-way RM ANOVA followed by SNK test. n = 5 (D1→D1), 4 (D2→D2), 4 (D1→D2) mice.

4.4. Discussion

Using the rabies virus-mediated retrograde monosynaptic tracing system, the present study investigated the inputs onto pDMS D1-MSNs and D2-MSNs and examined the distribution pattern of brain-wide extra-striatal D1R- and D2R-expressing inputs to these MSNs. We found that the cortex, including the secondary motor and cingulate cortices, preferentially projects to pDMS D1-MSNs, whereas the thalamus, including the central and ventromedial thalamic nuclei, preferentially innervates pDMS D2-MSNs. In addition, while providing fewer inputs than the cortex and thalamus to the pDMS, the BNST and CeA contained more D2R-expressing than D1R-expressing neurons. Lastly, we discovered that MSN-projecting neurons exhibited distinct distribution of the D1R and D2R across the whole brain. These results suggest that the segregation of connections between upstream brain regions and pDMS D1- or D2-MSNs may provide the basis for biased information propagation to basal ganglia structures, resulting in differential effects on behavior. In addition, D2R-expressing neurons in the BNST and CeA may exert distinct roles in anxiety and addiction.

4.4.1. Distinct monosynaptic inputs to pDMS D1-MSNs and D2-MSNs

Given the broad roles of the striatum in motor execution, action selection, learning, behavioral flexibility and reinforcement-associated behaviors such as reward-seeking and reinstatement (Ragozzino ME et al., 2002; Bamford et al., 2018; Roltsch Hellard et al., 2019), improving our understanding of how individual brain regions precisely innervate two major subtypes of striatal neuron represent an essential step towards dissecting the circuits that impact on striatal function. The present study

discovered that pDMS D1-MSNs and D2-MSNs received asymmetric inputs from other brain regions. We employed a monosynaptic rabies virus system (Wall et al., 2013) to label brain-wide neurons with direct connections to pDMS D1-MSNs or D2-MSNs. We discovered that these two MSN subtypes received asymmetric inputs from other whole brain regions. Dense D1-MSN innervations were originated primarily from the orbital frontal, secondary motor, cingulate, and secondary visual cortices. These prefrontal and limbic association structures are devoted mainly to reward motivation, emotional regulation, planning of complex cognitive behaviors, and decision making (Floresco et al., 2008; Balleine et al., 2009; Gremel et al., 2016; Barthas and Kwan, 2017). Therefore, our results suggested that information related to reward, based on past experience, may be preferentially passed to the direct pathway circuit and thus facilitate actions likely to procure a reward. In contrast, D2-MSNs received inputs that mainly originated from the primary motor cortex, primary sensory cortex, central thalamic nucleus, and ventromedial thalamic nucleus. Concurrent activation of D1- and D2-MSNs has been reported during action initiation (Hikida et al., 2010; Cui et al., 2013). Biased projections from the primary motor and sensory cortices onto D2-MSNs may contribute to the suppression of unwanted behavior via activation of D2-MSNs. In addition, there is growing evidence that the thalamostriatal pathway plays an essential role in responses to salient stimuli and behavioral flexibility; projections from the central median and parafascicular nuclei onto cholinergic interneurons, which have also been found to express the D2R, appear to be particularly important in this context (Smith et al., 2011; Bradfield et al., 2013; Guo et al., 2015). The present study used D2-Cre mice to identify

extra-striatal inputs onto D2-MSNs. Despite the relatively low abundance of striatal cholinergic interneurons (Kreitzer and Malenka, 2008) , we cannot rule out the possibility that the observed connections between central and ventromedial thalamic regions and D2-expressing striatal neurons may also have included some projections to cholinergic interneurons. This architecture suggests that salient information from the thalamus may be differentially transmitted to D2R-expressing cholinergic interneurons and D2-MSNs to stop a current ongoing action and initiate a new action, thus facilitating flexible switching between behaviors.

The pDMS appears to be more involved in the acquisition of goal-directed actions than the aDMS (Yin et al., 2005a; Corbit and Janak, 2010; Shiflett et al., 2010), and the present study, therefore, focused on inputs to the pDMS. Our results were mostly consistent with other recent studies, which identified major inputs onto D1-MSNs and D2-MSNs that arose in the cortex and thalamus (Doig et al., 2010; Wall et al., 2013; Hunnicutt et al., 2016). Interestingly, in contrast to a previous observation (Wall et al., 2013), we identified significant projections from the secondary motor cortex and cingulate cortex to the pDMS. These inputs selectively innervated D1-MSNs. Anatomical and functional studies have suggested that the dorsomedial, dorsolateral, and ventral striatum received preferential inputs from the associative, sensorimotor, and limbic structures, respectively (Burton et al., 2015; Hunnicutt et al., 2016). Thus, this discrepancy may reflect the medial injection site employed in the present study.

4.4.2. Distinct expression of D1Rs and D2Rs in the BNST and CeA

Interestingly, we observed that D2R-expressing neurons predominated in the BNST and CeA, which are closely associated with anxiety and addictive disorders (Davis et al., 2010; Kim et al., 2018). This was consistent with previous anatomical studies that identified a high proportion of D2R-expressing cells in the BNST and CeA using D2-GFP transgenic animals and D2 *in situ* hybridization (Perez de la Mora et al., 2012; De Bundel et al., 2016). The CeA and BNST receive dense dopaminergic inputs that originate in the ventral tegmental area (Hasue and Shammah-Lagnado, 2002; Krawczyk et al., 2011). A study using a mouse behavioral paradigm for auditory threat response generalization found that dopamine facilitated the consolidation of fear memory through concomitant activation of D2Rs in the CeA and BNST (De Bundel et al., 2016). A previous immunohistochemical study revealed that most D2R-expressing cells were also positive for protein kinase C-δ-positive (Kim et al., 2018), a marker previously shown to identify GABAergic neurons. Selective expression of D2Rs in the BNST and CeA may have a critical impact on final behavioral outcomes in anxiety- and reward-related processes.

4.4.3. D1R- or D2R-expressing inputs to D1- and D2-MSNs in the pDMS

Dopaminergic modulation of corticostriatal neurotransmission is particularly crucial during reward-based behaviors (Luscher and Malenka, 2011; Bamford et al., 2018; Ma et al., 2018). Our recent anatomical study observed high expression levels of D1Rs and D2Rs in the medial prefrontal cortex, orbital frontal cortex, and amygdala (Wei et al., 2018). Furthermore, these D1R- and D2R-expressing neurons were highly

segregated, with a low percentage of neurons co-expressing both D1Rs and D2Rs (Wei et al., 2018). Importantly, we found that D1R- or D2R-expressing neurons within the cortex and amygdala sent projections to the DMS, and formed functional connections with D1-MSNs or D2-MSNs (Lu et al., 2019). Thus, we expected that there would be strong anatomical connections between extra-striatal D1R- or D2R-expressing DMS-projecting neurons and D1-MSNs or D2-MSNs. Surprisingly, we did not detect a high level of overlap between extra-striatal neurons expressing D1Rs or D2Rs and D1- or D2-MSNs; this suggested that the majority of extra-striatal neurons projecting to D1- or D2-MSNs did not express these receptors. Although only a minority of neurons with inputs to D1- or D2-MSNs expressed D1Rs or D2Rs, increasing evidence indicates that presynaptic D1Rs and D2Rs are essential for dopamine-dependent modulation of glutamate release at corticostriatal synapses (Wang and Goldman-Rakic, 2004; Bamford et al., 2018; Cui et al., 2018; Lu et al., 2019).

When the cortical inputs are stimulated at a low frequency, activation of presynaptic D1Rs was shown to boost glutamate release to D1- and D2-MSNs, whereas activation of presynaptic D2Rs suppressed glutamate release (Wang et al., 2012b; Cui et al., 2018; Lu et al., 2019). When the cortical inputs are stimulated at a higher frequency, this dopaminergic modulation of glutamate release was blocked by adenosine and endocannabinoids (Wang et al., 2012b; Bamford et al., 2018). This type of presynaptic dopaminergic modulation facilitates the appropriate selection and transmission of excitatory inputs via corticostriatal synapses during learning (Bamford et al., 2018). The

D1R- and D2R-expressing inputs to D1-MSNs or D2-MSNs may play important roles in this presynaptic filtration.

We observed that D1R- or D2R-expressing neurons with inputs to pDMS D1- or D2-MSNs had distinct brain distribution patterns. Cortical regions contained a higher percentage of D1→D1 or D1→D2 connections, as compared with D2→D2, while thalamic areas had more D2→D2 connections, as compared with either D1→D1 or D1→D2. It is known that D1Rs exhibit a relatively low affinity for dopamine and are mainly activated by fast phasic release of high concentrations of dopamine, while D2Rs have a higher affinity for dopamine and mainly respond to slow tonic dopamine release (Richfield EK et al., 1989; Grieder et al., 2012). The relative levels of D1R- and D2R-expressing inputs to MSNs from cortical and thalamic regions observed in this study suggest that the corticostriatal pathway may be more sensitive to phasic dopamine release. In contrast, the thalamostriatal pathway would be modulated by an increased basal dopamine level. These anatomical findings indicate that phasic dopamine release would preferentially initiate an action, while an increased basal dopamine level would stop an action. In addition, the SNc, lateral habenula, and BNST were similar to thalamic regions in that they expressed high levels of D2Rs than of D1Rs (Krawczyk et al., 2011; Ford, 2014). As we did not examine the anatomical connections between D2R-expressing inputs and D1-MSNs in the present study, it is not surprising that D2→D2 connections were more prevalent than either D1→D1 or D1→D2 in these regions.

In summary, we have demonstrated that pDMS D1-MSNs and D2-MSNs receive differential innervation from cortical and thalamic structures. Additionally, we found

that the majority of brain-wide extra-striatal inputs to D1-MSNs or D2-MSNs did not express D1Rs or D2Rs, and that the input neurons that did express these receptors exhibited distinct distribution patterns. These findings provide a foundation for the understanding of information segregation in pDMS circuits that will guide future studies.

4.5. Materials and methods

4.5.1. Reagents

Two Cre-dependent (Flex) adeno-associated virus (AAV) serotype 8 vectors were employed in this study; one expressed rabies glycoprotein (RG) (AAV8-Flex-RG) and the other expressed an avian membrane EnvA receptor protein (TVA) and mCherry (AAV8-Flex-TVA-mCherry). These helper viruses were purchased from the University of North Carolina Vector Core. Pseudotyped rabies viruses, EnvA-SADΔG-mCherry and EnvA-SADΔG-GFP (2.04 x10^8 TU/mL), were obtained from the Salk Institute Vector Core. All other reagents were purchased from Sigma.

4.5.2. Animals

Drd1a-Cre (D1-Cre) and Drd2-Cre (D2-Cre) mice were acquired from Mutant Mouse Regional Resource Centers. Snap 25 mice and D1-TdTomato mice were purchased from the Jackson Laboratory. D1-Cre and D2-Cre mice were crossed with Snap25 mice on a C57BL/6J background to produce D1-Cre;Snap25 and D2-Cre;Snap25 offspring, respectively. D2-Cre mice were also crossed with D1-tdTomato mice on a C57BL/6J background to produce D1-tdTomato;D2-Cre offspring. Mouse genotypes were determined by PCR analysis of Cre or the fluorescent protein gene in tail DNA (Cre for D1-Cre and D2-Cre mice; tdT for D1-tdTomato; GFP for Snap25 mice)

(Wang et al., 2011; Wang et al., 2015; Cheng et al., 2017; Wei et al., 2018; Lu et al., 2019). Mice were group housed at 23 degrees Celsius with a 12 hour light: dark cycle (lights on at 11:00 pm). Food and water were provided ad libitum. Male 2- to 3-month-old mice were used in this study. All animal care procedures and experimental protocols were approved by the Texas A&M University Institutional Animal Care and Use Committee and were performed in agreement with the National Research Council Guide for the Care and Use of Laboratory Animals.

4.5.3. Stereotaxic virus infusion

Stereotaxic viral infusions were performed as described previously (Wang et al., 2015; Cheng et al., 2017; Ma et al., 2017; Ma et al., 2018; Lu et al., 2019; Roltsch Hellard et al., 2019). Briefly, mice were anesthetized using isoflurane and mounted in a rodent stereotaxic frame (Kopf). A three-axis micromanipulator was used to measure spatial coordinates for Bregma and Lambda. Small drill holes were made in the skull at the appropriate coordinates, according to the Paxinos atlas (Franklin and Paxinos, 2007). Two microinjectors were loaded with 0.5 µL of a 1:1 mixture of AAV8-Flex-RG and AAV8-Flex-TVA-mCherry and then lowered into the pDMS (AP: 0.0 mm, ML: ± 1.87 mm, DV: -2.90 mm). This helper virus mixture was infused into the brain at a rate of 0.1 µL/min. To avoid backflow of virus, microinjectors were left in place for 10 minutes after the infusion was complete, and were then removed. The skin was sutured, and the mice were allowed to recover for 3 weeks prior to the infusion of pseudotyped rabies virus (EnvA-SADΔG-mCherry or EnvA-SADΔG-eGFP). The rabies virus was injected at the same site and using the same injection volume as the initial helper virus injection.

To prevent coincident rabies infection along the AAV injection tract, the rabies virus was infused at an angle of 10 degrees (Wall et al., 2013) into adapted coordinates (AP, 0.0 mm; ML, ± 2.42 mm; DV, -2.94 mm). The modified coordinates were calculated by measuring from the midline and parallel to the dorsal-ventral axis.

4.5.4. Confocal imaging and cell counting

Rabies virus was allowed to replicate and spread for 7 days prior to perfusing the mice intracardially with 4% paraformaldehyde (PFA) in phosphate-buffered saline (PBS) (Wall et al., 2013). The brains were extracted and post-fixed overnight in 4% PFA/PBS solution, followed by dehydration in 30% sucrose. Each whole brain was sectioned serially into 50-μm coronal sections using a cryostat. We mounted sections in a 1 in 4 series. Confocal images were obtained using a confocal laser-scanning microscope (Fluoview 1200, Olympus). Fluorescent images were reconstructed in three dimensions, and cell counts from these scans were manually acquired using the Bitplane Imaris 8.3.1 (Bitplane, Zurich, Switzerland), as previously reported (Wei et al., 2018; Lu et al., 2019). Green and red neurons were counted using the Spot module within Imaris, which also calculate co-localization. Brain structures were registered using the Paxinos mouse atlas as a reference (Franklin and Paxinos, 2007).

4.5.5. Statistical analysis

Data were analyzed by two-tailed t test, two-way ANOVA with repeated measurement, or one-way ANOVA followed by the Student-Newman-Keuls (SNK) post hoc test. Significance was determined if $p < 0.05$. Statistical analysis was conducted by SigmaPlot.

CHAPTER V

CONCLUSIONS

Striatal circuits exert powerful control over reward-driven behaviors. Alcohol-evoked aberrant synaptic plasticity in the DMS might drive compulsive alcohol-seeking and alcohol-taking behaviors in the AUD. Thus, exploring the input-specific and cell type-specific contributions of striatal circuits to AUD is important for elucidating the mechanism by which aberrant glutamatergic synaptic plasticity potentially drives excessive alcohol intake.

In chapter II, I demonstrated that glutamatergic inputs to the DMS can be classified in a cell type-specific manner and that the strengths of their glutamatergic connections with two types of MSN were not identical. One major finding of this chapter is that striatal synapses containing presynaptic D2Rs and postsynaptic D1Rs (D2→D1) exhibited stronger glutamatergic connectivity than the other tested synapses (D1→D1, D1→D2, and D2→D2). Additionally, I discovered that excessive alcohol consumption induced a long-lasting potentiation of glutamatergic transmission at the corticostriatal D2→D1 synapse. To our knowledge, we provide the first demonstration that corticostriatal circuits can be further characterized according to the cell type-specific inputs. The main reason why we classified glutamatergic inputs based on presynaptic dopamine receptor expression is that during reward-based behaviors, dopamine acts on not only its postsynaptic receptors but also its presynaptic ones; the latter provides presynaptic filtering to select appropriate excitatory synapses, allowing their specific signals to pass to the direct and indirect pathway of the basal ganglia (Bamford et al.,

2004; Bamford et al., 2018). Appropriate presynaptic filtering may be critical to select the most effective corticostriatal synapses during learning (Bamford et al., 2018). Since D1Rs and D2Rs are major dopamine receptors at the corticostriatal pathway (Wei et al., 2018) and they are few overlapped, we think that there are at least four pathways that can be examined: D1→D1, D1→D2, D2→D1, and D2→D2. The finding showing intrinsic differences of glutamatergic connectivity at four types of striatal synapses with both pre-and postsynaptic dopamine receptors may provide a foundation for understanding how different inputs onto distinct DMS neurons are regulated by dopamine. Furthermore, these findings also provide new insights into alcohol-evoked circuit-specific plasticity at the behavior level. D2Rs are linked to Gαi (Xing et al., 2016), activation of which negatively regulates neuronal activity; this suggested that activation of the presynaptic D2Rs may negatively regulate glutamatergic transmission of corticostriatal D2→D1 circuit. The reduced dopamine levels induced by chronic alcohol intake (Barak et al., 2011) may decrease D2R signaling and consequently disinhibit the regulation of "Go" actions by DMS D1-MSNs (Cheng et al., 2017). The elucidation of this alcohol-evoked circuit-specific plasticity could provide the basis for new neuronal therapeutic targets for the treatment of alcohol use disorder.

Another major finding of chapter II is that D2R-mediated inhibition of glutamatergic transmission in the DMS is mediated by distinct pre- and postsynaptic mechanisms. It is known that D2R activation inhibits corticostriatal transmission, but the underlying mechanism is not completely understood (Bamford et al., 2004; Yin and Lovinger, 2006; Bamford et al., 2018). Since we can selectively measure the

glutamatergic transmission at D2→D1 or D1→D2, which did not express postsynaptic D2Rs or presynaptic D2Rs, respectively, we are able to separate the contribution of presynaptic and postsynaptic D2Rs to their inhibitory role on corticostriatal transmission. Our results contribute to the clarification of previous controversial findings (Bamford et al., 2004; Yin and Lovinger, 2006) relating to the role of the D2R in inhibitory presynaptic filtering of cortical inputs. Postsynaptic D2R-mediated suppression of glutamatergic transmission required eCB signaling, whereas presynaptic D2Rs mediated eCB-independent suppression.

In chapter III, I employed activity-dependent genetic labeling using the FosTRAP method and found a higher percentage of DMS D1R-expressing neurons were activated by excessive intake of ethanol, as compared with water only. These data are consistent with previous studies showing that excessive alcohol consumption is associated with elevated D1-MSN activity (Cheng et al., 2017; Ma et al., 2018). Then, using optogenetics and whole-cell patch clamp recording, I observed alcohol-induced circuit-specific potentiation at mPFC inputs onto D1-MSNs. This enhanced synaptic strength was due to both stronger postsynaptic AMPAR- and GluN2B-containing NMDAR-mediated responses, and an enhanced probability of presynaptic transmitter release. This is consistent with other studies showing that addictive substances, including ethanol, potentiated glutamatergic responses in D1-MSNs, but not D2-MSNs (MacAskill et al., 2014; Cheng et al., 2017; Ma et al., 2018).

Accumulating evidence indicates that the reinforcement behavior induced by addictive substances requires dopamine-dependent long-term synaptic plasticity in the

striatum (MacAskill et al., 2014; Pascoli et al., 2015; Bamford et al., 2018). We utilized dual-channel optogenetic approaches to manipulate synaptic plasticity at the mPFC onto DMS D1R-MSN synapse, mimicking the ethanol-mediated potentiation. We provide direct evidence that induction of LTP specifically at corticostriatal synapses reinforced operant behavior. Our findings will facilitate future research exploring the neurons and circuits that are responsible for the regulation of long-term behaviors relevant to addition.

Another major finding in chapter III is that time-locked depression of mPFC→D1-MSN transmission persistently decreased ethanol-seeking behavior. This finding was made using an experimental design where ethanol-seeking behavior in rats triggered an *in vivo* dual-channel optogenetic post-pre spike-timing dependent plasticity protocol that induced LTD of mPFC→D1-MSN synapses. This plasticity-based reduction in ethanol-seeking behavior represents a potential therapeutic strategy to modulate dysregulated brain circuits in addiction.

In chapter IV, we generated a brain-wide map showing the distribution of neurons outside of striatum that project to pDMS D1-MSNs or D2-MSNs using recently developed rabies virus-mediated monosynaptic tracing approach. Although a variety of cortical, thalamic, amygdala, and midbrain structure send equivalent inputs onto D1-MSNs and D2-MSNs, we discovered that orbital frontal cortex, secondary motor and visual cortex, as well as cingulate cortex preferentially targeted pDMS D1-MSNs, whereas primary motor, primary sensory, and thalamic inputs preferentially projected to pDMS D2-MSNs. The prefrontal and limbic association structures that are devoted

mainly to reward motivation, emotional regulation, planning of complex cognitive behaviors, and decision making preferentially innervated D1-MSNs (Floresco et al., 2008; Balleine et al., 2009; Gremel et al., 2016; Barthas and Kwan, 2017). Thus, rewarded information based on the past experience may be preferentially passed to the direct pathway circuit to facilitate prior rewarded actions to procure a reward. It has been reported that during action initiation, D1-MSNs and D2-MSNs are concurrently activated (Hikida et al., 2010; Cui et al., 2013). Biased projections from primary motor and sensory cortex onto D2-MSNs may contribute to suppression of unwanted behavior via activation of D2-MSNs.

In chapter II, I found that extra-striatal D1R- or D2R-expressing neurons formed strong glutamatergic connections with D1-MSNs or D2-MSNs. Surprisingly, in chapter IV, we found that majority of extra-striatal neurons that innervated D1-MSNs or D2-MSNs do not contain D1Rs (or D2Rs). While the number of D1R- or D2R-expressing neurons that projected to pDMS MSNs was low, but they exhibited distinct distribution across the different brain regions. Increasing evidence has indicated that presynaptic D1Rs and D2Rs present in cortical terminals are important for dopamine-dependent modulation of glutamate release at corticostriatal synapses (Wang and Goldman-Rakic, 2004; Bamford et al., 2018; Cui et al., 2018). It has been shown that at low stimulation frequency of cortical inputs, the presynaptic D1Rs boost, whereas the presynaptic D2Rs suppress glutamate release to D1-MSN and D2-MSNs (Wang et al., 2012b; Cui et al., 2018). At higher stimulation frequency of cortical inputs, this dopaminergic modulation of glutamatergic terminals is occluded by adenosine and endocannabinoids (Wang et al.,

2012b; Bamford et al., 2018).These findings lay a foundation for future understanding of how pDMS sorts information from multiple upstream brain regions to determine the action.

In summary, my research provides an insight into the detailed circuit mechanisms underlying the control of alcohol consumption. It establishes a causal link between corticostriatal synaptic potentiation and alcohol-seeking behavior. As mentioned, current treatments for alcohol addiction are limited since they fail to achieve long-term treatment goals. This research is highly significant because it aims to address this gap by establishing reversal of alcohol-evoked long-term synaptic plasticity. It is also highly innovative because it applied several state-of-the-art approaches, including rabies virus-mediated retrograde monosynaptic tracing, dual-channel optogenetics, Fos promoter-based TRAP techniques, and transgenic mice, which allow us to manipulate the specific circuit. These data will enrich and help specify the understanding of how this glutamatergic plasticity controls alcohol-seeking behavior, and these results can guide subsequent manipulation studies.

REFERENCES

Abrahao KP, Salinas AG, Lovinger DM (2017) Alcohol and the brain: neuronal molecular targets, synapses, and circuits. Neuron 96:1223-1238.

Ade KK, Wan Y, Chen M, Gloss B, Calakos N (2011) An improved BAC transgenic fluorescent reporter line for sensitive and specific identification of striatonigral medium spiny neurons. Frontiers in Systems Neuroscience 5:32.

Allen WE, DeNardo LA, Chen MZ, Liu CD, Loh KM, Fenno LE, Ramakrishnan C, K. D, Luo L (2017) Thirst-associated preoptic neurons encode an aversive motivational drive. Science 357:1149-1155.

Bahi A, Dreyer JL (2012) Involvement of nucleus accumbens dopamine D1 receptors in ethanol drinking, ethanol-induced conditioned place preference, and ethanol-induced psychomotor sensitization in mice. Psychopharmacology (Berl) 222:141-153.

Balleine BW, O'Doherty JP (2010) Human and rodent homologies in action control: corticostriatal determinants of goal-directed and habitual action. Neuropsychopharmacology 35:48-69.

Balleine BW, Liljeholm M, Ostlund SB (2009) The integrative function of the basal ganglia in instrumental conditioning. Behav Brain Res 199:43-52.

Bamford NS, Wightman RM, Sulzer D (2018) Dopamine's effects on corticostriatal synapses during reward-based behaviors. Neuron 97:494-510.

Bamford NS, Zhang H, Schmitz Y, Wu NP, Cepeda C, Levine MS, Schmauss C, Zakharenko SS, Zablow L, Sulzer D (2004) Heterosynaptic dopamine neurotransmission selects sets of corticostriatal terminals. Neuron 42:653-663.

Barak S, Carnicella S, Yowell QV, Ron D (2011) Glial cell line-derived neurotrophic factor reverses alcohol-induced allostasis of the mesolimbic dopaminergic system: implications for alcohol reward and seeking. J Neurosci 31:9885-9894.

Barthas F, Kwan AC (2017) Secondary motor cortex: where 'sensory' meets 'motor' in the rodent frontal cortex. Trends Neurosci 40:181-193.

Batman AM, Miles MF (2015) Translating alcohol research: opportunities and challenges. Alcohol Research 37:7-14.

Beaulieu JM, Gainetdinov RR (2011) The physiology, signaling, and pharmacology of dopamine receptors. Pharmacological Reviews 63:182-217.

Belin D, Everitt BJ (2008) Cocaine seeking habits depend upon dopamine-dependent serial connectivity linking the ventral with the dorsal striatum. Neuron 57:432-441.

Ben Hamida S, Darcq E, Wang J, Wu S, Phamluong K, Kharazia V, Ron D (2013) Protein tyrosine phosphatase alpha in the dorsomedial striatum promotes excessive ethanol-drinking behaviors. J Neurosci 33:14369-14378.

Blackwell KT, Czubayko U, Plenz D (2003) Quantitative estimate of synaptic inputs to striatal neurons during up and down states in vitro. J Neurosci 23:9123-9132.

Bradfield LA, Bertran-Gonzalez J, Chieng B, Balleine BW (2013) The thalamostriatal pathway and cholinergic control of goal-directed action: interlacing new with existing learning in the striatum. Neuron 79:153-166.

Bromberg-Martin ES, Matsumoto M, Hikosaka O (2010) Dopamine in motivational control: rewarding, aversive, and alerting. Neuron 68:815-834.

Brown P (2007) Abnormal oscillatory synchronisation in the motor system leads to impaired movement. Curr Opin Neurobiol 17:656-664.

Burton AC, Nakamura K, Roesch MR (2015) From ventral-medial to dorsal-lateral striatum: neural correlates of reward-guided decision-making. Neurobiology of Learning and Memory 117:51-59.

Calabresi P PA, Mercuri NB, Bernardi G. (1992) Long-term potentiation in the striatum is unmasked by removing the voltage-dependent magnesium block of NMDA receptor channels. Eur J Neurosci 4:6.

Chan CS, Surmeier DJ, Yung WH (2005) Striatal information signaling and integration in globus pallidus: timing matters. Neurosignals 14:281-289.

Cheng Y, Huang CC, Ma T, Wei X, Wang X, Lu J, Wang J (2017) Distinct synaptic strengthening of the striatal direct and indirect pathways drives alcohol consumption. Biol Psychiatry 81:918-929.

Cheng Y, Wang X, Wei X, Xie X, Melo S, Miranda RC, Wang J (2018) Prenatal exposure to alcohol induces functional and structural plasticity in dopamine D1 receptor-expressing neurons of the dorsomedial striatum. Alcohol Clin Exp Res 42:1493-1502.

Corbit LH, Janak PH (2010) Posterior dorsomedial striatum is critical for both selective instrumental and Pavlovian reward learning. The European Journal of Neuroscience 31:1312-1321.

Corbit LH, Leung BK, Balleine BW (2013) The role of the amygdala-striatal pathway in the acquisition and performance of goal-directed instrumental actions. J Neurosci 33:17682-17690.

Creed M, Pascoli V, Lüscher C (2015) Refining deep brain stimulation to emulate optogenetic treatment of synaptic pathology. Science 347:659-664.

Cruikshank SJ, Urabe H, Nurmikko AV, Connors BW (2010) Pathway-specific feedforward circuits between thalamus and neocortex revealed by selective optical stimulation of axons. Neuron 65:230-245.

Cui G, Jun SB, Jin X, Pham MD, Vogel SS, Lovinger DM, Costa RM (2013) Concurrent activation of striatal direct and indirect pathways during action initiation. Nature 494:238-242.

Cui Q, Li Q, Geng H, Chen L, Ip NY, Ke Y, Yung WH (2018) Dopamine receptors mediate strategy abandoning via modulation of a specific prelimbic cortex-nucleus accumbens pathway in mice. Proc Natl Acad Sci U S A 115:E4890-E4899.

Davis M, Walker DL, Miles L, Grillon C (2010) Phasic vs sustained fear in rats and humans: role of the extended amygdala in fear vs anxiety. Neuropsychopharmacology 35:105-135.

De Bundel D, Zussy C, Espallergues J, Gerfen CR, Girault JA, Valjent E (2016) Dopamine D2 receptors gate generalization of conditioned threat responses through mTORC1 signaling in the extended amygdala. Mol Psychiatry 21:1545-1553.

DeLong M (1990) Primate models of movement disorders of basal ganglia origin. Trends Neurosci 13:281-285.

DeNardo LA, Liu CD, Allen WE, Adams EL, Friedmann D, Fu L, Guenthner CJ, Tessier-Lavigne M, Luo L (2019) Temporal evolution of cortical ensembles promoting remote memory retrieval. Nat Neurosci 22:460-469.

Ding J, Peterson JD, Surmeier DJ (2008) Corticostriatal and thalamostriatal synapses have distinctive properties. J Neurosci 28:6483-6492.

Doig NM, Moss J, Bolam JP (2010) Cortical and thalamic innervation of direct and indirect pathway medium-sized spiny neurons in mouse striatum. J Neurosci 30:14610-14618.

Dumartin B, Doudnikoff E, Gonon F, Bloch B (2007) Differences in ultrastructural localization of dopaminergic D1 receptors between dorsal striatum and nucleus accumbens in the rat. Neurosci Lett 419:273-277.

Durieux PF, Schiffmann SN, de Kerchove d'Exaerde A (2012) Differential regulation of motor control and response to dopaminergic drugs by D1R and D2R neurons in distinct dorsal striatum subregions. EMBO J 31:640-653.

Ehrie J, Hartwell EE, Morris PE, Mark TL, Kranzler HR (2020) Survey of addiction specialists' use of medications to treat alcohol use disorder. Front Psychiatry 11:47.

Floresco SB, St Onge JR, Ghods-Sharifi S, Winstanley CA (2008) Cortico-limbic-striatal circuits subserving different forms of cost-benefit decision making. Cogn Affect Behav Neurosci 8:375-389.

Ford CP (2014) The role of D2-autoreceptors in regulating dopamine neuron activity and transmission. Neuroscience 282:13-22.

Franklin KBJ, Paxinos G (2007) The mouse brain in stereotaxic coordinates, 3rd Edition: Elsevier.

Gerfen CR, Surmeier DJ (2011) Modulation of striatal projection systems by dopamine. Annu Rev Neurosci 34:441-466.

Gong S, Doughty M, Harbaugh CR, Cummins A, Hatten ME, Heintz N, Gerfen CR (2007) Targeting Cre recombinase to specific neuron populations with bacterial artificial chromosome constructs. J Neurosci 27:9817-9823.

Gremel CM, Chancey JH, Atwood BK, Luo G, Neve R, Ramakrishnan C, Deisseroth K, Lovinger DM, Costa RM (2016) Endocannabinoid modulation of orbitostriatal circuits gates habit formation. Neuron 90:1312-1324.

Grieder TE, George O, Tan H, George SR, Le Foll B, Laviolette SR, van der Kooy D (2012) Phasic D1 and tonic D2 dopamine receptor signaling double dissociate the motivational effects of acute nicotine and chronic nicotine withdrawal. Proc Natl Acad Sci U S A 109:3101-3106.

Guo Q, Wang D, He X, Feng Q, Lin R, Xu F, Fu L, Luo M (2015) Whole-brain mapping of inputs to projection neurons and cholinergic interneurons in the dorsal striatum. PLoS One 10:e0123381.

Hasue RH, Shammah-Lagnado SJ (2002) Origin of the dopaminergic innervation of the central extended amygdala and accumbens shell: a combined retrograde tracing and immunohistochemical study in the rat. The Journal of Comparative Neurology 454:15-33.

Hernandez VM, Hegeman DJ, Cui Q, Kelver DA, Fiske MP, Glajch KE, Pitt JE, Huang TY, Justice NJ, Chan CS (2015) Parvalbumin+ neurons and npas1+ neurons are distinct neuron classes in the mouse external globus pallidus. J Neurosci 35:11830-11847.

Higley MJ, Gittis AH, Oldenburg IA, Balthasar N, Seal RP, Edwards RH, Lowell BB, Kreitzer AC, Sabatini BL (2011) Cholinergic interneurons mediate fast VGluT3-dependent glutamatergic transmission in the striatum. PLoS One 6:e19155.

Hikida T, Kimura K, Wada N, Funabiki K, Nakanishi S (2010) Distinct roles of synaptic transmission in direct and indirect striatal pathways to reward and aversive behavior. Neuron 66:896-907.

Hooks BM, Lin JY, Guo C, Svoboda K (2015) Dual-channel circuit mapping reveals sensorimotor convergence in the primary motor cortex. J Neurosci 35:4418-4426.

Hu Y, Salmeron BJ, Krasnova IN, Gu H, Lu H, Bonci A, Cadet JL, Stein EA, Yang Y (2019) Compulsive drug use is associated with imbalance of orbitofrontal- and

prelimbic-striatal circuits in punishment-resistant individuals. Proc Natl Acad Sci U S A 116:9066-9071.

Huang CCY, Ma T, Roltsch Hellard EA, Wang X, Selvamani A, Lu J, Sohrabji F, Wang J (2017) Stroke triggers nigrostriatal plasticity and increases alcohol consumption in rats. Sci Rep 7:2501.

Hunnicutt BJ, Jongbloets BC, Birdsong WT, Gertz KJ, Zhong H, Mao T (2016) A comprehensive excitatory input map of the striatum reveals novel functional organization. Elife 5:e19103.

Jeanblanc J (2015) Comorbidity between psychiatric diseases and alcohol use disorders: impact of adolescent alcohol consumption. Current Addiction Reports 2:293-301.

Kim B, Yoon S, Nakajima R, Lee HJ, Lim HJ, Lee YK, Choi JS, Yoon BJ, Augustine GJ, Baik JH (2018) Dopamine D2 receptor-mediated circuit from the central amygdala to the bed nucleus of the stria terminalis regulates impulsive behavior. Proc Natl Acad Sci U S A 115:E10730-E10739.

Klapoetke NC et al. (2014) Independent optical excitation of distinct neural populations. Nature Methods 11:338-346.

Koob GF, Volkow ND (2010) Neurocircuitry of addiction. Neuropsychopharmacology 35:217-238.

Kranzler HR, Soyka M (2018) Diagnosis and pharmacotherapy of alcohol use disorder: a review. JAMA 320:815-824.

Kravitz AV, Tye LD, Kreitzer AC (2012) Distinct roles for direct and indirect pathway striatal neurons in reinforcement. Nat Neurosci 15:816-818.

Krawczyk M, Georges F, Sharma R, Mason X, Berthet A, Bezard E, Dumont EC (2011) Double-dissociation of the catecholaminergic modulation of synaptic transmission in the oval bed nucleus of the stria terminalis. J Neurophysiol 105:145-153.

Kreitzer AC (2009) Physiology and pharmacology of striatal neurons. Annu Rev Neurosci 32:127-147.

Kreitzer AC, Malenka RC (2008) Striatal plasticity and basal ganglia circuit function. Neuron 60:543-554.

Kuei-Sen Hsu C-CH, Cheng-Hsun Yang, Po-Wu Gean (1995) Presynaptic D2 dopaminergic receptors mediate inhibition of excitatory synaptic transmission in rat neostriatum. Brain Research 690:264-268.

Lalive AL, Lien AD, Roseberry TK, Donahue CH, Kreitzer AC (2018) Motor thalamus supports striatum-driven reinforcement. Elife 7:pii: e34032.

Lee CR, Abercrombie ED, Tepper JM (2004) Pallidal control of substantia nigra dopaminergic neuron firing pattern and its relation to extracellular neostriatal dopamine levels. Neuroscience 129:481-489.

Lee CR, Yonk AJ, Wiskerke J, Paradiso KG, Tepper JM, Margolis DJ (2019) Opposing influence of sensory and motor cortical input on striatal circuitry and choice behavior. Curr Biol 29:1313-1323.

Li YC, Yang SS, Gao WJ (2016) Disruption of Akt signaling decreases dopamine sensitivity in modulation of inhibitory synaptic transmission in rat prefrontal cortex. Neuropharmacology 108:403-414.

Lobo MK, Covington HE, Chaudhury D, Friedman AK, Sun H, Damez-Werno D, Dietz DM, Zaman S, Koo JW, Kennedy PJ, Mouzon E, Mogri M, Neve RL, Deisseroth K, Han MH, Nestler EJ (2010) Cell type-specific loss of BDNF signaling mimics optogenetic control of cocaine reward. Science 330:385-390.

Lovinger DM (2010) Neurotransmitter roles in synaptic modulation, plasticity and learning in the dorsal striatum. Neuropharmacology 58:951-961.

Lovinger DM, Abrahao KP (2018) Synaptic plasticity mechanisms common to learning and alcohol use disorder. Learn Mem 25:425-434.

Lu J, Cheng Y, Wang X, Woodson K, Kemper C, Disney E, Wang J (2019) Alcohol intake enhances glutamatergic transmission from D2 receptor-expressing afferents onto D1 receptor-expressing medium spiny neurons in the dorsomedial striatum. Neuropsychopharmacology 44:1123-1131.

Luscher C, Malenka RC (2011) Drug-evoked synaptic plasticity in addiction: from molecular changes to circuit remodeling. Neuron 69:650-663.

Luscher C, Robbins TW, Everitt BJ (2020) The transition to compulsion in addiction. Nat Rev Neurosci 21:247-263.

Ma T, Barbee B, Wang X, Wang J (2017) Alcohol induces input-specific aberrant synaptic plasticity in the rat dorsomedial striatum. Neuropharmacology 123:46-54.

Ma T, Cheng Y, Roltsch Hellard E, Wang X, Lu J, Gao X, Huang CCY, Wei XY, Ji JY, Wang J (2018) Bidirectional and long-lasting control of alcohol-seeking behavior by corticostriatal LTP and LTD. Nat Neurosci 21:373-383.

Ma YY, Lee BR, Wang X, Guo C, Liu L, Cui R, Lan Y, Balcita-Pedicino JJ, Wolf ME, Sesack SR, Shaham Y, Schluter OM, Huang YH, Dong Y (2014) Bidirectional modulation of incubation of cocaine craving by silent synapse-based remodeling of prefrontal cortex to accumbens projections. Neuron 83:1453-1467.

MacAskill AF, Cassel JM, Carter AG (2014) Cocaine exposure reorganizes cell type- and input-specific connectivity in the nucleus accumbens. Nat Neurosci 17:1198-1207.

Madisen L, Zwingman TA, Sunkin SM, Oh SW, Zariwala HA, Gu H, Ng LL, Palmiter RD, Hawrylycz MJ, Jones AR, Lein ES, Zeng H (2010) A robust and high-throughput Cre reporting and characterization system for the whole mouse brain. Nat Neurosci 13:133-140.

Madisen L et al. (2012) A toolbox of Cre-dependent optogenetic transgenic mice for light-induced activation and silencing. Nat Neurosci 15:793-802.

Madisen L et al. (2015) Transgenic mice for intersectional targeting of neural sensors and effectors with high specificity and performance. Neuron 85:942-958.

Malenka RC, Bear MF (2004) LTP and LTD: an embarrassment of riches. Neuron 44:5-21.

Mansouri F, Fettes P, Schulze L, Giacobbe P, Zariffa J, Downar J (2018) A real-time phase-locking system for non-invasive brain stimulation. Front Neurosci 12:877.

Maroteaux M, Mameli M (2012) Cocaine evokes projection-specific synaptic plasticity of lateral habenula neurons. J Neurosci 32:12641-12646.

Matamales M, McGovern A, Mi J, Mazzone S, Balleine B, J. B-G (2020) Local D2- to D1-neuron transmodulation updates goal-directed learning in the striatum. Science 367:549-555.

Mateo Y, Johnson KA, Covey DP, Atwood BK, Wang HL, Zhang S, Gildish I, Cachope R, Bellocchio L, Guzman M, Morales M, Cheer JF, Lovinger DM (2017) Endocannabinoid Actions on Cortical Terminals Orchestrate Local Modulation of Dopamine Release in the Nucleus Accumbens. Neuron 96:1112-1126 e1115.

McCool BA (2011) Ethanol modulation of synaptic plasticity. Neuropharmacology 61:1097-1108.

Ogawa SK, Watabe-Uchida M (2018) Organization of dopamine and serotonin system: Anatomical and functional mapping of monosynaptic inputs using rabies virus. Pharmacol Biochem Behav 174:9-22.

Oldenburg IA, Ding JB (2011) Cholinergic modulation of synaptic integration and dendritic excitability in the striatum. Curr Opin Neurobiol 21:425-432.

Partridge JG TK, Lovinger DM. (2000) Regional and postnatal heterogeneity of activity-dependent long-term changes in synaptic efficacy in the dorsal striatum. J Neurophysiol 84:9.

Pascoli V, Turiault M, Luscher C (2012) Reversal of cocaine-evoked synaptic potentiation resets drug-induced adaptive behaviour. Nature 481:71-75.

Pascoli V, Terrier J, Hiver A, Luscher C (2015) Sufficiency of mesolimbic dopamine neuron stimulation for the progression to addiction. Neuron 88:1054-1066.

Pascoli V, Terrier J, Espallergues J, Valjent E, O'Connor EC, Luscher C (2014) Contrasting forms of cocaine-evoked plasticity control components of relapse. Nature 509:459-464.

Pascoli V, Hiver A, Van Zessen R, Loureiro M, Achargui R, Harada M, Flakowski J, Luscher C (2018) Stochastic synaptic plasticity underlying compulsion in a model of addiction. Nature 564:366-371.

Perez de la Mora M, Gallegos-Cari A, Crespo-Ramirez M, Marcellino D, Hansson AC, Fuxe K (2012) Distribution of dopamine D(2)-like receptors in the rat amygdala and their role in the modulation of unconditioned fear and anxiety. Neuroscience 201:252-266.

Perreault ML, Hasbi A, O'Dowd BF, George SR (2014) Heteromeric dopamine receptor signaling complexes: emerging neurobiology and disease relevance. Neuropsychopharmacology 39:156-168.

Peterchev AV, Wagner TA, Miranda PC, Nitsche MA, Paulus W, Lisanby SH, Pascual-Leone A, Bikson M (2012) Fundamentals of transcranial electric and magnetic stimulation dose: definition, selection, and reporting practices. Brain Stimul 5:435-453.

Pina MM, Cunningham CL (2014) Effects of dopamine receptor antagonists on the acquisition of ethanol-induced conditioned place preference in mice. Psychopharmacology (Berl) 231:459-468.

Ragozzino ME, Ragozzino KE, Mizumori SJ, RP. K (2002) Role of the dorsomedial striatum in behavioral flexibility for response and visual cue discrimination learning. Behav Neurosci 116:105-115.

Regier PS, Amemiya S, Redish AD (2015) Hippocampus and subregions of the dorsal striatum respond differently to a behavioral strategy change on a spatial navigation task. J Neurophysiol 114:1399-1416.

Rehm J, Mathers C, Popova S, Thavorncharoensap M, Teerawattananon Y, Patra J (2009) Global burden of disease and injury and economic cost attributable to alcohol use and alcohol-use disorders. Lancet 382:1575-1586.

Renteria R, Baltz ET, Gremel CM (2018) Chronic alcohol exposure disrupts top-down control over basal ganglia action selection to produce habits. Nat Commun 9:211.

Renteria R, Maier EY, Buske TR, Morrisett RA (2017) Selective alterations of NMDAR function and plasticity in D1 and D2 medium spiny neurons in the nucleus accumbens shell following chronic intermittent ethanol exposure. Neuropharmacology 112:164-171.

Richfield EK, Penney JB, AB. Y (1989) Anatomical and affinity state comparisons between dopamine D1 and D2 receptors in the rat central nervous system. Neuroscience 30:767-777.

Roltsch Hellard E, Binette A, Zhuang X, Lu J, Ma T, Jones B, Williams E, Jayavelu S, Wang J (2019) Optogenetic control of alcohol-seeking behavior via the dorsomedial striatal circuit. Neuropharmacology 155:89-97.

Sacks JJ, Gonzales KR, Bouchery EE, Tomedi LE, Brewer RD (2015) 2010 national and state costs of excessive alcohol consumption. Am J Prev Med 49:e73-e79.

Shen W, Hamilton SE, Nathanson NM, Surmeier DJ (2005) Cholinergic suppression of KCNQ channel currents enhances excitability of striatal medium spiny neurons. J Neurosci 25:7449-7458.

Shen W, Flajolet M, Greengard P, Surmeier DJ (2008) Dichotomous dopaminergic control of striatal synaptic plasticity. Science 321:848-851.

Shen W, Hernandez-Lopez S, Tkatch T, Held JE, Surmeier DJ (2004) Kv1. 2-containing K+ channels regulate subthreshold excitability of striatal medium spiny neurons. Journal of Neurophysiology 91:1337-1349.

Shiflett MW, Brown RA, Balleine BW (2010) Acquisition and performance of goal-directed instrumental actions depends on ERK signaling in distinct regions of dorsal striatum in rats. J Neurosci 30:2951-2959.

Silvanto J, Muggleton N, Walsh V (2008) State-dependency in brain stimulation studies of perception and cognition. Trends Cogn Sci 12:447-454.

Smith JB, Klug JR, Ross DL, Howard CD, Hollon NG, Ko VI, Hoffman H, Callaway EM, Gerfen CR, Jin X (2016) Genetic-based dissection unveils the inputs and outputs of striatal patch and matrix compartments. Neuron 91:1069-1084.

Smith Y, Surmeier DJ, Redgrave P, Kimura M (2011) Thalamic contributions to Basal Ganglia-related behavioral switching and reinforcement. J Neurosci 31:16102-16106.

Surmeier DJ, Bargas J, Kitai S (1989) Two types of A-current differing in voltage-dependence are expressed by neurons of the rat neostriatum. Neuroscience Letters 103:331-337.

Surmeier DJ, Plotkin J, Shen W (2009) Dopamine and synaptic plasticity in dorsal striatal circuits controlling action selection. Curr Opin Neurobiol 19:621-628.

Surmeier DJ, Stefani A, Foehring RC, Kitai S (1991) Developmental regulation of a slowly-inactivating potassium conductance in rat neostriatal neurons. Neuroscience Letters 122:41-46.

Trantham-Davidson H, Chandler LJ (2015) Alcohol-induced alterations in dopamine modulation of prefrontal activity. Alcohol 49:773-779.

Verena Pawlak JNDK (2008) Dopamine receptor activation is required for corticostriatal spike-timing-dependent plasticity. J Neurosci 28:11.

Volkow ND, Morales M (2015) The brain on drugs: from reward to addiction. Cell 162:712-725.

Volkow ND, Koob GF, McLellan AT (2016) Neurobiologic advances from the brain disease model of addiction. N Engl J Med 374:363-371.

Volkow ND, Wang GJ, Telang F, Fowler JS, Logan J, Childress AR, Jayne M, Ma Y, Wong C (2006) Cocaine cues and dopamine in dorsal striatum: mechanism of craving in cocaine addiction. J Neurosci 26:6583-6588.

Wall NR, De La Parra M, Callaway EM, Kreitzer AC (2013) Differential innervation of direct- and indirect-pathway striatal projection neurons. Neuron 79:347-360.

Wang H, Pickel VM (2002) Dopamine D2 receptors are present in prefrontal cortical afferents and their targets in patches of the rat caudate-putamen nucleus. The Journal of Comparative Neurology 442:392-404.

Wang J, Lanfranco MF, Gibb SL, Ron D (2011) Ethanol-mediated long-lasting adaptations of the NR2B-containing NMDA receptors in the dorsomedial striatum. Channels (Austin) 5:205-209.

Wang J, Lanfranco MF, Gibb SL, Yowell QV, Carnicella S, Ron D (2010) Long-lasting adaptations of the NR2B-containing NMDA receptors in the dorsomedial striatum play a crucial role in alcohol consumption and relapse. J Neurosci 30:10187-10198.

Wang J, Ben Hamida S, Darcq E, Zhu W, Gibb SL, Lanfranco MF, Carnicella S, Ron D (2012a) Ethanol-mediated facilitation of AMPA receptor function in the dorsomedial striatum: implications for alcohol drinking behavior. J Neurosci 32:15124-15132.

Wang J, Cheng Y, Wang X, Roltsch Hellard E, Ma T, Gil H, Ben Hamida S, Ron D (2015) Alcohol elicits functional and structural plasticity selectively in dopamine D1 receptor-expressing neurons of the dorsomedial striatum. J Neurosci 35:11634-11643.

Wang J, Carnicella S, Phamluong K, Jeanblanc J, Ronesi JA, Chaudhri N, Janak PH, Lovinger DM, Ron D (2007) Ethanol induces long-term facilitation of NR2B-NMDA receptor activity in the dorsal striatum: implications for alcohol drinking behavior. J Neurosci 27:3593-3602.

Wang W, Dever D, Lowe J, Storey GP, Bhansali A, Eck EK, Nitulescu I, Weimer J, Bamford NS (2012b) Regulation of prefrontal excitatory neurotransmission by dopamine in the nucleus accumbens core. The Journal of Physiology 590:3743-3769.

Wang Y, Goldman-Rakic PS (2004) D2 receptor regulation of synaptic burst firing in prefrontal cortical pyramidal neurons. Proc Natl Acad Sci U S A 101:5093-5098.

Wei X, Ma T, Cheng Y, Huang CCY, Wang X, Lu J, Wang J (2018) Dopamine D1 or D2 receptor-expressing neurons in the central nervous system. Addict Biol 23:569-584.

White NM HN (1998) Preferential localization of self-stimulation sites in striosomes/patches in the rat striatum. Proc Natl Acad Sci USA 95:6486-6491.

Whiteford HA, Degenhardt L, Rehm J, Baxter AJ, Ferrari AJ, Erskine HE, Charlson FJ, Norman RE, Flaxman AD, Johns N, Burstein R, Murray CJL, Vos T (2013) Global burden of disease attributable to mental and substance use disorders: findings from the Global Burden of Disease Study 2010. The Lancet 382:1575-1586.

Williams ZM, Eskandar EN (2006) Selective enhancement of associative learning by microstimulation of the anterior caudate. Nat Neurosci 9:562-568.

Wilson CJ, Kawaguchi Y (1996) The origins of two-state spontaneous membrane potential fluctuations of neostriatal spiny neurons. Journal of Neuroscience 16:2397-2410.

Wu YW, Kim JI, Tawfik VL, Lalchandani RR, Scherrer G, Ding JB (2015) Input- and cell-type-specific endocannabinoid-dependent LTD in the striatum. Cell Rep 10:75-87.

Xing B, Li YC, Gao WJ (2016) Norepinephrine versus dopamine and their interaction in modulating synaptic function in the prefrontal cortex. Brain Res 1641:217-233.

Yin HH, Knowlton BJ (2004) Contributions of striatal subregions to place and response learning. Learn Mem 11:459-463.

Yin HH, Lovinger DM (2006) Frequency-specific and D2 receptor-mediated inhibition of glutamate release by retrograde endocannabinoid signaling. Proc Natl Acad Sci U S A 103:8251-8256.

Yin HH, Knowlton BJ, Balleine BW (2005a) Blockade of NMDA receptors in the dorsomedial striatum prevents action-outcome learning in instrumental conditioning. The European Journal of Neuroscience 22:505-512.

Yin HH, Ostlund SB, Knowlton BJ, Balleine BW (2005b) The role of the dorsomedial striatum in instrumental conditioning. The European Journal of Neuroscience 22:513-523.

Yin HH, Park BS, Adermark L, Lovinger DM (2007) Ethanol reverses the direction of long-term synaptic plasticity in the dorsomedial striatum. The European Journal of Neuroscience 25:3226-3232.

Zucker RS, Regehr WG (2002) Short-term synaptic plasticity. Annu Rev Physiol 64:355-405.